

**Methane Homologation by the Two-Step Cycle
on Co Catalysts**

by

Jaafar Sadegh | Soltan Mohammad Zadeh

B.Sc., Abadan Institute of Technology, 1987

M.Sc., The University of Shiraz, 1993

**A THESIS SUBMITTED IN PARTIAL FULFILLMENT OF THE REQUIREMENTS
FOR THE DEGREE OF DOCTOR OF PHILOSOPHY**

in

**THE FACULTY OF GRADUATE STUDIES
(Department of Chemical Engineering)**

**We accept this thesis as confirming
to the required standard**

THE UNIVERSITY OF BRITISH COLUMBIA

January, 1998

© J.S. Soltan Mohammad Zadeh, 1998

In presenting this thesis in partial fulfilment of the requirements for an advanced degree at the University of British Columbia, I agree that the Library shall make it freely available for reference and study. I further agree that permission for extensive copying of this thesis for scholarly purposes may be granted by the head of my department or by his or her representatives. It is understood that copying or publication of this thesis for financial gain shall not be allowed without my written permission.

Department of Chemical Engineering

The University of British Columbia
Vancouver, Canada

Date Jan. 22, 1998

Abstract

Conversion of natural gas to liquid hydrocarbons upgrades a low density fuel to a valuable source of chemicals and liquid fuel. To eliminate the expensive intermediate step of methane-steam reforming in the commercial Fischer-Tropsch, methanol to gasoline and Shell middle distillate synthesis processes, a direct method of CH_4 conversion to higher hydrocarbons is very desirable. In direct conversion of CH_4 to higher hydrocarbons in the presence of O_2 (e.g. oxidative coupling and partial oxidation), deep oxidation of CH_4 to CO and CO_2 is a major drawback. In the two-step homologation of CH_4 in the absence of O_2 , CH_4 is first activated on a reduced transition metal catalyst at high temperature (e.g. $450\text{ }^\circ\text{C}$) to produce H_2 and carbon species on the catalyst. The carbon species are then hydrogenated in the second step at a lower temperature (e.g. $100\text{ }^\circ\text{C}$) to produce CH_4 and higher hydrocarbons.

In the present study of the two-step homologation of CH_4 , SiO_2 supported Co catalysts were prepared by incipient impregnation. The catalysts were characterized by BET surface area and pore volume measurement, powder X-ray diffraction, temperature programmed reduction, H_2 chemisorption and Co re-oxidation. Carbon species deposited in the activation step were recovered by isothermal hydrogenation at $100\text{ }^\circ\text{C}$, temperature programmed surface reaction and temperature programmed oxidation to account for the reactivity of different carbon species.

The effect of catalyst loading, activation time, activation temperature, carbon aging, reaction cycle and isothermal medium on both the CH_4 activation step and the isothermal hydrogenation to C_{2+} hydrocarbons, were studied.

Based on the findings from deposition of more than a nominal monolayer carbon coverage on the supported metal, a semi-empirical kinetic model for the activation of CH_4 on Co- SiO_2 catalysts was developed. In the kinetic model, gas phase CH_4 is first activated on Co to produce adsorbed H and CH_3 species. Migration of some of the CH_3 species from the metal to the support liberates Co sites for further reaction. H_2 is generated by further dehydrogenation of CH_3 species on the metal and support, and desorption of adsorbed H.

The kinetic model and rate constants of different steps were used to interpret the effect of changes in operating conditions on the rate of different steps of the CH_4 activation reaction. Metal-support interactions in the Co- SiO_2 system play an important role in CH_4 activation and in determining the activity of carbon species.

With more than a nominal monolayer coverage of metal by carbon, a considerable amount of inactive carbon, which can only be removed by high temperature oxidation, is produced on the support. Hydrogen content and age of the carbon species were among the important factors affecting C_{2+} production in isothermal hydrogenation. It was shown that C-C bond formation occurs to a great extent before the isothermal hydrogenation step.

Table of Contents

Abstract	ii
Table of Contents	iv
List of Tables	ix
List of Figures	xi
Nomenclature	xiv
Acknowledgments	xviii
Chapter 1 Introduction	1
1.1 Conversion of Methane	1
1.2 Two-step Homologation of Methane	4
1.3 Motivation	7
1.4 Objectives of the Research	8
Chapter 2 Literature Review	10
2.1 Methane Upgrading	10
2.2 Homologation of Methane Using a Two-Step Cycle	12
2.2.1 Methane Homologation Using a Temperature Cycle	15
2.2.2 Methane Homologation Using a Pressure Cycle	20
2.3 Carbonaceous Deposits on Group VIII Metal Catalysts	24
2.4 Modifications of the Catalyst and Reactor for the two-step Cycle	29
2.4.1 Effect of the Catalyst Support on the Two-Step Cycle	29
2.4.2 Effect of a Catalyst Promoter on the Two-Step Cycle	30

2.4.3	Bimetallic Catalysts for the Two-Step Cycle	31
2.4.4	Molecular Sieve Catalysts for the Two-Step Cycle	32
2.4.5	Membrane Reactors for the Two-Step Cycle	33
2.5	Summary	33
Chapter 3	Experimental Methods	34
3.1	Overview	34
3.2	Catalyst Preparation	35
3.3	Experimental Set-Up	36
3.3.1	Kinetic Apparatus	36
3.3.2	Diffuse Reflectance IR Spectroscopy	39
3.4	Catalyst Characterization	42
3.4.1	Temperature Programmed Reduction	42
3.4.2	H ₂ Desorption	43
3.4.3	Co Re-Oxidation	43
3.4.4	Powder X-Ray Diffraction	44
3.4.5	BET Surface Area	45
3.5	Two-Step Reaction Cycles	47
3.5.1	Methane Activation	47
3.5.2	Isothermal Hydrogenation	48
3.5.3	Temperature Programmed Surface Reaction	49
3.5.4	Temperature Programmed Oxidation	49
3.6	DRIFTS Experiments	50

Chapter 4	Catalyst Characterization	52
4.1	Overview	52
4.2	Surface Area and Pore Volume	53
4.3	Bulk Phase Analysis	57
4.4	Reduction Properties of Calcined Co-SiO ₂ Catalysts	61
4.5	H ₂ Chemisorption on Co-SiO ₂ Catalysts	64
4.6	Extent of Catalyst Reduction	67
4.7	DRIFTS Study	70
4.8	Discussion	74
Chapter 5	Activation of CH ₄	78
5.1	Overview	78
5.2	Activation of CH ₄	79
5.3	Kinetics of CH ₄ Activation	82
5.3.1	Coverage of Surface Species	89
5.4	Parametric Study of the Kinetic Model	93
5.4.1	Initial Activation of CH ₄	94
5.4.2	Carbon Migration	96
5.4.3	Hydrogen Desorption	98
5.4.4	Dehydrogenation of Surface CH ₃	100
5.5	Effect of Operating Variables	102
5.5.1	Effect of Reaction Time	102
5.5.2	Effect of Metal Loading	105

5.5.3	Effect of Activation Temperature	106
5.5.4	Effect of Support and K Promoter on the Activation of CH ₄	108
5.6	Conclusions	110
Chapter 6	Hydrogenation	111
6.1	Overview	111
6.2	Carbon Recovery	113
6.2.1	Isothermal Hydrogenation	113
6.2.2	Temperature Programmed Surface Reaction	115
6.2.3	Temperature Programmed Oxidation	117
6.2.4	Carbon Balance	119
6.3	Effect of Operating Variables	121
6.3.1	Effect of Loading	121
6.3.2	Activation Time	124
6.3.3	Activation Temperature	126
6.3.4	Carbon Aging	128
6.3.5	Reaction Cycle	131
6.3.6	Isothermal Medium	133
6.4	Conclusion	137
Chapter 7	Conclusions and Recommendations for Future Work	139
7.1	Conclusions	139
7.2	Recommendations for Future Work	143
References		145

Appendices	152
1.1 Calibration of Mass Flow Controllers	153
1.2 Conditions of BET Analysis	156
1.3 Analysis with Gas Chromatograph	158
1.4 Calibration of Quadrupole Mass Spectrometer	162
1.5 Analysis Conditions of Infra-Red Spectroscopy	167
2.1 Temperature Programmed Reduction Profiles	169
2.2 Experimental Data	173
2.3 Equations for Calculations	181
2.4 Study of the Effect of Activation Temperature by the Kinetic Model	182
3.1 Computer Program Listing	187

List of Tables

Table 1.1	Operating conditions and yield of some direct CH ₄ upgrading processes.	3
Table 2.1	Selectivity of different catalysts in two step homologation of CH ₄ .	18
Table 2.2	Effect of K and Cu promoter on Co catalysts.	30
Table 2.3	Kinetic parameters of hydrogenation step on [Co _x] _{red} /NaY and Co/SiO ₂ .	32
Table 4.1	Average pore diameter and pore size distribution for the support and A series Co- SiO ₂ calcined catalysts.	57
Table 4.2	Peak 2 Θ location and the relative peak intensity of different phases in Co-SiO ₂ system in the 2 Θ range of 30-50°.	58
Table 4.3	Co dispersion based on the PXRD of the calcined catalysts.	61
Table 4.4	Extent of reduction of Co catalysts based on TPR.	64
Table 4.5	Moles of chemisorbed H ₂ and surface Co in Co-SiO ₂ catalysts.	67
Table 4.6	Extent of reduction of Co catalyst based on re-oxidation of the reduced Co.	70
Table 4.7	Summary of the Co-SiO ₂ catalyst characteristics.	75
Table 5.1	Effect of metal loading on the reaction rate constants.	106
Table 5.2	Effect of temperature on CH ₄ activation over 12% Co-SiO ₂ catalyst.	107
Table 5.3	Effect of support and K promoter on CH ₄ activation.	109
Table 6.1	Summary of carbon balance calculations for A-12% Co-SiO ₂ catalyst.	120
Table 6.2	Effect of the catalyst metal loading on its hydrogenation performance.	122
Table 6.3	Effect of activation time on the hydrogenation step.	125
Table 6.4	Effect of activation temperature on the hydrogenation step.	127

Table 6.5	Effect of carbon aging on the hydrogenation step.	130
Table 6.6	Effect of reaction cycle on the hydrogenation step.	132
Table 6.7	Effect of the isothermal medium on the product distribution.	135

List of Figures

Figure 1.1	Schematic representation of the two-step cycle for the homologation of CH ₄ .	5
Figure 2.1	Gibbs free energy as a function of temperature for activation of CH ₄ on Co and hydrogenation of cobalt carbide to C ₂ H ₆ .	14
Figure 2.2	CH ₄ production profile as a function of temperature in a TPSR.	17
Figure 2.3	A probable reaction sequence for activation of CH ₄ (step 1) and hydrogenation of surface species (step 2).	26
Figure 3.1	Block diagram of the experimental set-up.	37
Figure 3.2	DRIFTS reaction cell.	40
Figure 3.3	Block diagram of the DRIFTS reaction cell connections.	41
Figure 4.1	N ₂ adsorption and desorption on SiO ₂ as a function of relative pressure (P/P ₀).	54
Figure 4.2	BET plot for N ₂ adsorption on SiO ₂ .	56
Figure 4.3	PXRD diffractogram of the calcined A series 12%Co-SiO ₂ catalyst.	59
Figure 4.4	Profile of the temperature programmed reduction (TPR) of the A series 12%Co-SiO ₂ catalyst with 54 ml/min of 20%H ₂ /Ar gas mixture.	62
Figure 4.5	Profile of temperature and H ₂ desorption from A series 12%Co-SiO ₂ catalyst in 15 ml/min of Ar flow.	66
Figure 4.6	O ₂ uptake profile from pulses of 1.0 ml O ₂ in 15 ml/min of He flow by the reduced A series 12%Co-SiO ₂ catalyst during the Co oxidation step.	69

Figure 4.7	Diffuse reflectance infra-red Fourier transform spectra of the dilute passivated A series 12%Co-SiO ₂ catalyst with respect to pure KBr background.	71
Figure 4.8	Diffuse reflectance infra-red Fourier transform spectra of the diluted A series 12%Co-SiO ₂ reduced catalyst after activation, subsequent evacuation and hydrogenation with respect to the reduced, diluted catalyst background.	73
Figure 4.9	Schematic diagram of the two types of metal-support interaction (MSI) on Co-SiO ₂ catalyst.	77
Figure 5.1	Rate of CH ₄ consumption and H ₂ generation per mole of Co during 2 min flow of 5%CH ₄ /95%Ar gas mixture at 54 ml/min and 450 °C over A series 12%Co-SiO ₂ catalyst.	80
Figure 5.2	Cumulative moles of CH ₄ consumed per mole of surface Co and the value of x in the CH _x surface species during 2 min flow of 5%CH ₄ /95%Ar gas mixture at 54 ml/min and 450 °C over A series 12%Co-SiO ₂ catalyst.	81
Figure 5.3	Cumulative moles of CH ₄ consumed per mole of surface Co measured during 2 min flow of 5%CH ₄ /95%Ar gas mixture and 54 ml/min at 450 °C over A series 12%Co-SiO ₂ catalyst, compared to model fit.	88
Figure 5.4	Results of simulation of reaction rates for 2 min activation of 5%CH ₄ /95%Ar gas mixture at 450 °C over A series 12%Co-SiO ₂ catalyst.	90
Figure 5.5	Results of simulation of surface coverage for 2 min activation of 5%CH ₄ /95%Ar gas mixture at 450 °C over A series 12%Co-SiO ₂ catalyst.	91
Figure 5.6	Effect of k ₁ on nominal metal coverage, θ_c .	95
Figure 5.7	Effect of k ₂ on nominal metal coverage, θ_c .	97

Figure 5.8	Effect of k_3 on nominal metal coverage, θ_c .	99
Figure 5.9	Effect of k_4 on nominal metal coverage, θ_c .	101
Figure 5.10	Cumulative moles of CH_4 consumed per mole of surface Co measured during 7 min flow of 5% CH_4 /95%Ar gas mixture at 54 ml/min and 450 °C over the A series 12%Co-SiO ₂ catalyst, compared to model fit.	103
Figure 5.11	Value of x in the CH_x surface species during 2 min and 7 min flow of 5% CH_4 /95%Ar gas mixture at 54 ml/min and 450 °C over the A series 12%Co-SiO ₂ catalyst.	104
Figure 6.1	Profile of CH_4 , C_2H_4 and C_2H_6 production as a function of isothermal hydrogenation at 100 °C in 11 ml/min H_2 flow over the A series 12%Co-SiO ₂ catalyst after 2 min activation with a 5% CH_4 /Ar mixture at 450 °C.	114
Figure 6.2	Profile of CH_4 production and temperature as a function of time during temperature programmed surface reaction (TPSR) in 11 ml/min of H_2 flow on A series 12%Co-SiO ₂ catalyst.	116
Figure 6.3	Profile of CO_2 production and temperature as a function of time in temperature programmed oxidation (TPO) in 11 ml/min of O_2 flow on A series 12%Co-SiO ₂ catalyst.	118

Nomenclature

a	absorptivity
AES	Auger electron spectroscopy
a.u.	arbitrary unit
BET	Brunauer-Emmett-Teller
C	concentration (mol/l)
C	constant (Section 3.4.5)
C ₂₊	hydrocarbons with carbon number of 2 and higher
CH _x	carbon species on the surface with the H/C ratio of x
C _α	active carbon on the surface that hydrogenates at a temperature below 100 °C
C _β	moderately active carbon on the surface that hydrogenates at a temperature of about 200 °C
C _γ	least active carbon on the surface that hydrogenates at a temperature of about 500 °C
d	average pore diameter (Å)
DRIFTS	diffuse reflectance infra-red Fourier transform spectroscopy
FID	flame ionization detector
FT	Fischer-Tropsch
GC	gas chromatograph
HREELS	high resolution electron energy loss spectroscopy
IR	infra-red
IVS	injection valve system
k	reaction rate constant

K	Scherrer constant (=0.9)
LEED	low energy electron diffraction
LNG	liquefied natural gas
M	reduced metal
MCT	mercury-cadmium-telluride
MSI	metal-support interaction
MTG	methanol to gasoline
N_0	Avogadro's number ($=6.02 \times 10^{23}$ molecules/mol)
OC	oxidative coupling
P	pressure (Pa)
P_0	saturation pressure of the adsorbate at the adsorption temperature (Pa)
PO	partial oxidation
PXRD	powder X-ray diffraction
QMS	quadrupole mass spectrometer
R	gas constant ($8.314 \text{ J}\cdot\text{mol}^{-1}\cdot\text{K}^{-1}$)
R'	relative reflectance
R^2	correlation parameter
S	scattering coefficient (Section 3.6)
S	surface site
S_1	active site on the metal surface
S_2	active site on the support surface
S_{BET}	specific surface area measured by BET method (m^2/g)
SMDS	Shell middle distillate synthesis

t	crystal size (Å)
T	temperature (°C or K)
TCD	thermal conductivity detector
TCM	trillion cubic meters (10^{12} m^3)
TOF	turn over frequency (min^{-1})
TPD	temperature programmed desorption
TPO	temperature programmed oxidation
TPR	temperature programmed reduction
TPSR	temperature programmed surface reaction
UHP	ultra high purity
UHV	ultra high vacuum
V_a	volume of gas adsorbed per gram of adsorbent at STP (ml/g)
V_{BET}	specific pore volume measured by BET method (m^3/g)
V_m	monolayer capacity of the adsorbent (ml/g)
w	instrumental peak broadening in Scherrer's equation (radians) = 0.11 degrees
W	peak width at half height (radians)
Wt%	weight percent
XPS	X-ray photoelectron spectroscopy

Greek Letters

α	molecular cross-section of adsorbate ($\approx 0.162 \text{ nm}^2/\text{molecule of N}_2$)
α	chain growth probability in Schulz-Flory model (Section 2.2.1)
β	peak broadening in PXRD (radians)
ΔG°	standard Gibbs free energy change (J/mol)
Φ	catalyst metal dispersion (mol metal on surface/mol metal in the catalyst)
λ	radiation wavelength in Scherrer's equation (1.5406 Å)
θ	coverage
θ	peak position in PXRD (radians) (Section 3.4.4)
θ_c	nominal metal coverage by carbon (mol CH ₄ /mol surface Co)
σ	standard deviation

Acknowledgments

I am deeply indebted to my supervisor Dr. Kevin J. Smith for his support, guidance and enthusiasm throughout my graduate career at UBC. My thanks are also due to my supervisory committee members Dr. John Grace, Dr. Keith Mitchell and Dr. A.P. Watkinson for their help and contribution to this work.

Special thanks must go to the staff of the Mechanical Shop, Electronic Shop and Stores, and Office of the Chemical Engineering Department and UBC Libraries for all the skill, patience and kindness that made an experimental graduate research work possible.

Finally, I would like to dedicate this thesis to my family and to my first grade teacher, Mr. Hasan Mahdad.

Chapter 1

Introduction

1.1. Conversion of Methane

CH₄ is the primary constituent of both natural gas and the gas resulting from crude oil production and processing. Currently, natural gas is used mostly as a fuel in industrial and domestic applications. However, the low energy density of natural gas makes its transport from production site to the consumer difficult and expensive. Fox (1993) reported that the cost of transporting natural gas as liquefied natural gas (LNG) over a 1000 km distance can be about six times the value of the natural gas at the well. Conversion of CH₄ to higher hydrocarbons and transportable liquid fuels would make natural gas a more attractive fuel and source of chemicals.

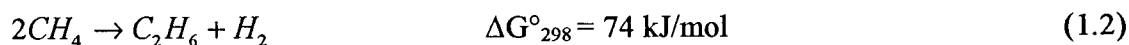
Currently, two approaches for the conversion of CH₄ to liquid hydrocarbons are practiced commercially (Anderson, 1989; Fox et al., 1990; Fox, 1993). Both begin with the production of synthesis gas from CH₄ steam reforming (reaction 1.1) which is a high temperature, endothermic and costly operation.



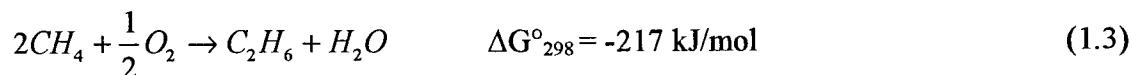
In the Fischer-Tropsch (FT) process (Anderson, 1984), the synthesis gas is converted to a range of higher hydrocarbons, including gasoline, by polymerization reactions on Fe based catalysts. In the methanol to gasoline (MTG) process (Anderson, 1989), CH₃OH is first produced from CO and H₂. The CH₃OH is subsequently dehydrated to (CH₃)₂O which is

passed over a ZSM-5 zeolite catalyst. The gasoline product is the result of a complex series of oligomerization, cracking, cyclization and aromatization reactions. The gasoline produced by either the FT or the MTG process is more expensive than gasoline obtained from crude oil. This higher production cost arises mainly from the reforming of the natural gas which accounts for more than 60% of the total cost of these processes (Poirier et al., 1991; Mc Carty, 1992; Sundset et al., 1994; Ross et al., 1996; Lange and Tijm, 1996; Rostrup-Nielsen, 1994; Lange et al., 1997; Rostrup-Nielsen et al., 1997; Vora et al., 1997). As a result, direct conversion of CH₄ to higher hydrocarbons without reforming to synthesis gas is a very attractive alternative (Fox et al., 1990).

Direct conversion of CH₄ to higher hydrocarbons is not practical under normal industrial operating conditions because of the positive Gibbs free energy change associated with reaction 1.2.



One approach to overcoming the Gibbs free energy change barrier is to add O₂ to the reaction system, producing H₂O or oxygenates instead of H₂. In oxidative coupling (OC) reactions (Amenomiya et al., 1990), CH₄ and O₂ react on an alkali metal supported on BeO, MgO and other alkaline earth oxides to give a higher hydrocarbon (e.g. C₂H₆) and H₂O:



Deep oxidation of hydrocarbons to carbon oxides (CO and CO₂) are important undesirable reactions in this route.

In the partial oxidation of CH₄ (PO) (Pitchai and Klier, 1986), CH₃OH and CH₂O are produced from O₂ plus CH₄, but this process also suffers from CO and CO₂ producing side

reactions. The product yield from both of the above routes is too low for a viable commercial operation (see Table 1.1).

In other processes, CH_4 /halogen or CH_4 / halogen/ O_2 mixtures are used (Oxyhydrohalogenation) to produce CH_3X (X is a halogen) which is then converted to higher hydrocarbons and HX or hydrolyzed to CH_3OH (Anderson, 1989). In other direct CH_4 conversion reactions, CH_4 is coupled with C_3H_6 or $\text{C}_6\text{H}_5\text{CH}_3$ to produce higher hydrocarbons (Fox, 1993). The yield from all of these processes is too low for commercial application, as shown in Table 1.1, in which the operating temperature and catalyst for these reactions are compared.

Table 1.1. Operating conditions and yield of some direct CH_4 upgrading processes.

<i>process</i>	<i>Temperature</i> °C	<i>Yield</i> %	<i>Catalyst</i>	<i>Reference</i>
OC	<800	15-25	Metal oxide	Amenomiya et al., 1990
PO	350-500	<8	MoO_3	Pitchai and Klier, 1986
Oxyhydrohalog.	100-250	<30 (based on Cl)	Pt	Fox et al., 1990
C_1 - C_3 Coupling	350	4	Ni	Ovalles et al., 1991

Another approach to overcome the Gibbs free energy change barrier of direct homologation of CH_4 (equation 1.2) in the absence of O_2 , is to perform the reaction in two steps. The temperature and pressure of each step of the cycle is chosen to overcome the

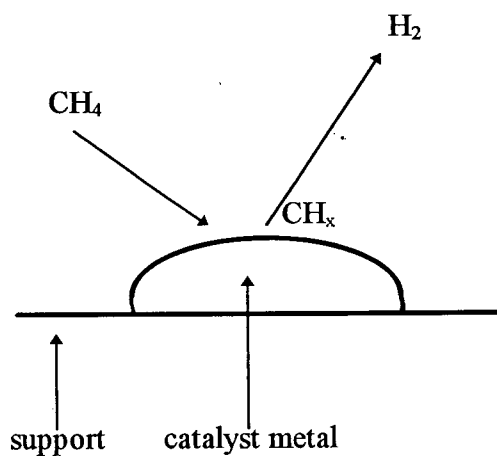
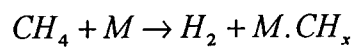
positive Gibbs free energy change of the overall reaction (Koerts and van Santen, 1991; Koerts et al. 1992; Belgued et al., 1992).

1.2. Two-Step Homologation of Methane

In the two-step homologation of CH_4 to higher hydrocarbons, CH_4 is first activated on a transition metal catalyst at high temperature and low H_2 partial pressure, generating H_2 and surface carbonaceous species. The carbon species are subsequently hydrogenated in the second step at low temperature and high H_2 partial pressure to produce CH_4 and higher hydrocarbons such as C_2H_6 and C_3H_8 , herein referred to collectively as C_{2+} products. The different temperatures and H_2 partial pressures of the two steps are necessary to overcome the positive Gibbs free energy change associated with the single-step CH_4 homologation reaction (1.2). Figure 1.1 shows a schematic illustration of the two-step CH_4 homologation cycle.

In previous studies of the two-step homologation reaction, CH_4 activation was performed over supported Group VIII metal catalysts either at high temperature ($>300^\circ\text{C}$) in a dilute stream of CH_4 (Koerts et al., 1992; Koranne et al., 1995), or with short pulses of CH_4 introduced to the feed gas (Carstens and Bell, 1996), or at temperatures below 300°C (Belgued et al., 1992). In each case, the number of moles of CH_4 converted was less than the number of moles of surface metal atoms available on the catalyst, suggesting less than a nominal monolayer coverage of the metal by the resulting CH_x species (i.e. the moles of CH_4 reacted per mole of surface metal atoms was less than one).

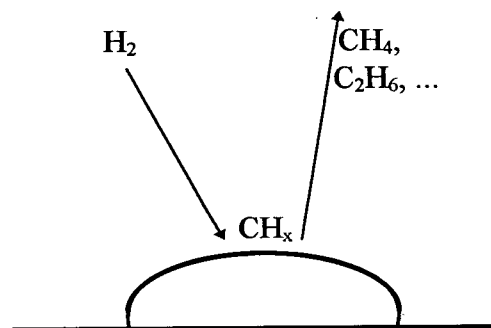
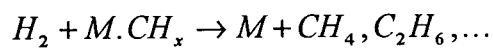
1. Activation Step⁺



High Temperature (450 °C)

Remove H₂ (low P_{H2})

2. Hydrogenation Step⁺



Low Temperature (100 °C)

Supply H₂ (high P_{H2})

Figure 1.1. Schematic representation of the two-step cycle for the homologation of CH₄.

M designates the reduced metal.

⁺ Equations are not stoichiometrically balanced.

A consequence of the low metal coverage was a low C_{2+} mole yield in the subsequent hydrogenation step since the moles of carbonaceous species available for hydrogenation were limited. In terms of moles of C_{2+} product per mole of surface metal of the catalyst, the yield reported by van Santen and coworkers (Koerts et al., 1992), Amariglio and coworkers (1994) and Koranne et al. (1995) was less than 1%.

One possible approach to increasing the yield of the two-step cycle is to increase the concentration of the carbonaceous species on the surface by reacting more CH_4 during the activation step. This may be achieved by, for example, operating with a higher concentration of CH_4 in the feed.

Despite the fact that in recent years different research groups in the Netherlands (Koerts and van Santen, 1990, 1991a, 1991b; Koerts et al., 1992a, 1992b), France (Amariglio et al., 1994; Belgued et al., 1992, 1996a, 1996b, 1996c) the United States (Koranne et al., 1995; Carstens and Bell, 1996) and Hungary (Solymosi et al., 1992; Gucczi et al., 1996b, 1997) have worked on various aspects of the two-step cycle for the homologation of CH_4 , this is a new approach in the early stages of development. Consequently, despite the contributions made in previous studies, many unanswered questions remain. In particular, the fate of the carbon deposited on the catalyst surface during the activation of CH_4 and the sequence of carbon-carbon bond formation and product generation steps, is not well understood.

Other points relevant to the two-step CH_4 homologation reaction that require further attention include the following:

1. The kinetics of CH_4 activation on supported metal catalysts are not known.

2. The properties of the carbonaceous deposits resulting from CH_4 activation and how these affect C-C bond formation need to be established.
3. The role of H_2 , as opposed to other reactants, in the second step of the two-step homologation reaction needs clarification.

The present research is motivated by the need to address these issues, as described in detail in the following section.

1.3. Motivation

With a higher concentration of CH_4 in the feed of the activation step, the rate of CH_4 activation and the fate of the generated carbon species are unknown. Previous studies of the two-step cycle, in which the coverage of the metal by carbonaceous species was nominally less than a monolayer, identified three different types of carbon species on the catalyst surface. These species were identified according to their reactivity in H_2 during temperature programmed surface reaction (TPSR). Only the most active carbon species are capable of producing C_{2+} in the second step of the two-step cycle. By exposure of the carbon species to high temperature, an “aging” phenomenon occurs in which active carbon species transform to less active species (Koerts and van Santen, 1991b; Koerts et al., 1992b). With higher concentrations of CH_4 in the feed, higher activation temperatures and with the deposition of more than a nominal monolayer of carbon species on the catalyst, the relative amount and activity of the surface carbon species needs to be determined. Also, the significance and effect of aging of the carbonaceous deposit on reactivity need to be evaluated. It is also important to

determine the operating conditions that maximize the amount of active carbon species and minimize the loss of carbon reactivity due to aging.

After CH_4 activation in the first step of the homologation cycle, an isothermal hydrogenation follows to produce C_{2+} and CH_4 . The significance of the isothermal medium and the importance of its chemical reactivity has not been addressed in previous studies (Koerts and van Santen, 1991b; Koerts et al., 1992a; Koranne et al., 1995; Belgued et al., 1996a, 1996b, 1996c; Carstens and Bell, 1996). Clarification of the role of the isothermal medium in the two-step cycle would help to identify the best isothermal gas for higher C_{2+} production. From a mechanistic point of view, it is not known at what stage of the two-step cycle C-C bond formation occurs and reaction products desorb. Clarification of this point is needed to maximize the production of C_{2+} hydrocarbons and to minimize the production of CH_4 and inactive carbon in the complete cycle.

1.4. Objectives of the Research

The present study focuses on the effect of using a higher concentration of CH_4 in the feed of the two-step cycle. The specific objectives are:

1. To prepare and characterize SiO_2 supported Co catalysts.
2. To study the kinetics of the CH_4 activation step, to develop a kinetic model for CH_4 activation and to obtain the reaction rate equations.
3. To use the kinetic model and rate equations as a quantitative tool to interpret some of the experimental observations and to quantify the effect of operating conditions on the activation step.

4. To evaluate the reactivity of the carbonaceous surface species after the activation step.

5. To determine whether the carbon combination, which generates the desired C_{2+} products, occurs in the hydrogenation step or the CH_4 activation step.

6. To clarify the significance of the chemical reactivity of the isothermal gas in the second step of the two-step cycle.

7. To determine the effect of operating variables such as activation temperature, catalyst metal loading and carbon aging on the overall performance of the two-step cycle.

Chapter 2

Literature Review

2.1. Methane Upgrading

The world supply of natural gas continues to increase as a result of the discoveries of new fields and the conservation methods being employed during gas and oil production (Vora et al., 1997). In 1992, the proven gas reserves of the world stood at 145 trillion (10^{12}) cubic meters (TCM), and annual production was 2.5 TCM, an increase of more than 60% from the 1973 production of about 1.6 TCM. The composition of natural gas varies widely but it consists predominantly of CH_4 . The heavier hydrocarbon components of natural gas are usually separated for use as fuel or as feedstocks for chemical processes.

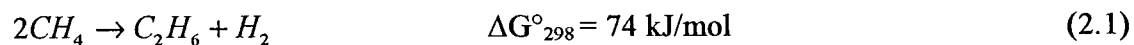
Transportation of natural gas from production site to the remote consumer is difficult and costly. An attractive solution is to convert the natural gas to higher hydrocarbons at the production site. The product liquid hydrocarbon could then be more easily transported and it would be a valuable source of chemicals and fuel in the consumer market.

Activation of CH_4 is difficult because it is a thermodynamically stable compound with very strong tetrahedral C-H bonds (bond energy of 435 kJ/mole), stronger than any C-H or C-C bond present in higher hydrocarbons. Current practice for converting natural gas to higher hydrocarbons proceeds by an indirect route in which natural gas is converted at high temperature (450-550 °C) to synthesis gas (Fox et al., 1990; Ib and Hansen, 1997).

Hydrocarbons are produced at lower temperature from exothermic synthesis gas reactions,

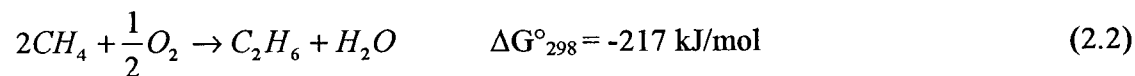
either by the Fischer-Tropsch (FT) process (Anderson, 1984), the methanol to gasoline (MTG) process (Anderson, 1989) or by the Shell middle distillate synthesis (SMDS) process (Sie et al., 1991). The gasoline produced by either of these indirect processes is more expensive than that obtained from crude oil refining. The higher production costs arise mainly from the reforming of natural gas which accounts for more than 60% of the cost of production (Poirier et al., 1991; Ross et al., 1996; Lange and Tijm, 1996; Rostrup-Nielsen, 1994)

Direct CH₄ conversions such as pyrolysis to acetylene or benzene operate at temperatures above 1000 °C and generate coke as a side product. At moderate reaction conditions, direct conversion of CH₄ to higher hydrocarbons is thermodynamically unfavorable because of the positive Gibbs free energy change of the reaction 2.1.



One approach to overcome the Gibbs free energy change barrier is to add oxygen to the reaction system and produce oxygenates or water instead of hydrogen.

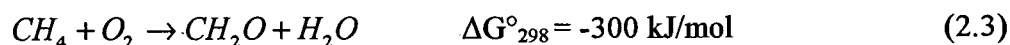
In oxidative coupling (OC) reactions (Lunsford, 1995) CH₄ and O₂ react at a temperature of about 800 °C on an alkali metal supported on BeO, MgO and other alkaline earth oxides to produce C₂H₆ and H₂O.



In OC, the role of the catalyst is to activate CH₄ by abstraction of H from CH₄ to generate a methyl radical. Subsequent coupling of the radicals yields C₂H₆. Abstracted hydrogen is removed by water formation using both oxygen from the gas phase and oxygen adsorbed on the catalyst surface.

Deep oxidation of hydrocarbons to carbon oxides is an undesirable reaction in OC which limits the C₂₊ yield to about 25%.

In partial oxidation (PO), CH₄ is partially oxidized to methanol and formaldehyde at a temperature range of 350 to 500 °C in an oxygen deficient atmosphere. MoO₃ based catalysts have been widely used for partial oxidation reactions.



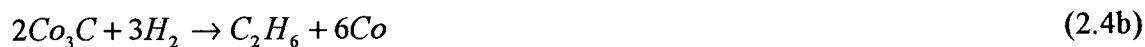
Deep oxidation of CH₄ to CO and CO₂ is also the most important drawback of this process limiting the reaction yield to less than 8%.

Reacting O₂ with CH₄ is beneficial in overcoming the Gibbs free energy change barrier of the direct homologation of CH₄, but it leads to the non-selective conversion of CH₄ to CO and CO₂. Another approach is needed to overcome the Gibbs free energy change barrier of the direct homologation of CH₄ in the absence of O₂ and to avoid deep oxidation to CO and CO₂ that occurs with OC and PO.

2.2. Homologation of Methane Using a Two-Step Cycle

In another approach to overcome the Gibbs free energy change barrier of direct homologation of CH₄ to higher hydrocarbons, the effect of temperature and pressure on the Gibbs free energy change is utilized in a two-step cycle (Guczi et al., 1996). In the first step, CH₄ is activated at high temperature on a transition metal catalyst to produce hydrogen and carbonaceous deposits on the catalyst. In the second step, the carbonaceous species are hydrogenated at a lower temperature to produce C₂₊ products.

For illustration purposes, assume that the reaction of CH₄ with a Co catalyst produces H₂ and Co₃C (eq. 2.4a) in the first step of the cycle (Koerts et al., 1992a). The Co₃C species are hydrogenated (eq. 2.4b) in the second step to produce C₂H₆. For the CH₄ activation on Co to produce Co₃C in the first step and hydrogenation of Co₃C to produce C₂H₆ in the second step, the ΔG° vs. temperature diagram is shown in Figure 2.1.



The activation of CH₄ on Co forming cobalt carbide (eq. 2.4a) is endothermic with a positive change in entropy. This reaction is only possible at temperatures above 360 °C at standard conditions. The hydrogenation of cobalt carbide to form ethane (eq. 2.4b) is exothermic with a negative change in entropy. This reaction is favorable at low temperature and can occur below 77 °C. There is no common temperature at which both reactions 2.4a and 2.4b can occur, so that the temperature gap of 283 °C is a thermodynamic stipulation to meet the condition of negative Gibbs free energy change for a favorable reaction. This temperature gap can be decreased by the partial pressure effect. The effect of pressure on the Gibbs free energy of the two steps is expressed by equations 2.5a and 2.5b.

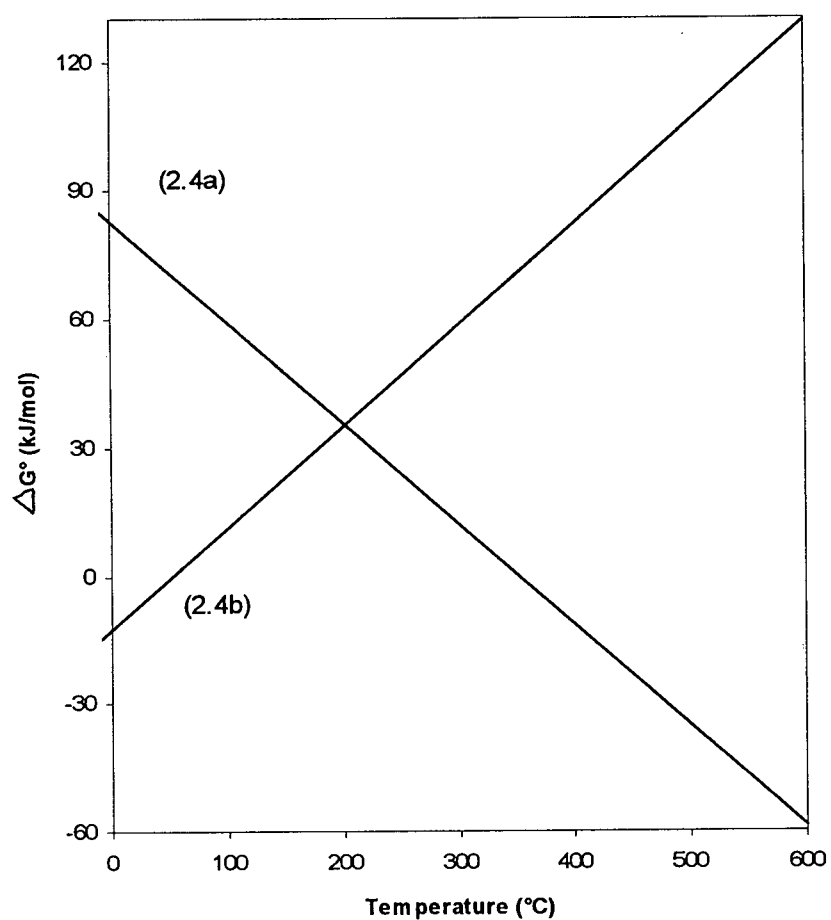


Figure 2.1. Gibbs free energy as a function of temperature for activation of CH₄ on Co

(2.4a) and hydrogenation of cobalt carbide to C₂H₆ (2.4b).



$$\left(\frac{P_{H_2}^2}{P_{CH_4}}\right)^2 = \exp\left[\frac{-\Delta G^{\circ}_{step1}}{RT}\right] \quad (2.5a)$$

$$\frac{P_{C_2H_6}}{P_{H_2}^3} = \exp\left[\frac{-\Delta G^{\circ}_{step2}}{RT}\right] \quad (2.5b)$$

Instead of using the effect of temperature, it is possible to use the effect of partial pressure to overcome the Gibbs free energy change barrier of reaction 2.4. Lower H₂ partial pressure and higher CH₄ partial pressure in the first step, by continuous removal of the H₂ produced, makes reaction 2.4a more favorable at low temperature. Low partial pressure of C₂H₆ (by removal of C₂H₆ from the system) and high partial pressure of H₂ in the second step (eq. 2.4b) utilizes the effect of pressure on Gibbs free energy change and makes an isothermal two-step cycle possible. Although reactions 2.4a, 2.4b and 2.4 are used as an example to illustrate the concept of the two-step cycle, Co₃C species are reportedly involved in the two-step cycle reactions over Co catalysts (Koerts and van Santen, 1991a; Koerts et al., 1992a).

2.2.1. Methane Homologation Using a Temperature Cycle

Van Santen and co-workers (Koerts and van Santen, 1990, 1991a, 1991b; Koerts et al., 1992a, 1992b) reported a two-step CH₄ activation and hydrogenation sequence for C₂₊ hydrocarbon formation. At a temperature between 170 and 520 °C, CH₄ was activated on reduced Group VIII metal catalysts to produce H₂ and adsorbed surface carbonaceous species. In the second step, hydrogenation of the surface species at 30-130 °C produced hydrocarbons. Among the Group VIII metal catalysts studied, they reported a maximum C₂₊ yield of 13% for a silica-supported Ru catalyst.

Van Santen and co-workers (Koerts and van Santen, 1990, 1991a, 1991b; Koerts et al., 1992a, 1992b) also studied the CH₄ activation activity of silica-supported Ru, Rh, and Co catalysts as a function of temperature. From these studies they reported the activation energy of the CH₄ activation reaction on Ru, Rh and Co as 26, 31 and 42 kJ/mole, respectively. By subsequent temperature-programmed hydrogenation of the carbonaceous deposits, three types of surface carbon species were identified (Figure 2.2). A very reactive surface carbon species C_α could be hydrogenated at ≤50 °C to CH₄ and C₂₊ hydrocarbons. Single crystal studies have identified the C_α carbon to be carbidic (Koerts and van Santen, 1992). A less reactive surface carbon species designated C_β could be hydrogenated between 100 and 300 °C. During the hydrogenation of C_β only traces of higher hydrocarbons up to hexanes were detected. The C_β species from studies of CO disproportion on Ru was identified as an amorphous carbon (Koerts et al., 1992a). At temperatures above 400 °C, the poorly reactive C_γ reacted to produce only CH₄. The C_γ type surface carbon was reportedly a graphitic phase which was probably located partially on the support (Nakamura et al., 1987; Koerts et al., 1992a).

By analyzing hydrocarbons produced by hydrogenation of surface carbon species, van Santen and co-workers (Koerts et al., 1992a) found that hydrocarbon selectivity followed a Schulz-Flory type distribution, indicating that adsorbed surface C_xH_y species can either be hydrogenated to C_xH_{2x+2} or increase in carbon number to C_{x+1}H_z species. The chain growth probability α, was reported as 0.25 for Co and Ru catalysts.

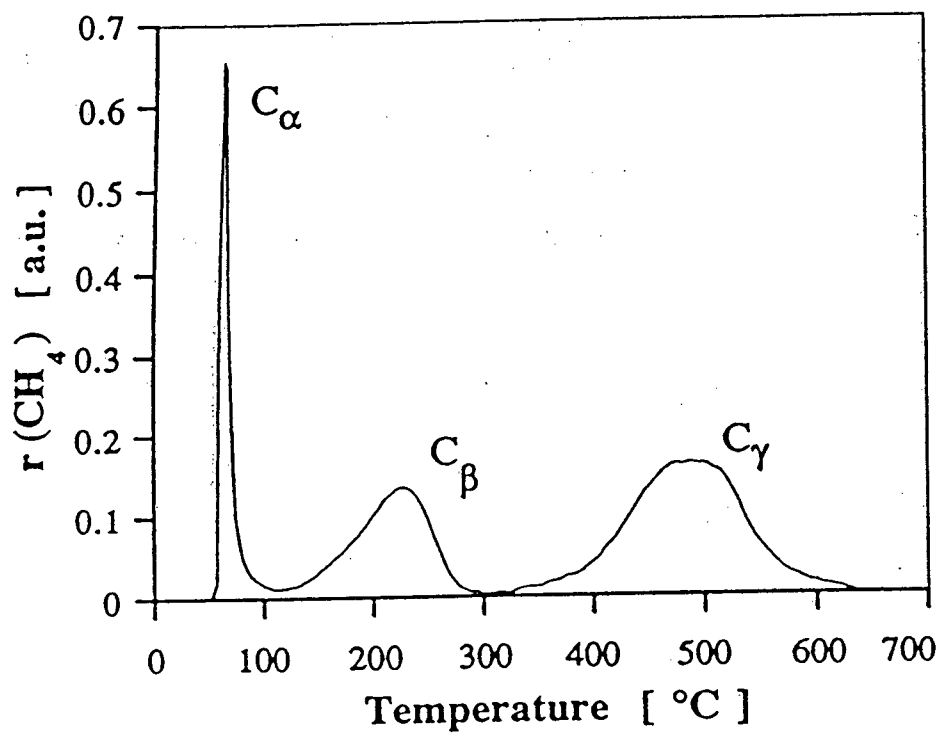


Figure 2.2. CH_4 production profile as a function of temperature in a TPSR (Koerts and van Santen, 1992).

a.u. is an arbitrary unit.

Table 2.1 shows the product selectivity of different transition metal catalysts supported on silica reported by van Santen and co-workers (Koerts et al., 1992a).

Table 2.1. Selectivity of different catalysts in two-step homologation of CH₄
(Activation at 460 °C, Hydrogenation at 95°C).

catalyst	<i>selectivity for hydrocarbons (%)</i>			
	<i>CH₄</i>	<i>C₂H₆</i>	<i>C₃H₈</i>	<i>C₄H₁₀</i>
10% Co	79.6	11.3	6.11	2.92
5% Ru	80.5	15.8	2.69	1.00
10% Ni	89.3	7.3	1.89	1.40
3% Rh	95.8	4.12	0.09	0
4% Pt	91.3	8.4	0.23	0
5% Re	98.4	1.3	0	0.29

Since only the reactive C_α type carbon has reasonable selectivities for C₂₊ hydrocarbon formation upon hydrogenation, it is desirable to maximize the amount of C_α carbon generated during CH₄ activation. Parameters that affect the amount of C_α are CH₄ deposition temperature, time, CH₄ concentration, gas velocity and aging time. It has been found that a high selectivity for reactive C_α type carbon is only obtained at low surface coverage by carbon. The selectivity of more reactive carbidic type carbon is related to the ability of the catalyst to form multiple bonded surface carbon species. It has been proposed that CH₄ is initially activated into carbidic C_α carbon and that there is an interconversion between C_α and C_β

carbon with a dynamic equilibrium of conversion of C_α to C_β (Koerts et al., 1992a) and transformation of C_β to C_α (Carstens and Bell, 1996).

Carstens and Bell (1996) studied the two-step CH_4 homologation reaction on a 2.75% Ru-SiO₂ catalyst. In this work, pulses of 10.4% CH_4/He mixture were used in the activation of CH_4 on the reduced catalyst in the temperature range of 200 to 400 °C with exposure times of less than 40 s, producing a nominal metal coverage (θ_c) of less than 80%. The results from this study showed that CH_4 underwent dissociative adsorption on Ru at temperatures above 100 °C. The pre-exponential factor for dissociative adsorption was 2×10^{-7} to $5.7 \times 10^{-7} \text{ s}^{-1}$ and the activation energy was 24.8 to 29.4 kJ/mole. Based on TPSR in H_2 , three types of carbon species were distinguished, namely C_α , C_β and C_γ carbons. The distribution among these carbon species was dependent on the total carbon coverage and the length of time that the carbon had been aged at a given temperature after deposition. For the first time in this study, the conversion of C_β to C_α and its activation energy of 92.4 kJ/mole, was reported.

In the two-step cycle using high temperature CH_4 activation in the first step and lower temperature hydrogenation in the second step, the effect of both temperature and H_2 partial pressure on the Gibbs free energy change is utilized. From a practical point of view, the temperature cycle has an undesirable energy flow. The exothermic low temperature hydrogenation step cannot provide heat for the endothermic high temperature activation step. Using a pressure cycle in which both the activation and hydrogenation steps are carried out at the same temperature does not have an unfavorable energy flow. In the pressure cycle two-step homologation of CH_4 , removal of the H_2 produced in the activation step and provision of

high partial pressure of H_2 in the hydrogenation step, provides the driving force to overcome the Gibbs free energy change barrier of direct homologation of CH_4 .

2.2.2. Methane Homologation Using a Pressure Cycle

Instead of working in a temperature cycle, Belgued and co-workers (Belgued et al., 1992; Amariglio et al., 1994; Belgued et al., 1996a, 1996b, 1996c) performed the two-step reaction isothermally in a pressure cycle. CH_4 was activated on Ru and Pt supported catalysts producing adsorbed CH_x fragments and H_2 . Subsequently, the CH_x fragments were hydrogenated in pure H_2 flow to produce C_{2+} hydrocarbons.

Belgued and co-workers (Belgued et al., 1992; Amariglio et al.; 1994) reported the production of higher hydrocarbons from CH_4 over EUROPT-1 (a standard Pt- Al_2O_3 catalyst in European catalysis laboratories) by using a two-step reaction sequence. In the first step, 100 mg of EUROPT-1 was exposed to pure CH_4 at a flow of 400 ml/min and 250 °C. They observed C_2H_6 evolution with a selectivity of 63.5%, which was equivalent to 40% of the amount of C_2H_6 formed in the reaction of $2CH_4 \rightarrow C_2H_6 + H_2$ at equilibrium. The total CH_4 conversion was 19.3% and this increased to 29% when the process was conducted at 200 °C, but the corresponding amount of higher hydrocarbons produced was lower since less CH_4 was adsorbed during the activation. The key factor of success in their experiments was the continuous removal of H_2 by the flow of CH_4 during activation.

These results were compared with those obtained on Ru and Co at low temperature (250 °C) (Belgued et al., 1992). On the basis of adsorbed CH_4 , the yields of C_{2+} hydrocarbons amounted to 19.3% on Pt at 250 °C, to 36.9% on Ru at 120 °C, but only 7.5% on Co at 270

°C. The distribution shifted toward products of higher molecular weight hydrocarbons at higher temperatures on Pt, but Co and Ru displayed an opposite trend. Strikingly, on Ru the pentanes were the most abundant products at 120 °C. The conversion of the adsorbed CH₄ and the distribution of the products were strongly influenced by the flow rate of CH₄ during the activation step. The product distribution was significantly affected by the flow of H₂, that is, at 300 °C with a H₂ flow rate of 50 ml/min, the C₂ selectivity on the Co catalyst was 85%, but at a H₂ flow rate of 300 ml/min, the C₂ selectivity decreased to 66%, but selectivity to C₃ and C₄ products increased.

Considerable improvement in selectivity was achieved in the work of Pareja et al. (1994). They established that during CH₄ adsorption on EUROPT-1, to increase the conversion of CH₄, the produced H₂ had to be removed. Therefore a hydrogen trap containing 5 wt% Pd on Al₂O₃ operating at room temperature was attached to the adsorption loop and during CH₄ activation H₂ was removed by the Pd trap. Using this device the conversion of CH₄ to higher hydrocarbons increased to about 40% at 250 °C, and the distribution of C₂₊ products shifted toward higher hydrocarbons when the exposure time increased from 3 to 16 min.

In a more recent work, Belgued and co-workers (1996a, 1996b) showed that at atmospheric pressure, CH₄ was activated on EUROPT-1 catalyst (6.3 wt% Pt-SiO₂) with parallel evolution of H₂ at temperatures above 150 °C. C₂H₆ was also produced at an order of magnitude lower rate, so that H deficient hydrocarbon fragments built up on the metal surface. Temperature programmed desorption (TPD) after CH₄ activation showed that CH₄ was desorbed in two peaks, one at about 60 °C and the other between 180 and 250 °C. TPD was

interrupted at 300 °C. During subsequent temperature programmed surface reaction with H₂, formation of CH₄ was accompanied by small amounts of C₂H₆ and traces of C₃H₈. They reported that the amount of chemisorbed CH₄ increased and the H content (i.e. the value of x) of surface CH_x species decreased when the temperature or the duration of exposure was increased. When a CH₄/Ar mixture was used instead of pure CH₄, the increase of the CH₄ content of the feed gas had an effect similar to that of an increase of either the temperature or the duration of exposure. In this study, out of 16 mmol of CH₄ fed to the reactor, only 1.8 to 12.6 μmol was reacted on the 21 μmol available Pt atoms. Hydrogenation of the adspecies formed from CH₄ chemisorption on EUROPT-1 produced a mixture of alkanes ranging from C₁ to C₈. They reported that the C₂₊ selectivity reached a maximum at a temperature of 250 to 260 °C, with a maximum C₂₊ yield occurring at about 210 °C. Increasing the duration of exposure to CH₄ in the activation step at 250 °C, increased the C₂₊ production for exposure times of less than 1 min. Exposure to static CH₄ at 250 °C resulted in negligible CH₄ activation, while increasing the flow rate to <400 ml/min increased both the CH₄ consumption and C₂₊ production. The effect of increasing CH₄ content in a CH₄/He feed in the activation step at 250 °C had a similar effect as the CH₄ flow rate. The effect of partial pressure of H₂ in the H₂/Ar mixture, which was used in the TPSR step, was also similar to the effect of flow rate in the activation step. They showed that with all other factors fixed, there existed an optimum temperature for the two-step isothermal homologation of CH₄ which resulted in maximum C₂₊ production. All the results were interpreted by assuming that C-C bond formation takes place between H-deficient CH_x fragments during the CH₄ chemisorption step. In the second step, H₂ saturates the alkane precursors and removes them from the surface.

From a conceptual point of view, the driving force for this isothermal homologation cycle in the absence of O_2 is the energy which would be required to compress the necessary quantity of H_2 from low partial pressure, at which it is produced in the first step, up to the operating pressure of the second step in order to make it able to remove alkanes from the Pt surface.

The two-step cycles used by Belgued et al. (pressure cycle) and van Santen and co-workers (temperature cycle), are similar since in both cases CH_4 forms an intermediate carbonaceous product on the catalyst which is subsequently hydrogenated to produce hydrocarbons. The main difference in the two approaches is in the hydrogen content of the carbonaceous species generated by the isothermal two-step cycle due to the lower temperature of the CH_4 activation step. Belgued argued that since C-C bond formation occurred during the activation step, a lower activation temperature decreased the possibility of hydrogenolysis reactions, leading to higher selectivity in the isothermal process.

In a similar study Belgued et al. (1996c) used a 4.7% Ru-SiO₂ catalyst instead of EUROPT-1 Pt-SiO₂ for the two-step reactions. The main contribution from this study constituted extension of the results obtained with Pt to Ru. The possibility of CH_4 adsorption at lower temperatures, no release of C_2H_6 during CH_4 adsorption, lower x value of CH_x surface fragments and stronger contribution of hydrogenolysis during the hydrogenation step were the main differences displayed by Ru.

In the pressure cycle two-step homologation of CH_4 , both the first step activation and the second step hydrogenation are performed at the same temperature of 200-300 °C. At this lower temperature of activation (compared to about 450 °C in the temperature cycle) the CH_4 activation is slow and a very small amount of carbon species is deposited on the catalyst. Low

temperature activation generates more active carbon species and more C-C bond formation occurs. The temperature of the hydrogenation step in the pressure cycle (200-300 °C) is higher than that of the temperature cycle (about 100 °C). Consequently the possibility of hydrogenolysis reactions that break the C-C bonds is higher in the pressure cycle case.

In both the temperature and pressure cycles for two-step homologation of CH₄, active carbon species are generated on the catalyst. Determination of the chemical nature of these species can enhance our understanding of the controlling mechanisms of the process.

2.3. Carbonaceous Deposits on Group VIII Metal Catalysts

In the first step of the two-step cycle, H₂ and surface carbonaceous species are produced by catalytic activation of CH₄. A temperature programmed surface reaction (TPSR) in which carbon species are removed by reaction with H₂ can differentiate the carbon species based on their reactivity with H₂. TPSR is a kinetic method of characterizing the reactivity of the deposited carbon species. The chemical nature of the deposited carbon species is often determined by surface science techniques.

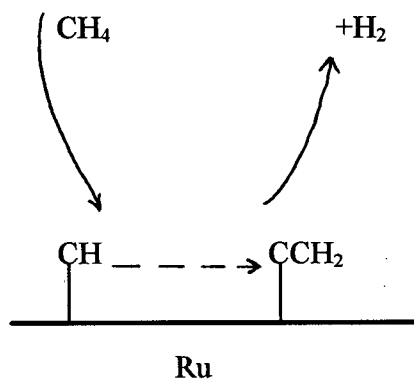
Goodman and co-workers (Lenz-Solomun et al., 1994; Wu et al. 1994) used an ultra high vacuum (UHV) system to study the surface intermediates and to elucidate the reaction mechanisms of the two-step CH₄ activation and hydrogenation reactions on single crystals of Ru. They studied C₂H₆ and C₃H₈ formation from CH₄ using combined elevated pressure kinetic measurements and surface analytical techniques. They acquired kinetic data in a combined elevated pressure reactor and UHV surface analysis chamber equipped with Auger electron spectroscopy (AES) and temperature programmed desorption (TPD). They employed

a separate UHV system containing high resolution electron energy loss spectroscopy (HREELS) and elevated pressure reactors to characterize various forms of surface hydrocarbon species from CH_4 activation reactions. Based on HREELS results of UHV experiments they identified two species, methylidyne (CH) and vinylidene (CCH_2) at temperatures between 130 and 430 °C. They identified another species, ethylidyne (CCH_3) below 130 °C.

In the elevated pressure kinetic studies, they measured turnover frequency (moles of hydrocarbon produced per mole of catalyst surface atoms per unit time) for C_2H_6 and C_3H_8 products on single crystals as a function of activation temperature. By subsequent hydrogenation at 102 °C, they detected, CH_4 , C_2H_6 , C_3H_8 and C_4H_{10} . The turnover frequencies for C_2H_6 and C_3H_8 products increased with increase in activation temperature and then decreased at temperatures exceeding 230 °C. At an activation temperature of 520 °C, C_2H_6 and C_3H_8 production was negligible.

It was observed that the surface concentration of methylidyne species first increased as activation temperature increased from 130 to 230 °C and then reached a plateau between 230 and 330 °C. At temperatures exceeding 330 °C the CH concentration decreased. The vinylidene species was found to be present in a narrow temperature range between 192 and 277 °C. From the comparison of the product turnover frequencies and the HREELS results at different temperatures, they concluded that the CCH_2 species was likely the key precursor to C_2H_6 and C_3H_8 . The possibility of methylidyne polymerization to vinylidyne intermediates and then hydrogenation to form C_2H_6 , was not rejected. Based on these findings they proposed the reaction sequence shown in Figure 2.3.

Step 1
activation (130-330 °C)



Step 2
hydrogenation (100°C)

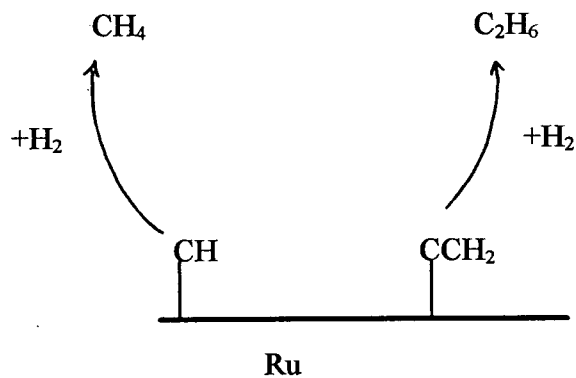


Figure 2.3. A probable reaction sequence for activation of CH_4 (step 1) and hydrogenation of surface species (step 2) proposed by Lenz-Solomun et al. (1994) and Wu et al. (1994).

In the first step of the reaction, CH_4 is activated on the surface to produce the methylidyne and vinylidene species at temperatures between 130 and 330 °C. Subsequent polymerization of the CH species to the vinylidene intermediates competes with direct hydrogenation to CH_4 . C_2H_6 is formed from the hydrogenation of vinylidene at about 100 °C.

Wu et al. (1994) compared the results of single crystal studies with the supported metal catalyst experiments of van Santen and co-workers (Koerts et al., 1992a). There was no strong one-to-one correlation between the detected surface intermediates and C_α , C_β and C_γ species that were considered to be carbidic, amorphous and graphitic carbons, respectively. However, the results from the supported catalyst experiments revealed that the C_α and C_β were associated with H. The average number of hydrogens contained in the surface carbon species following CH_4 activation was near one in the 280-530 °C activation temperature range. This result agreed with the single crystal studies in which methylidyne species were found to be dominant at activation temperatures above 270 °C. In addition, the results from the supported Ru catalysts indicated that higher hydrocarbon production was favored when the surface species were dehydrogenated. The optimum average number of hydrogens contained in the surface species was found to be near one, in agreement with single crystal studies that represented the surface species as CH and CCH_2 (Wu et al., 1994).

In an extension of the studies of CH_4 homologation on single crystal Ru, Goodman and co-workers (Koranne et al., 1995) examined the performance of supported Ru- SiO_2 catalysts. In these studies, CH_4 was activated on 3 wt% Ru- SiO_2 catalyst at temperatures between 130 and 530 °C to produce surface carbon species, followed by hydrogenation of these species to higher hydrocarbons at 95 °C. It was found that the Ru- SiO_2 supported

catalyst exhibited a trend similar to that of single crystal Ru. However, the temperature at which a maximum in C_2H_6 selectivity occurred shifted toward higher temperature.

Shen and Ichikawa (1997) used transmission IR to compare a $Co_4(Co)_{12}$ cluster catalyst with supported 10% Co-SiO₂ catalysts in the two-step homologation of CH₄. In this study, an IR wafer of $[Co_x]_{red}$ -NaY (reduced form of the $Co_4(Co)_{12}$ -NaY catalyst) was briefly exposed to a flow of 20 ml/min of 5% CH₄/He at high temperature, quickly cooled to 25 °C and then in situ IR spectra were recorded. The weak and medium bands observed at 2960, 2880, 1520 and 1393 cm⁻¹ were attributed to CH₄ dissociation products. Comparison of these IR bands with vibrational bands of hydrocarbon species suggested that the 2960 and 2880 cm⁻¹ bands were due to C-H stretching of CH and CH₂ adspecies and the 1520 and 1393 cm⁻¹ bands arose from the deformation vibrations of CH₂ adspecies. From a comparison of the band intensity due to activation in the temperature range of 200 to 400 °C, it was concluded that the dissociated fragments increased with increasing activation temperature. By admission of H₂ into the IR cell with heating, the bands of CH_x adspecies disappeared and new bands at 3024 and 1310 cm⁻¹ appeared, an indication of physisorbed CH₄. The dissociation of CD₄ studied in the same manner as CH₄ generated new bands due to CD_x adspecies. The trends of changes in band intensity observed with CD₄ were the same as with CH₄. However, with the same procedure of activation on a Co-SiO₂ catalyst, no carbon species was detected by IR.

After activation of CH₄ on $[Co_x]_{red}$ -NaY catalyst, the carbon species were treated with D₂ at 200 °C and the product distribution was analyzed by mass spectroscopy. The distribution of reaction products showed that the carbon species in the form of CH₂, CH and carbidic carbon were present on $[Co_x]_{red}$ -NaY. The same experimental method with Co-SiO₂

catalyst showed that only CH and carbidic carbon were present. The presence of CH_x on the [Co_x]_{red}-NaY catalyst was essential for production of high molecular weight products of hydrogenation of [Co_x]_{red}-NaY compared to Co-SiO₂.

2.4. Modifications of the Catalyst and Reactor for the Two-Step Cycle

The effect of various parameters of the catalyst, process and reactor configuration on the performance of the two-step cycle for CH₄ homologation, has also been studied by different research groups.

2.4.1. Effect of the Catalyst Support on the Two-Step Cycle

Solymosi and Cserenyi (1994) activated CH₄ on Ir supported on TiO₂, Al₂O₃, SiO₂, MgO and ZSM-5 and subsequently hydrogenated the produced carbon species. Ir-MgO proved to be the most effective catalyst for CH₄ activation. Ir-Al₂O₃ catalyst produced the highest C₂₊ selectivity upon hydrogenation. This study proved the significance of the support in the performance of the catalyst metal for both CH₄ activation and hydrogenation. Infra-red (IR) study of the activation of CH₄ identified CH₃ as a reaction intermediate.

In another study Solymosi et al. (1994b) used 5 wt% Pd supported on TiO₂, Al₂O₃, SiO₂ and MgO for CH₄ activation and subsequent hydrogenation of the carbon species. This study identified Pd-TiO₂ as the most effective catalyst for the CH₄ activation reaction, whereas a large amount of C₂H₆ was produced by Pd-SiO₂.

2.4.2. Effect of a Catalyst Promoter on the Two-Step Cycle

Smith and co-workers (Boskovic et al., 1996, 1997; Boskovic and Smith, 1997) studied the activation of CH_4 at 450 °C and hydrogenation of the resulting carbon species at 100 °C with subsequent TPSR characterization of the unreacted carbon species. This study reported that 10 wt% Co- Al_2O_3 catalyst was more active than Co- SiO_2 catalyst for the CH_4 activation reaction, while Co- SiO_2 proved to be more effective in the hydrogenation of carbon species to higher hydrocarbons. Addition of 1% K promoter to the Co supported on both Al_2O_3 and SiO_2 catalysts increased the CH_4 activation on both the catalysts, while Cu promoter increased the activity of Co- SiO_2 and decreased the activity of Co- Al_2O_3 . K promoter increased the C_{2+} selectivity of the Co- SiO_2 catalyst from 14% to 36%, while it had a very small effect on the selectivity of Co- Al_2O_3 catalyst. Cu promoter decreased the C_{2+} selectivity of both the catalysts. Table 2.2 summarizes the effect of K and Cu promoters on the Co- Al_2O_3 and Co- SiO_2 catalysts (Boskovic et al., 1997).

Table 2.2. Effect of K and Cu promoter on Co catalysts (Data from Boskovic et al., 1997).

<i>Catalyst</i>	Θ_c	CH_4	C_{2+}	C_{2+}
	<i>mol CH₄/mol Co</i>	<i>μmol/g cat</i>	<i>μmol/g cat</i>	<i>C atom%</i>
Co- SiO_2	1.15	7.57	0.63	14.2
K-Co- SiO_2	1.33	1.55	0.44	36.0
Cu-Co- SiO_2	1.31	3.79	0.23	10.8
Co- Al_2O_3	1.92	4.11	0.25	10.8
K-Co- Al_2O_3	2.88	3.16	0.20	11.3
Cu-Co- Al_2O_3	1.84	3.28	0.09	5.0

2.4.3. Bimetallic Catalysts for the Two-Step Cycle

Guczi et al.(1996b) reported the results of a study of CH_4 activation and coupling of CH_x species formed from CH_4 into higher hydrocarbons over NaY, Pt-NaY, Co-NaY, Co-Pt-NaY and Co-Pt- Al_2O_3 catalysts. Co-Pt-NaY and Co-Pt- Al_2O_3 showed high yields, referred to the adsorbed CH_x species, and high selectivity for the formation of C_{2+} hydrocarbons (84 and 92% respectively) at 250 °C activation and hydrogenation conditions. However, the amount of CH_x after activation was four times higher on Co-Pt-NaY than Co-Pt- Al_2O_3 . The synergistic effect was interpreted as insertion of Co into Pt inside the zeolite cages which caused a preferred coupling of CH_x versus its hydrogenation to CH_4 . Experiments carried out for the removal of CH_x species with D_2 showed that deep dissociation of CH_4 did not occur on bimetallic catalysts and weakly bound CH_x species easily participated in a chain building reaction on the surface.

Dissociative chemisorption of CH_4 over Ru, Co and Ru-Co bimetallic catalysts supported on Al_2O_3 , SiO_2 and NaY was investigated in the temperature range of 150 to 450 °C (Guczi et al., 1997). Based on this study it was reported that the amount of chemisorbed CH_4 and the evolution of H_2 during CH_4 activation increased with temperature and followed the sequence of reducibility of the supported metals and the particle size, which in turn depends on the support and the alloy formed. CH species prevailed on Al_2O_3 and SiO_2 supported catalysts while on NaY supported metals, CH_2 species were dominant when the metal particles were stabilized inside the super cage.

2.4.4. Molecular Sieve Catalysts for the Two-Step Cycle

Shen and Ichikawa (1997) compared the reduced $\text{Co}_4(\text{CO})_{12}\text{-NaY}$ and 10% Co-SiO_2 catalysts in the two-step cycle. Pulses of CH_4/He were used to activate CH_4 at 450 °C and the generated carbon species were hydrogenated in TPSR in the temperature range of 27 to 400 °C. The result of hydrogenation after 20 μmol CH_4 activation on the two catalysts in terms of product selectivity and the temperature for optimum selectivity of each product, is shown in Table 2.3 (Shen and Ichikawa, 1997).

Table 2.3. Kinetic parameters of hydrogenation step on $[\text{Co}_x]_{\text{red}}\text{-NaY}$ and Co-SiO_2 .

<i>hydrocarbon</i>	<i>$[\text{Co}_x]_{\text{red}}\text{-NaY}$</i>		<i>Co-SiO_2</i>	
	<i>optimum temp, °C</i>	<i>selectivity, %</i>	<i>optimum temp, °C</i>	<i>selectivity, %</i>
C_2	60	2.4	270	3.7
C_3	210	17.7	270	6.6
C_4	150	11.7	-	-
C_5	180	46.9	-	-

$[\text{Co}]_x\text{-NaY}$ showed a high activity in the CH_4 activation step. TPSR experiments proved that $[\text{Co}]_x\text{-NaY}$ produced higher hydrocarbons at lower temperatures compared to the Co-SiO_2 catalyst. Based on the IR studies, CH_2 species were detected on the encapsulated Co catalysts which were believed to be responsible for propagation of C-C bond formation in the $[\text{Co}]_x\text{-NaY}$ catalysts.

2.4.5. Membrane Reactors for the Two-Step Cycle

Garnier et al. (1997) used a 5% Ru-Al₂O₃ catalyst in a Pd-Ag membrane reactor for activation of CH₄ at 450 °C for a 2.4% mixture of CH₄ in a 3 min pulse. Upon hydrogenation of the carbon species to form higher hydrocarbons it was reported that the use of the Pd-Ag membrane reactor significantly enhanced the CH₄ conversion into H₂ and carbon species in the first step and the yield of hydrocarbons in the second step.

2.5. Summary

In the two-step CH₄ homologation, H₂ and carbon species are generated in the activation step. Subsequent hydrogenation of the carbon species produces CH₄ and C₂₊ hydrocarbons. Although no clear understanding of the effect of metal, support and promoter has been attained, transition metal catalysts have proved effective in the two-step cycle. In a temperature cycle two-step sequence, Co-SiO₂ catalyst has produced a high C₂₊ selectivity. Because of the small amount of carbon deposited in the activation step, a maximum C₂₊ yield per site of about 1% has been reported.

Because of better C₂₊ selectivity, Co-SiO₂ catalysts will be used in the present work. Since a temperature cycle in a flow system uses the effect of both the temperature and pressure on the Gibbs free energy, a flow system based on temperature cycle is used in this work. To increase the C₂₊ yield per site, more than a nominal monolayer of carbon will be deposited on the catalyst by a 2 min activation of 5% CH₄/Ar at 450 °C.

Chapter 3

Experimental Methods

3.1. Overview

In this chapter the details of the experimental methods used in the present study for catalyst preparation, catalyst characterization and CH₄ homologation by the two-step cycle are presented. In section 3.2 the preparation method of two different SiO₂-supported Co catalysts is discussed. The two catalysts, designated as A series Co-SiO₂ and B series Co-SiO₂, are referred to as A-X%Co-SiO₂ and B-X%Co-SiO₂, where X% is the nominal weight percent of Co in the catalyst.

In section 3.3 the experimental set-ups are discussed. Section 3.3.1 gives the details of the kinetic apparatus used for some of the catalyst characterization and all of the two-step homologation reactions. Section 3.3.2 gives the details of the diffuse reflectance infra-red Fourier transform spectrometer (DRIFTS) that was used to study the catalyst and deposited carbon species during the two-step cycle reactions.

In section 3.4 the details of the catalyst characterization methods are given. Catalysts were characterized by a sequence of temperature programmed reduction (TPR), H₂ desorption and Co re-oxidation. TPR in H₂ was used to study the reduction characteristics of the calcined Co-SiO₂ catalysts and to estimate the extent of reduction of the cobalt oxide to Co. H₂ desorption experiments were used to determine the number of surface Co atoms available for H₂ chemisorption, and this was taken as the number of active metal sites of the

catalyst. In the Co re-oxidation experiments, the amount of reduced Co atoms was determined by re-oxidation of the reduced Co catalyst. Catalyst characterization experiments by TPR, H₂ desorption and Co re-oxidation were performed using the kinetic apparatus. For further characterization of the catalysts (BET surface area, BET pore volume and powder X-ray diffraction) standard procedures were followed using commercial equipment.

The experimental methods for the two-step homologation of CH₄ are discussed in section 3.5. In a complete sequence of experiments, the reduced Co-SiO₂ catalysts were used for activation of CH₄ (section 3.5.1), isothermal hydrogenation of the deposited carbon species (section 3.5.2), temperature programmed surface reaction (section 3.5.3) and temperature programmed oxidation (section 3.5.4). The sequence of the four experiments was performed using the kinetic apparatus.

Diffuse reflectance infra-red Fourier transform spectroscopy (DRIFTS) was used to study the catalyst during the reaction cycle and to characterize the carbon species generated by activation of CH₄ on the Co-SiO₂ catalysts. The DRIFTS study experimental method is presented in section 3.6.

3.2. Catalyst Preparation

The cobalt catalysts were prepared by incipient wetness impregnation of the silica support (Silica gel, grade 62, 60-200 mesh, 15A, Aldrich 24398-1) using an aqueous solution (de-ionized water) of Co(NO₃)₂·6H₂O (98+%, Aldrich 23926-7). For catalyst series A, silica gel was used as the support following calcination in air at 500°C for 25 hours. After impregnation of the support, the catalysts were dried under 98.6 kPa vacuum for 37 hours at

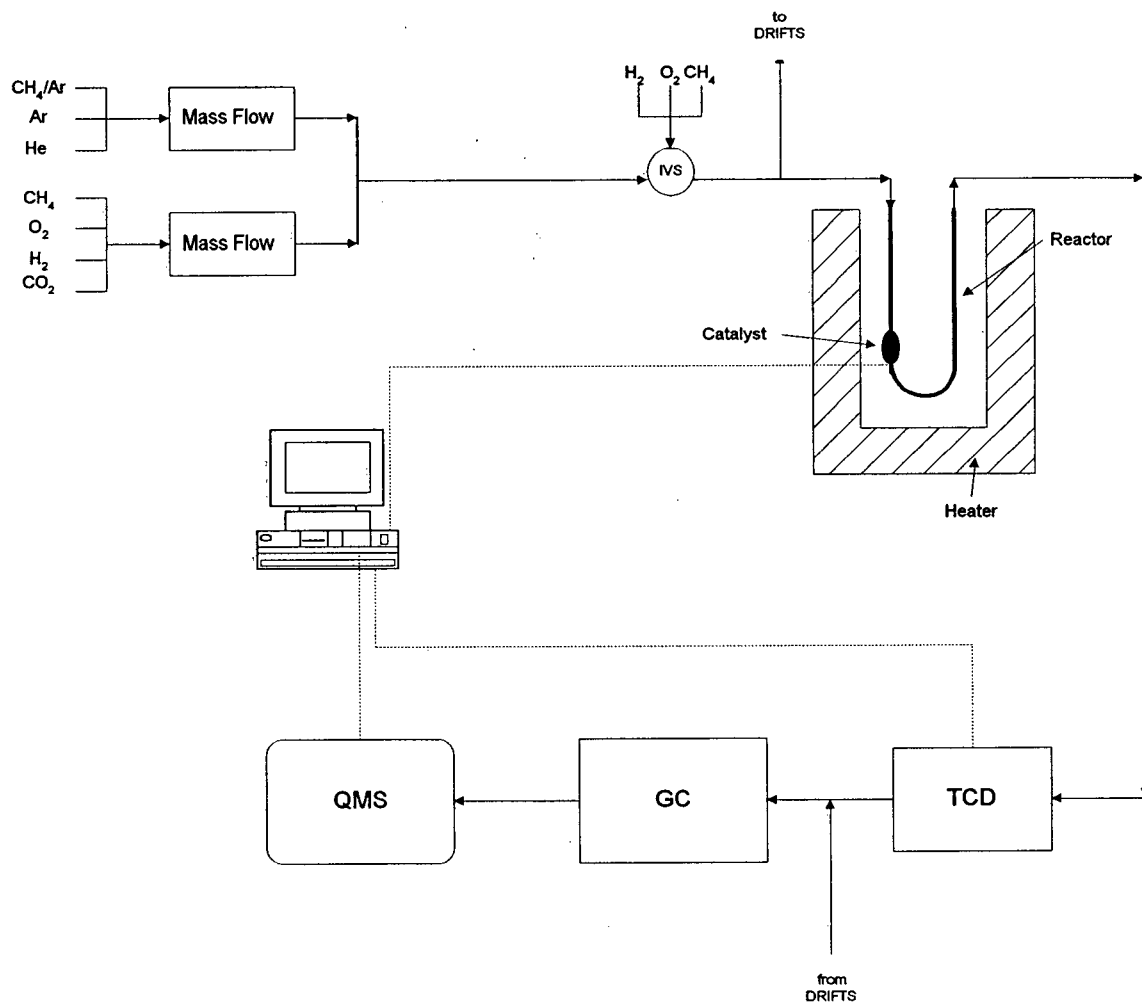
110 °C and then calcined in air for 10 minutes at 450 °C. Series B catalysts were prepared similarly except that there was no high temperature calcination step and the drying time was extended to at least 10 days in vacuum. The catalysts were reduced using the temperature-programmed reduction procedure. Similar preparation procedures using extended drying times and short calcination times have been shown to provide improved Co dispersions on SiO₂ supports (Ho et al., 1990; Coulter and Sault, 1995).

3.3. Experimental Set-Up

An experimental set up (referred to as the kinetic apparatus) was used for the two-step cycle kinetic studies and some of the catalyst characterization experiments. In addition a diffuse reflectance Fourier transform infra-red spectrometer (DRIFTS) was used to study the catalyst during the two-step cycle and to characterize the carbon species generated after activation of CH₄ on the Co-SiO₂ catalyst.

3.3.1. Kinetic Apparatus

A flow diagram of the reactor and the on-line analytical equipment used in the present study is shown in Figure 3.1. The reactor feed gas flow rate was controlled by calibrated Brooks 5878 mass flow controllers and two Whitey flow selector valves were used to introduce different gas mixtures to the reactor feed. The calibration data of the mass flow controllers are given in Appendix 1.1. 1/8" (3.2 mm) gas flow lines with Swagelok connections were used in the experimental system.



DRIFTS: diffuse reflectance Fourier transform infra-red spectrometer

GC: gas chromatograph

IVS: injection valve system

QMS: quadrupole mass spectrometer

TCD: thermal conductivity detector

Figure 3.1. Block diagram of the experimental set-up.

Air actuated valves with known-volume sample loops (0.1 and 1 ml) installed in a 5710A Hewlett Packard Gas Chromatograph were used for injection of doses of gas into the reactor feed stream (injection valve section in Figure 3.1). A connection was provided to direct the feed gas stream to the reaction cell of the DRIFTS set up. The 20 cm long fixed-bed differential micro-reactor was made from quartz glass (i.d. = 4 mm) and included an in-bed thermowell and fused silica catalyst bed support. The catalyst particles (0.074 to 0.27 mm with average size 0.17 mm) were placed on the support and held in place with glass wool. The total volume of the reactor and the tubing system between the two by-pass valves was about 5 ml. The gas flowrate and catalyst particle size were chosen to eliminate any external or internal mass transfer effects. The reactor was placed in a Hoskins cylindrical furnace and the reactor temperature was controlled by an Omega linear temperature-programmable controller. Rapid cooling of the reactor was achieved by lowering the furnace from the reactor.

Product analysis was achieved in a variety of ways, depending on the type of experiment being performed. Hydrogen consumption during catalyst reduction was determined using the thermal conductivity detector (TCD) of the 5710A Hewlett Packard Gas Chromatograph. In this case the reactor feed gas was passed through the reference side of the TCD prior to entering the reactor, while the reactor effluent was passed through the sample side of the same TCD. A Spectramass DAQ100/DXM quadrupole mass spectrometer (QMS) was used to continuously monitor the reaction products and a Varian 3400CX gas chromatograph (GC), equipped with a 10 loop Valco sampling valve, was used to calibrate the QMS and store samples during the short reaction time for subsequent analysis.

The Labtech Notebook[®] and Model PCL-718 Pc-Lab Card (Advantech) computer interface were used for data logging and recording. Reactor temperature, TCD response and QMS mass number recordings were logged by the computer. The gas analysis section could also be used to analyze the products from the FTIR reaction cell.

3.3.2. Diffuse Reflectance IR Spectroscopy

FT-IR diffuse reflectance spectroscopy (DRIFTS) was performed with a Bio-Rad FTS 175 spectrometer. The spectrometer is equipped with a tungsten-halogen infra-red source, an extended range KBr beamsplitter and a liquid nitrogen-cooled mercury-cadmium-telluride (MCT) detector. A Harrick "praying mantis" diffuse reflectance accessory and an HVC-DR3 controlled atmosphere high temperature, high pressure reaction cell were used for studying the catalyst under treatment and reaction cycle experimental conditions. A schematic diagram of the diffuse reflectance attachment and the reaction cell is shown in Figure 3.2. The reaction cell was equipped with a thermocouple and a heater which was controlled by a Watlow Series 999 control unit.

Figure 3.3 shows a schematic diagram of the DRIFTS set-up. The gas mixture from the kinetic apparatus was diverted to the DRIFTS cell with a Nupro Bellows sealed open-close valve and a Nupro control valve. A sensitive pressure gauge which was connected to the reaction cell was used to indicate the pressure and vacuum level in the reaction cell. The reaction products then passed through a 15 μ m Swagelok filter. The reaction cell could be evacuated with an Edwards 1.5 vacuum pump via a Nupro Bellows sealed open-close valve and a Nupro control valve.

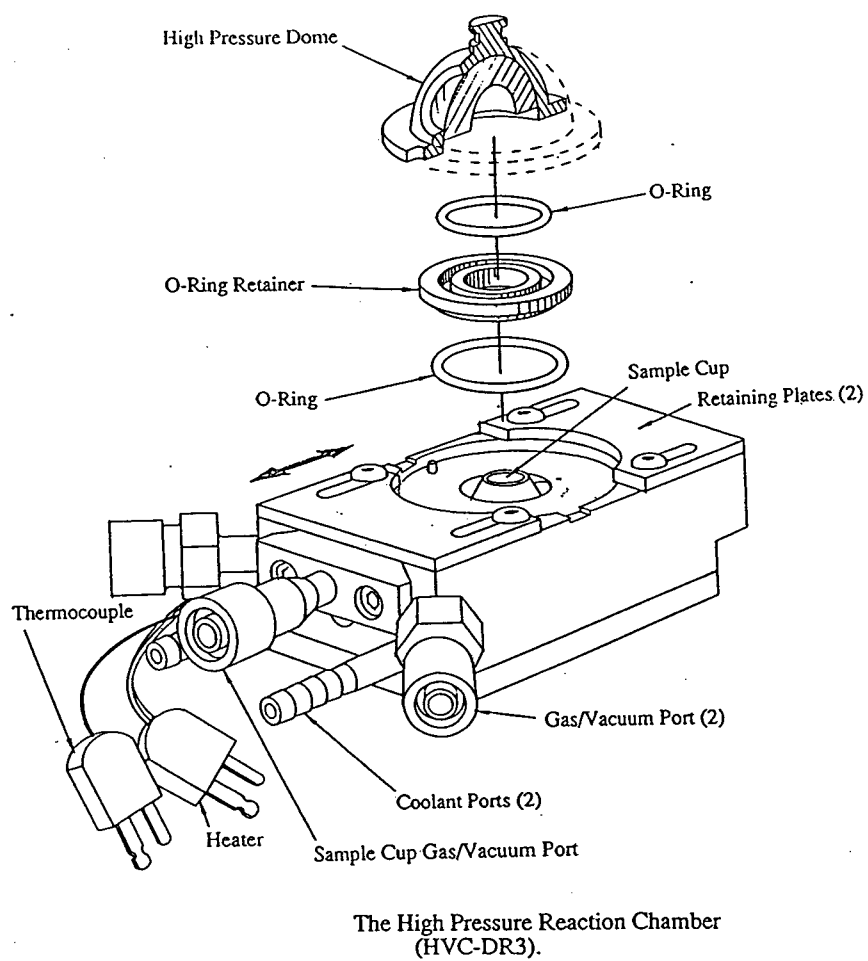
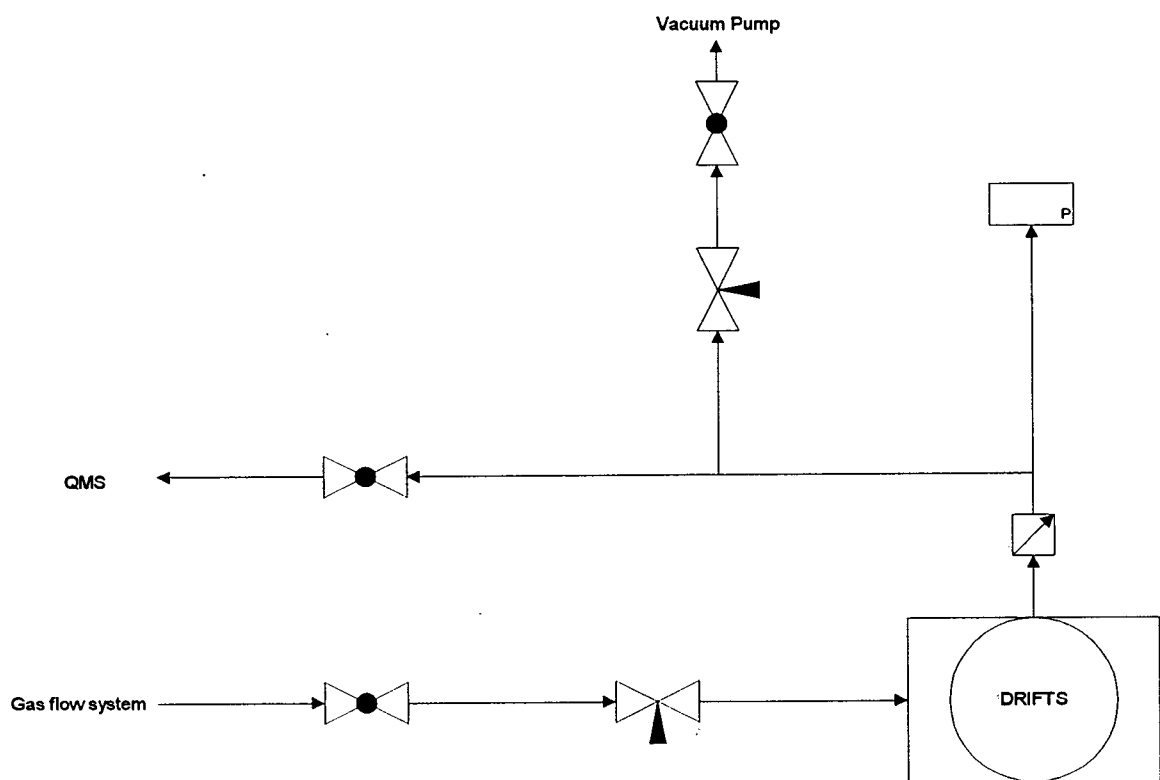


Figure 3.2. DRIFTS reaction cell.



QMS: quadrupole mass spectrometer

DRIFTS: diffuse reflectance Fourier transform infra-red spectrometer

P: pressure gauge

Figure 3.3. Block diagram of the DRIFTS reaction cell connections.

The effluent from the DRIFTS cell was connected to the GC and QMS in the analysis section of the kinetic apparatus with a Nupro Bellows sealed open-close valve.

3.4. Catalyst Characterization

To determine the turnover frequency (TOF) of a reaction on a catalyst it is essential to quantify the amount of active catalyst metal available for the reaction in a given amount of catalyst. Catalyst characterization is also important to quantify the effects of various treatments on the catalyst.

3.4.1. Temperature Programmed Reduction

Temperature programmed reduction (TPR) is used to monitor the reduction characteristics of the calcined catalysts. The shape of a TPR profile, the number of peaks, their corresponding temperature and area are useful information which can be extracted from a TPR experiment.

TPR profiles were recorded by placing 0.5 g of the calcined catalyst in the reactor and increasing the temperature from 30 °C to 450 °C at a ramp rate of 10 °C/min while flowing 60 ml/min of a 20% H₂/80% Ar feed gas mixture. UHP grade (Praxair) gases were used for the TPR experiments (without further treatment). During the TPR measurement, the effluent gas was passed through a dry ice trap prior to entering the sample side of the TCD. The TCD response, which was proportional to the H₂ consumption, was recorded by data acquisition software. The H₂ consumption profile was integrated and calibrated against the H₂ consumption of a CuO (99.9%) standard during TPR. Using the stoichiometry of reduction

of Co_3O_4 to Co (equation 3.1), the extent of reduction of the calcined catalysts could be calculated (Rosynek and Polansky, 1991).



3.4.2. H_2 Desorption

H_2 chemisorbs dissociatively on the reduced Co with a Co/H stoichiometric ratio of 1/1 (Reuel and Bartholomew, 1984). The chemisorbed H desorbs as H_2 at high temperature. Since only surface Co is available for H_2 chemisorption, the number of moles of surface Co is determined by quantifying the amount of the desorbed H_2 . Catalyst dispersion (Φ) is the ratio of the number of moles of surface Co to the total number of moles of reduced Co.

Co dispersions were measured by a H_2 desorption method. Following TPR, the catalyst was cooled to 30 °C in 20 ml/min of H_2 , and then purged with 15 ml/min of Ar at 30 °C for 30 min. The catalyst was then heated to 450 °C within 3 minutes in 15 ml/min of Ar, and the H_2 desorption was monitored with the TCD. The H_2 desorption profile was calibrated against 0.1 ml pulses of H_2 under the same flow conditions. Assuming a Co/H stoichiometric ratio of 1/1, the number of moles of surface Co atoms, and hence the catalyst dispersion, were calculated.

3.4.3. Co Re-Oxidation

The reduced Co can be oxidized with O_2 at 400 °C (Reuel and Bartholomew, 1984). By measuring the number of moles of O_2 consumed for Co oxidation, the number of moles of the reduced Co is calculated. Comparing the number of moles of the reduced Co to that of the

nominal Co loading of the catalyst, the degree of reduction of the Co catalyst after reduction in H₂ was determined.

After fast desorption of H₂, the catalyst was purged for 15 minutes at 400 °C in 15 ml/min of He. Subsequently, the extent of catalyst reduction was measured by injecting pulses of UHP grade O₂ (1 ml) into the He (UHP grade, Praxair) stream and monitoring the effluent with the TCD until no further O₂ uptake was observed. Assuming that during this process all the reduced Co was re-oxidized (equation 3.2) to Co₃O₄ at 400 °C, the degree of reduction of the catalyst was calculated.



3.4.4. Powder X-Ray Diffraction

Powder X-ray diffraction (PXRD) is a non-destructive, bulk sensitive characterization method to identify the type of crystalline phases in a catalyst and to estimate the size of the crystals.

For nominal Co loadings above 5 wt%, PXRD patterns of both the calcined and reduced catalysts were recorded with a Siemens D5000 powder diffractometer. With power settings of 40 kV and 30 mA a CuK α ($\lambda=1.5406$ Å) radiation source was used for PXRD. The powder samples were loaded into the powder sample holder without any treatment. The size of both the Co₃O₄ and Co crystallites were estimated from Scherrer's peak broadening equation:

$$t = \frac{K\lambda}{\beta \cos\theta} \quad (3.3)$$

where: $\beta = \sqrt{W^2 - w^2}$

t = Crystal size (Å)

λ = Radiation wavelength (1.5406 Å)

K = Scherrer constant (=0.9)

Θ = Peak position (radians)

W = Peak width at half height (radians)

w = Instrumental peak broadening (radians) = 0.004 radians

For the case where XRD of the reduced catalysts was not performed, the Co_3O_4 particle size was converted to the corresponding Co metal particle size using the equation $d_{\text{Co}} = 0.75d_{\text{Co}_3\text{O}_4}$, which is based on a comparison of the molar volumes of Co and Co_3O_4 (Schanke et al., 1995). Assuming cubic particles of Co on the support, catalyst dispersion (Φ) was found from the particle size (t) using the approximate equation $\Phi(\%) = \frac{1}{t(\text{nm})}$.

3.4.5. BET Surface Area

Based on physisorption of gases on porous surfaces, the BET (Brunauer-Emmett-Teller) method (Lowel, 1979; Iler, 1979) is used to determine the surface area and pore volume of the catalysts.

Brunauer-Emmett-Teller (Brunauer, et al., 1938) developed an adsorption isotherm which has been used to determine specific surface area from physisorption of gases on solid surfaces. The BET equation is of the form:

$$\frac{1}{V_a \left(\frac{P_0}{P} - 1 \right)} = \frac{1}{V_m C} + \frac{C-1}{V_m C} \frac{P}{P_0} \quad (3.4)$$

in which:

P = Adsorption pressure (Pa)

P_0 = Saturation pressure of the adsorbate at the adsorption temperature (Pa)

V_a = Volume of adsorbate gas adsorbed per gram of adsorbent solid at STP (ml/g)

V_m = Monolayer capacity of the adsorbent (ml/g)

C = Constant, depending on the temperature, adsorbate and adsorbent surface

By plotting $[V_a(P_0/P-1)]^{-1}$ versus P/P_0 a straight line is obtained with the slope of $(C-1)/(V_m C)$ and intercept of $1/(V_m C)$ from which the value of V_m can be obtained. The specific surface

area is obtained from $S_{BET} = \frac{V_m N_0 \alpha}{22414}$ in which:

S_{BET} = BET specific surface area of the adsorbent solid (m^2/g)

N_0 = Avogadro's number ($=6.02 \times 10^{23}$ molecule/mole)

α = Molecular cross section of the adsorbate gas ($\approx 0.162 \text{ nm}^2/\text{molecule of } N_2$)

Assuming that at $P/P_0=0.95$ the pores of the porous solid are filled with the liquid adsorbate, the pore volume of the porous solid (V_{BET}) can be calculated by determining the liquid volume of the corresponding adsorbed gas volume at $P/P_0=0.95$.

Assuming a cylindrical pore structure allows the average pore diameter to be estimated

by $d = 4 \frac{V_{BET}}{S_{BET}}$ in which:

V_{BET} = Pore volume (cm^3/g)

S_{BET} = BET surface area (cm^2/g)

d = Cylindrical pore diameter (cm)

BET surface area and pore volume of the support before impregnation and catalysts with different metal loadings were determined using a Micromeritics ASAP 2010 system. For each analysis about 0.2 g sample was used for N₂ adsorption at liquid nitrogen saturation temperature. The details of the experimental conditions are reported in Appendix 1.2.

3.5. Two-Step Reaction Cycles

Following TPR the reduced catalyst was used for two-step reaction cycles. In the first step of a complete cycle, CH₄ was activated on the reduced catalyst to deposit carbonaceous surface species on the catalyst. In the second step of the cycle, the carbon species were hydrogenated isothermally to produce higher hydrocarbons. Subsequently, a temperature programmed surface reaction and a temperature programmed oxidation were used to remove the unreacted carbon species from the catalyst. In all of the four steps of the complete run experiments, transport resistances and diffusion effects (mass transfer or heat transfer) were insignificant. Residence time distribution experiments showed that the flow pattern in the reactor was nearly ideal with an average residence time of about 0.1 min in the activation step and about 0.5 min in the isothermal hydrogenation, TPSR and TPO steps.

3.5.1. Methane Decomposition

Heterogeneous reaction of CH₄ on SiO₂-supported Co catalysts produces H₂ and generates carbon species on the catalyst. Activation of CH₄ on the catalyst to produce surface carbon species is the first step of the two-step CH₄ homologation cycle.

Decomposition of CH_4 on the supported Co catalysts was performed in the same quartz, fixed-bed micro-reactor, with the same amount of catalyst as was used for the TPR and H_2 desorption measurements. Following TPR, the reactor and catalyst were purged with 48 ml/min of Ar at 450 °C for 15 minutes. Once the temperature and flow had reached steady-state, the reduced catalyst was exposed to a 5% CH_4 /95% Ar gas mixture (premixed, analyzed Linde specialty gas) at a flow rate of 54 ml/min for periods of 2 to 7 minutes at 450 °C. During CH_4 activation, the reactor effluent was monitored continuously using the calibrated QMS. The catalyst was subsequently cooled to 100 °C in less than 30 s. The catalyst was then purged with 54 ml/min of Ar at 100 °C for 5 min.

3.5.2. Isothermal Hydrogenation

The second step of the two-step CH_4 homologation cycle is isothermal hydrogenation of the surface carbon species to generate C_{2+} and CH_4 .

After stabilizing the H_2 flow and QMS, the catalyst was exposed to 11 ml/min of H_2 at 100 °C for 10 min. The reaction products were monitored with the QMS and nine samples were taken with the GC multi-loop automatic sampling valve for subsequent analysis. A 5' (1.5 m) x 1/8" (3.2 mm) 60/80 Carbosive G packed column (Supelco Canada Ltd) was used for separation of CH_4 , C_2H_4 , C_2H_6 , C_3H_6 and C_3H_8 with 30 ml/min of UHP grade He carrier gas. A flame ionization detector (FID) was used for sample analysis. The GC was regularly calibrated with an analyzed calibration gas mixture (Praxair). The list of the GC control program for sampling and analysis is given in Appendix 1.3.

3.5.3. Temperature Programmed Surface Reaction

Not all the surface carbon species are active enough to react with H_2 at 100 °C during the isothermal hydrogenation. Using a temperature programmed surface reaction (TPSR) the amount and the activity of the less active carbon species are quantified. In TPSR the temperature of the reactor is increased linearly while H_2 flows through the reactor.

A TPSR in 11 ml/min of H_2 followed the isothermal hydrogenation step. For TPSR, the temperature was increased from 30 °C to 700 °C at a ramp rate of 15 °C/min and the reactor effluent was monitored with the calibrated QMS. The QMS calibration and calculation procedures are reported in Appendix 1.4.

3.5.4. Temperature Programmed Oxidation

Temperature programmed oxidation (TPO) was used to quantify the amount of any residual carbon species not removed in the TPSR. In TPO, the reactor temperature is increased linearly while O_2 flows through the reactor.

In TPO, (the last step of a complete reaction cycle) the catalyst was exposed to 11 ml/min of O_2 (UHP, Praxair) flow while the reactor temperature was increase from 40 °C to 700 °C at a ramp rate of 15 °C/min. To determine the amount of CO_2 production the reactor product was monitored with QMS.

3.6. DRIFTS Experiments

Infra-red techniques are very powerful to study the catalyst under actual reaction conditions. Unlike techniques such as X-ray photoelectron spectroscopy (XPS) and low-energy electron diffraction (LEED) spectroscopy, infra-red (IR) methods do not need an ultrahigh vacuum environment, which is an unrealistic operating condition for most catalytic reactions. Diffuse reflectance infra-red Fourier transform spectroscopy (DRIFTS) is based on the diffusely reflected radiation from the sample. Even though many strongly absorbing catalysts must be diluted with a nonabsorbing material such as KBr, the fact that pellet pressing is unnecessary for diffuse reflectance work has advantages. With DRIFTS, the catalysts are studied under more realistic reaction conditions. There is no need for difficult self-supporting disk preparation. In transmission infra-red, the KBr binder can inhibit diffusion of gases into the pellet and adsorption on the catalyst sites, whereas diffuse reflectance uses a physical mixture of catalyst and dispersant (usually KBr) in the form of a loose powder. To relate band intensity linearly to concentration in DRIFTS, the relative reflectance spectrum is converted using the Kubelca-Munk (K-M) equation (Blitz and Augustine, 1994).

$$f(R') = \frac{(1 - R')^2}{2R'} = 2.303 \frac{aC}{S}$$

where:

R' = Relative reflectance

a = Absorptivity

C = Concentration

S = Scattering coefficient

The mid-IR range ($400\text{-}4000\text{ cm}^{-1}$ wave number) DRIFTS is a useful method to monitor the changes in the reaction system during the reaction conditions close to the two-step cycle.

Passivated Co-SiO₂ catalysts were used in DRIFTS experiments. To prepare the passivated catalyst, the reduced Co-SiO₂ catalyst (reduction by TPR) was slowly oxidized in a 50 ml/min of 1.5% O₂/He flow at 30 °C for 30 min.

For DRIFTS studies about 0.08 g of a mixture of passivated 12% Co-SiO₂ catalyst and KBr was loaded into the reaction cell. Spectra were collected with respect to a KBr background. The catalyst was reduced with 10 ml/min of H₂ flow at 450 °C for 60 minutes. The reaction cell was purged with 10 ml/min of Ar and bypassed. Background spectra were recorded. 10 ml/min of a 5%CH₄/Ar was then admitted into the reaction cell at 450 °C for 7 min and spectra were recorded with respect to the dilute reduced catalyst background. The reaction cell was then evacuated for 30 min while cooling to 100 °C. 10 ml/min H₂ was admitted to the reaction cell at 100 °C and spectra were again collected. While flowing 10 ml/min H₂ through the reaction cell the temperature was increased stepwise from 100 °C to 400 °C with 100 °C increments and a temperature ramp of 100 °C/min holding at each temperature for 5 min and collecting spectra. DRIFTS data collection conditions are given in Appendix 1.5.

Chapter 4

Catalyst Characterization

4.1. Overview

Catalyst characterization is an important step in any study of catalytic reactions (Delannay, 1984; Imelik and Viedrine, 1994). By characterizing the catalyst, the physico-chemical state of the catalyst active species may be determined and changes in the state of the catalyst during various treatments can be observed. Perhaps one of the most important results from a catalyst characterization study is determination of the number of active sites exposed to the reaction medium on the surface of the catalyst. The actual nature of the active sites responsible for any particular reaction may be different for different reactions (Somorjai, 1994). In practice, for supported metal catalysts, the number of moles of the active metal on the surface of the catalyst metal crystallite is usually taken as a measure of the number of active sites. By expressing the rate of reaction in terms of the number of active sites, instead of the catalyst weight or reactor volume, a reaction frequency is obtained. The reaction frequency (moles of reactant consumed per mole of catalyst surface atoms per unit time) with the dimension of (time^{-1}) is referred to as the turnover frequency (TOF). Expressing the reaction rate in terms of TOF facilitates comparison of reaction rates reported by different research groups with different catalysts. To express the reaction rate in terms of TOF it is essential to determine the number of catalyst metal atoms on the surface of metal crystallites and hence catalyst dispersion.

In the present work different techniques were used for catalyst characterization. Surface areas and pore volumes of catalysts with different metal loadings were measured using the BET method. Powder X-ray diffraction (PXRD) was used to identify the presence of different bulk cobalt phases in the catalysts after calcination and reduction. PXRD was also used to estimate the size of the cobalt oxide particles in the calcined catalyst and Co particles in the reduced catalyst. To study the reduction behavior of the calcined catalysts and to estimate the extent of reduction of the catalyst, a temperature programmed reduction (TPR) technique was used. The number of moles of surface Co atoms and hence the catalyst metal dispersion were quantified by H₂ desorption. By re-oxidizing the reduced catalyst, the extent of reduction of catalysts was also determined.

The catalyst was also studied under reaction conditions similar to the kinetic studies using diffuse reflectance Fourier transform infra-red spectroscopy (DRIFTS) experiments. DRIFTS was also used to study the carbon species after catalyst activation.

In this chapter the findings from each characterization technique are reported and discussed. Since each characterization method provided a partial view of the catalyst properties, a conclusion section summarizes the overall catalyst characteristics.

4.2. Surface Area and Pore Volume

BET surface area, pore volume and average pore diameter of the calcined SiO₂ catalyst support and the calcined catalysts with different metal loadings were measured by the BET method using N₂ adsorption and desorption at the normal boiling point of N₂ (-196 °C).

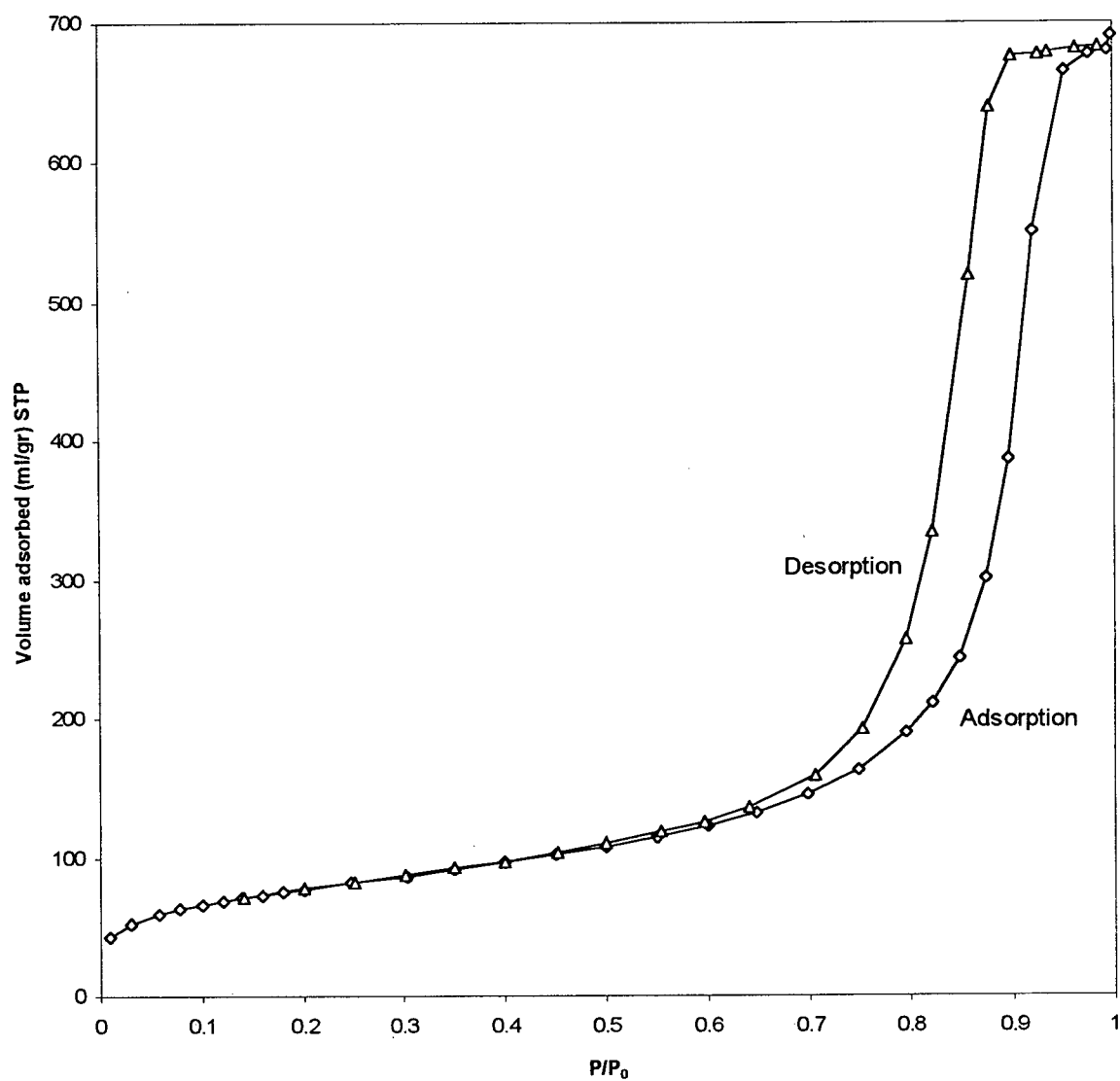


Figure 4.1. N₂ adsorption on (◊) and desorption from (Δ) SiO₂ as a function of relative pressure (P/P₀).

In Figure 4.1, the amount of adsorbed and desorbed N_2 is plotted as a function of the relative pressure (P/P_0) at N_2 normal saturation temperature of $-196\text{ }^\circ\text{C}$ measured on the SiO_2 support. N_2 adsorption and desorption curves showed that the support had a type IV isotherm with meso-pore structure (Lowell, 1979).

Figure 4.2 shows the BET surface area plot for the SiO_2 support. According to the BET method in the $P/P_0 < 0.2$ range, a plot of $[V_a(P_0/P-1)]^{-1}$ versus (P/P_0) is a straight line with slope of $(C-1)/(C.V_m)$ and intercept of $1/(C.V_m)$. The data of Figure 4.2 show a straight line. Using the slope and intercept of the best fit straight line, V_m and hence the specific surface area of the porous material were calculated. From repeat experiments, the BET surface area, pore volume and average pore diameter of the SiO_2 support were found to be $279.2 \pm 0.9\text{ m}^2/\text{g}$, $1.05 \pm 0.01\text{ ml/g}$ and $15.1 \pm 0.1\text{ nm}$, respectively. These values compare well with the technical specifications of specific surface area, pore volume and average pore diameter of $300\text{ m}^2/\text{g}$, 1.15 ml/g and 14 nm provided by the silica gel supplier (Aldrich).

Similar measurements were made on the series A Co- SiO_2 catalysts, and Table 4.1 reports their average pore diameters and pore size distributions.

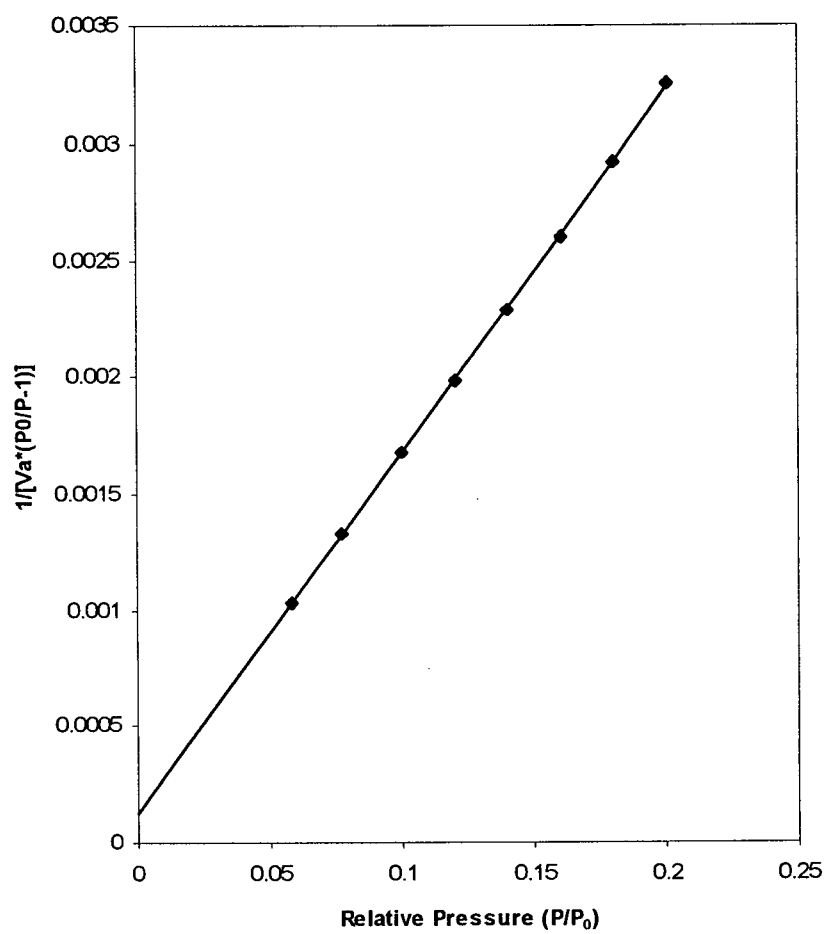


Figure 4.2. BET plot for N₂ adsorption on SiO₂.

Table 4.1. Average pore diameter and pore size distribution for the support and A series Co-SiO₂ calcined catalysts.

<i>Catalyst</i>	<i>Average Pore Dia.</i>	<i>% Area of pores in</i>		
	<i>(nm)</i>	<i>Micro</i> ¹	<i>Meso</i> ²	<i>Macro</i> ³
SiO ₂	15.1	9.0	90.9	0.1
0.6% Co-SiO ₂	14.5	11.8	88.0	0.2
2% Co-SiO ₂	14.4	12.1	87.6	0.3
5% Co-SiO ₂	14.3	12.3	87.5	0.2
12% Co-SiO ₂	14.1	12.2	87.7	0.1

¹ pores with diameter smaller than 20 Å.

² Pores with diameter in the range of 20 to 500 Å.

³ Pores with diameter larger than 500 Å.

The data of Table 4.1 showed that by increasing the metal loading of the catalyst the average pore diameter decreased. This is possibly due to partial coverage of meso-pore walls with cobalt oxide since the pore size distribution of the support and catalysts were similar except for a small decrease in the percentage of meso-pores of the catalyst.

4.3. Bulk Phase Analysis

Powder X-Ray Diffraction (PXRD) was used to determine the bulk phases and particle size of cobalt oxides in the calcined catalyst. The reduced catalysts were also examined by

PXRD to determine the presence of any cobalt oxide or cobalt silicate phase, and to estimate the reduced cobalt crystallite size.

Figure 4.3 shows the PXRD diffractogram of the calcined A series 12% Co-SiO₂ catalyst. In Table 4.2 the major peak location and relative intensity of peaks of different compounds in the Co-SiO₂ system in the 2 Θ range of 30° to 50° are reported (Data from ICDD, 1994). If one compares the peak location in Figure 4.3 with Table 4.2 it can be concluded that Co₃O₄ was the only major cobalt oxide phase present in the calcined catalyst. This is in accordance with previous characterizations of Co-SiO₂ catalysts (Khodakov et al., 1997).

Table 4.2. Peak 2 Θ location and the relative peak intensity of different phases in the Co-SiO₂ system in the 2 Θ range of 30-50° (ICDD, 1994).

<i>Crystalline phase</i>	<i>Peak 2Θ location, degrees (Peak Intensity)</i>
	<i>Degree, (%)</i>
Co	47.6 (100), 44.8 (60), 41.7 (20)
CoO	42.4 (100), 36.5 (67)
Co ₃ O ₄	36.9 (100), 31.3 (34), 44.8 (19)
Co ₂ O ₃	31.2 (100), 38.6 (100)
γ - Co ₂ SiO ₄	36.6 (100), 44.5 (43), 48.8 (10)
β - Co ₂ SiO ₄	36.5 (100), 44.5 (79), 33.9 (68), 33.1 (57)
Co ₂ SiO ₄	36.9 (100), 44.5 (44), 38.3 (13)
Co(NO ₃) ₂	40.5 (45), 42.2 (40), 29.5 (35)

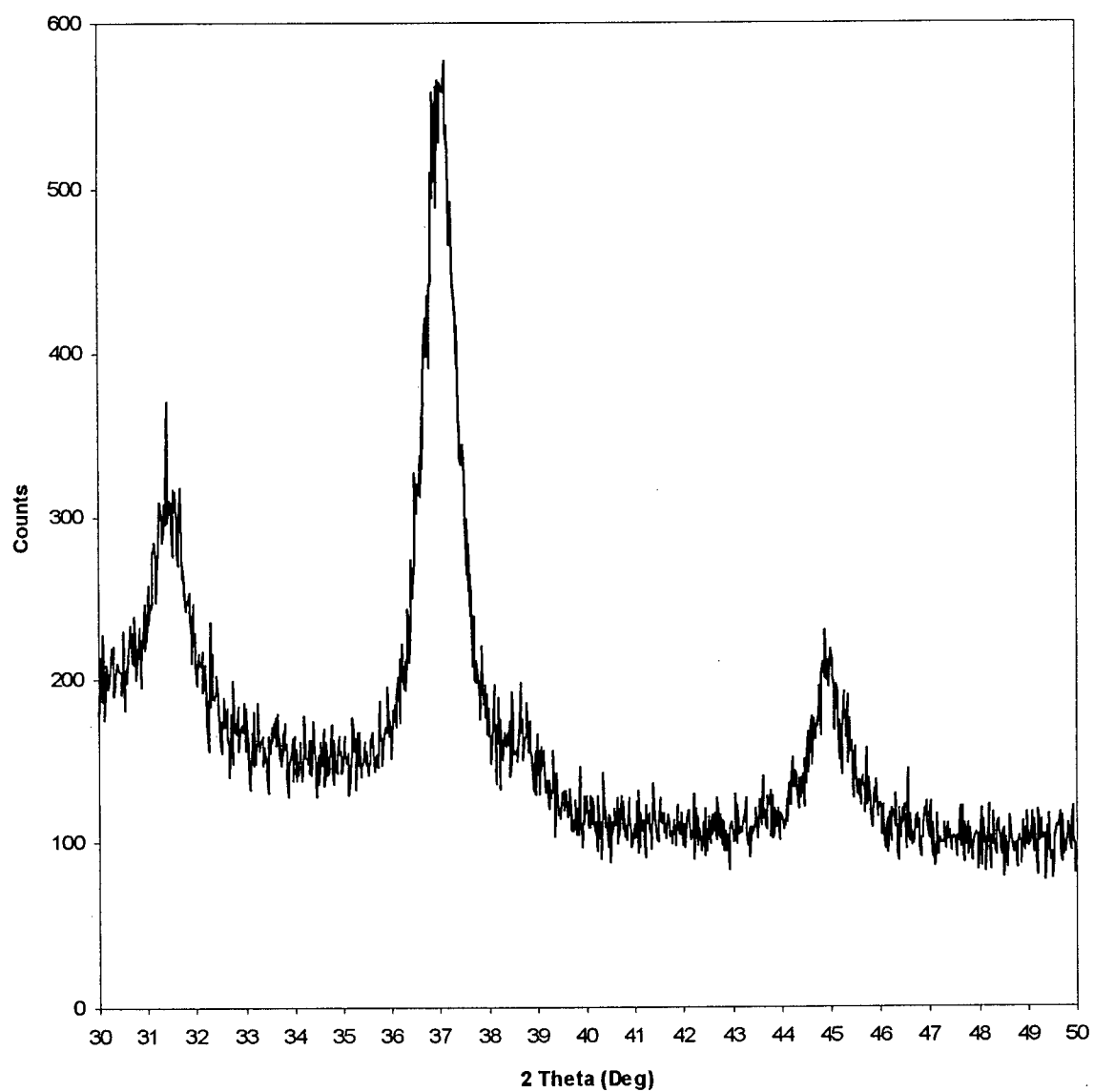


Figure 4.3. PXRD diffractogram of the calcined A series 12%Co-SiO₂ catalyst.

PXRD patterns of the reduced catalysts showed only metallic Co, indicating reduction of Co_3O_4 to Co. The absence of bulk cobalt oxide or cobalt silicate compounds does not completely exclude the possibility of their presence. As discussed in later sections of this chapter (Section 4.3, 4.4 and 4.5), other characterization techniques such as TPR, H_2 desorption and Co re-oxidation showed that not all the cobalt oxide of the calcined catalyst was reduced by TPR. Reports in the literature (Ming and Baker, 1995; van Steen et al., 1996) indicate that for Co- SiO_2 catalysts, unreduced cobalt silicate compounds existed after reduction under the same conditions as used in this work. Since PXRD is a bulk sensitive technique for catalyst characterization, it cannot detect amorphous phases and its detection limit of crystalline phases is about 3 wt% (Wachs, 1992). Because of the limitations of PXRD, the presence of cobalt silicates or other metal-support interaction products cannot be ruled out.

Using the line broadening equation (see Section 3.3.4), the crystallite particle size of Co_3O_4 and Co particles in the calcined and reduced catalysts, and hence percent dispersion of the Co, was estimated. Comparison of the Co dispersion calculated by PXRD line broadening of the Co_3O_4 in the calcined catalyst and Co in the reduced catalyst, showed that there was very good agreement between the two methods of measurement. For example, for B series 8% Co- SiO_2 catalyst, Co dispersion based on PXRD of the reduced catalyst was $7.3 \pm 1.0\%$, while Co dispersion based on the PXRD of the calcined catalyst was $8.8 \pm 1.0\%$. In Table 4.3 the catalyst Co dispersion, Φ (the ratio of the number of moles of surface Co atoms to the total number of moles of reduced Co in the catalyst) based on PXRD line broadening of Co_3O_4 is reported for the A and B series Co- SiO_2 catalysts.

Because of the detection limitation of the PXRD the 2% and 0.6% catalysts were not characterized by PXRD.

Table 4.3. Co dispersion based on the PXRD of the calcined catalysts.

<i>Catalyst</i>	<i>Co Dispersion(Φ)</i> (%)
A-12% Co-SiO ₂	10.0
A-5% Co-SiO ₂	11.0
B-8% Co-SiO ₂	8.8

4.4. Reduction Properties of Calcined Co-SiO₂ Catalysts

In temperature programmed reduction (TPR), the temperature of the catalyst is increased in a dilute H₂ flow and the H₂ consumption is recorded by a thermal conductivity detector (TCD) of a gas chromatograph (GC). TPR is a very useful technique in determining the operating conditions for catalyst reduction, the reduction behavior and the extent of reduction of a catalyst.

In the present work, TPR was used to study the reduction characteristics of the calcined Co-SiO₂ catalyst precursor. Figure 4.4 shows the TPR profile of the calcined A series 12% Co-SiO₂ catalyst. TPR profiles of the rest of A series catalysts are provided in Appendix 2.1.

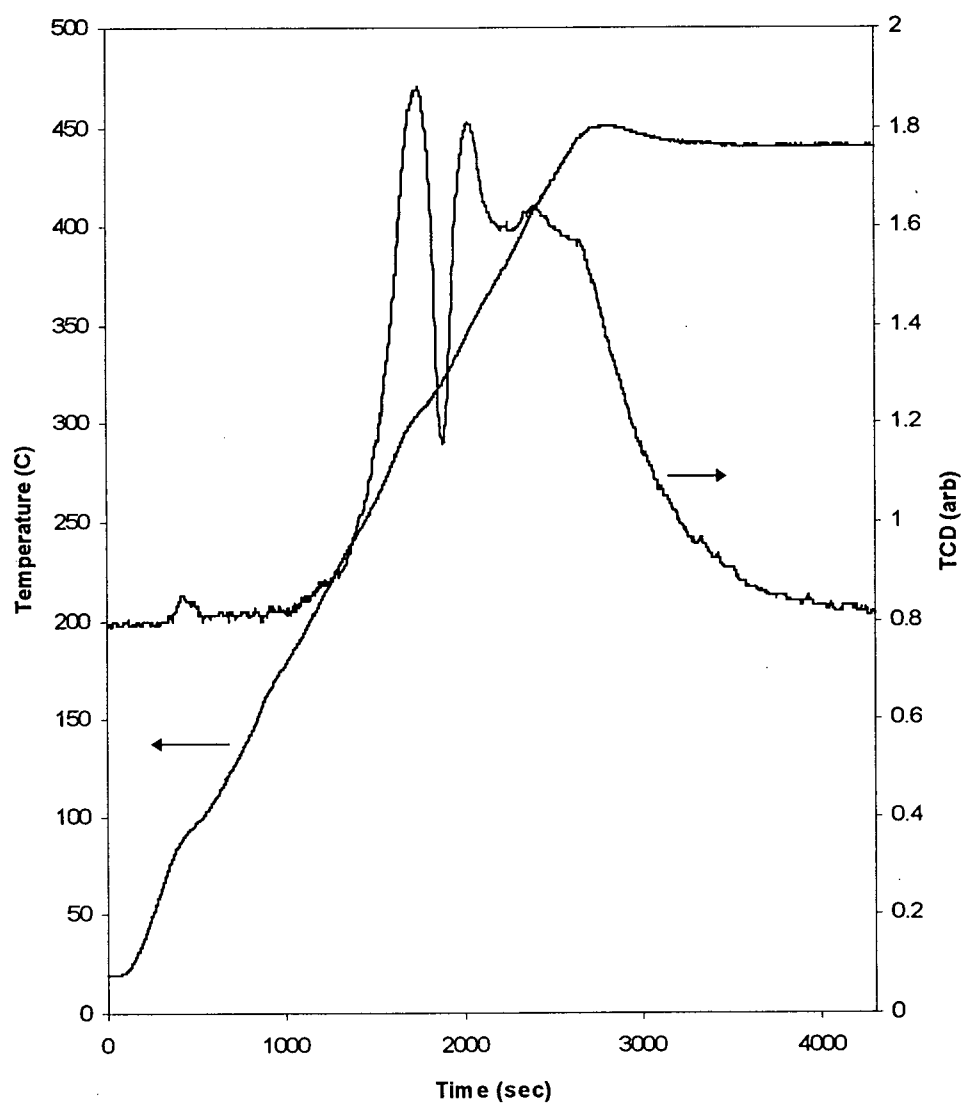


Figure 4.4. Profile of the temperature programmed reduction (TPR) of the A series 12%Co-SiO₂ catalyst with 54 ml/min of 20%H₂/Ar gas mixture.

The two H_2 consumption peaks of the TPR profile were due to the two-step reduction of Co_3O_4 according to the stoichiometry $Co_3O_4 + H_2 \rightarrow 3CoO + H_2O$ occurring at about 250 °C and $CoO + H_2 \rightarrow Co + H_2O$ which occurs at about 400 °C. The higher temperature reduction peak is an indication of a more difficult to reduce cobalt oxide (Lapidus et al., 1991).

Given the overall stoichiometry of reduction of Co_3O_4 to metallic Co $Co_3O_4 + 4H_2 \rightarrow 3Co + 4H_2O$ the total peak area of the TPR profile was used to quantify the extent of reduction of the calcined catalysts. The extent of reduction of the catalysts determined from TPR are reported in Table 4.4. Data in Table 4.4 showed that the reduction of Co-SiO₂ catalysts was not complete in the TPR. Incomplete reduction of the Co_3O_4 to Co is attributed to a metal-support interaction (MSI) and formation of cobalt silicates that are only reducible at temperatures higher than the maximum TPR temperature. (Rathousky et al., 1991; Jabionski et al., 1995; Rosynek and Polansky, 1991)

Although TPR is a powerful technique to determine the reduction behavior of the catalyst precursor, it provides only an approximate value for the degree of reduction. The fact that the TCD response is used for peak area calculations imposes some limitations on the accuracy of the calculation of H_2 consumption. The TCD detects only the difference between the thermal conductivity of the reactor feed and product streams. As a result, any change in gas composition due to liberation of non-condensable gases from the catalyst (e.g. due to the incomplete decomposition of nitrates in the calcination step), or H_2 uptake due to hydrogen spillover, or possible reduction of some support material, can have positive or negative effect on the peak area. In addition, the accuracy of the TPR is limited by the nonlinear response of

the TCD. The above errors become more significant at lower metal loadings. Because of these limitations the extent of reduction of the 0.6% Co-SiO₂ catalyst is clearly in error.

Table 4.4. Extent of reduction of Co catalysts based on TPR.

<i>Catalyst</i>	<i>Extent of Reduction</i> (%)
A-12% Co-SiO ₂	91
A-5% Co-SiO ₂	84
A-2% Co-SiO ₂	90
A-0.6% Co-SiO ₂	>100 ⁺
B-8% Co-SiO ₂	79

⁺ The calculated value was 105.

Nonetheless TPR is a valuable method for the preliminary study of catalyst reduction behavior and optimization of the reduction conditions. In the present work, TPR profiles were used primarily to quantitatively monitor the catalyst reduction behavior. Re-oxidation of the reduced catalysts at high temperature proved to be a more reliable method to quantify the extent of reduction of the catalysts.

4.5. H₂ Chemisorption on Co-SiO₂ Catalysts

In the temperature range 25 °C to 100 °C, hydrogen chemisorbs dissociatively on reduced Co with a H/Co stoichiometry of 1/1 (Reuel and Bartholomew, 1984). At high temperature, the chemisorbed H atoms combine and desorb as H₂. In the present study, the H₂

desorption technique was used to quantify the number of moles of surface Co atoms present in the reduced Co-SiO₂ catalysts. Based on the amount of H₂ desorbed from a known amount of catalyst, catalyst dispersion Φ was calculated. Catalyst dispersion (Φ) is the ratio of the number of moles of surface Co atoms to the total number of moles of reduced Co in the catalyst. The latter quantity was obtained from the re-oxidation of the reduced catalyst to be described in Section 4.5.

Figure 4.5 shows a typical H₂ desorption profile for the A series 12% Co-SiO₂ catalyst. The profile of temperature rise and the TCD response due to H₂ desorption are plotted as a function of time. The amount of desorbed H₂ was determined by comparing the H₂ desorption peak area with that of H₂ calibration peaks. In Table 4.5 the amount of desorbed H₂ and number of moles of surface Co for the catalysts of the present study are reported. From repeat experiments, the experimental error was established at less than $\pm 10\%$ of the reported values.

Previous experiments (not reported here) showed that the SiO₂ support did not chemisorb H₂. Hence the amount of desorbed H₂ reported in Table 4.5 was assumed to be chemisorbed on the surface Co atoms alone. Lower metal loading catalyst have less reduced Co content for H₂ chemisorption. Using the amount of desorbed H₂, the amount of surface Co atoms in the catalyst was determined.

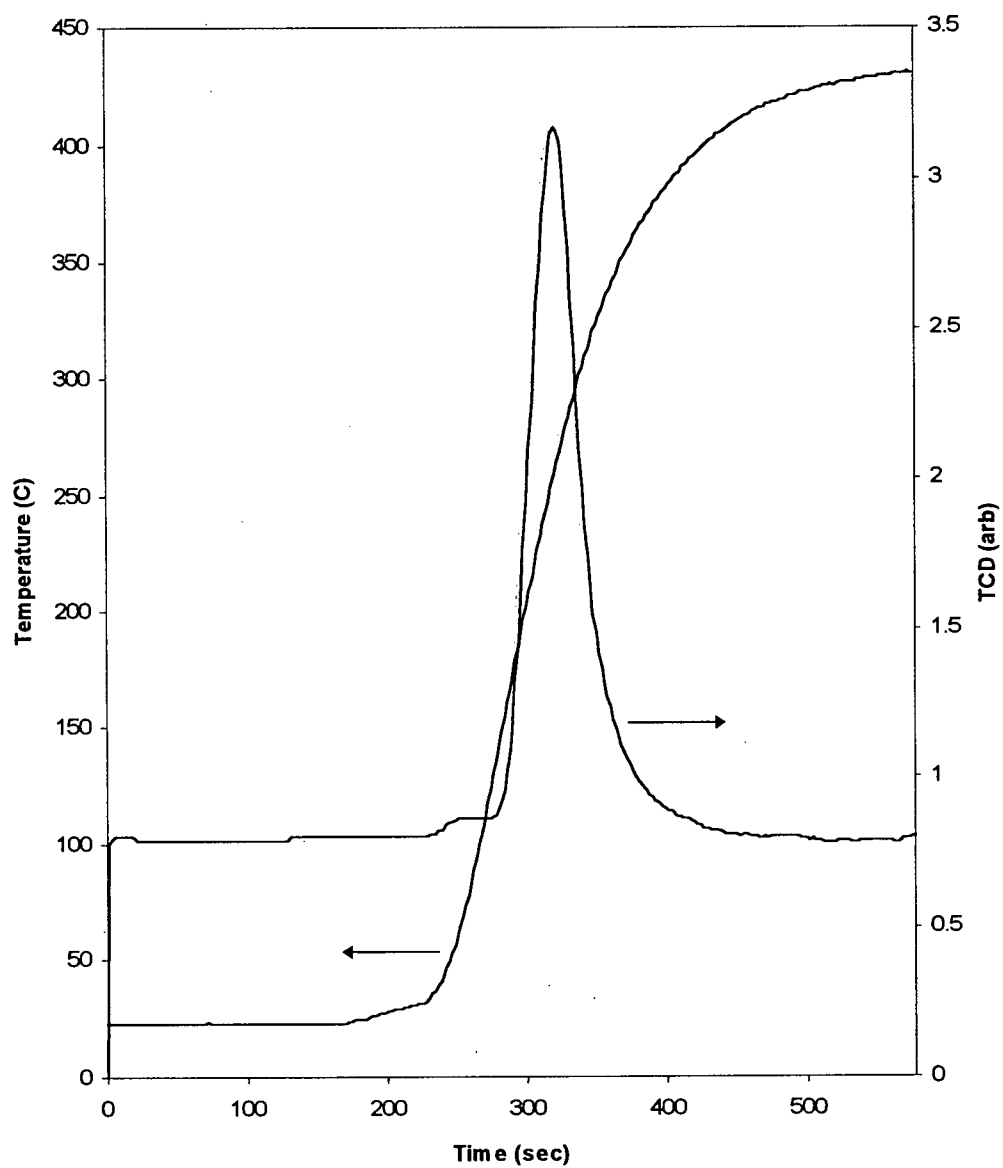


Figure 4.5. Profile of temperature and H₂ desorption from A series 12%Co-SiO₂ catalyst in 15 ml/min of Ar flow.

Table 4.5. Moles of chemisorbed H₂ and surface Co in Co-SiO₂ catalysts.

<i>Catalyst</i>	<i>Chemisorbed H₂</i> <i>μmol/g</i>	<i>Surface Co</i> <i>μmol/g</i>
A-12% Co-SiO ₂	49	98
A-5% Co-SiO ₂	17	33
A-2% Co-SiO ₂	4	8
A-0.6% Co-SiO ₂	2	4
B-8% Co-SiO ₂	24	49

4.6. Extent of Catalyst Reduction

PXRD showed that oxidation of the reduced catalyst at high temperature caused Co to be oxidized to Co₃O₄. To quantify the extent of reduction of the Co-SiO₂ catalysts, the re-oxidation of Co to Co₃O₄ ($3Co + 2O_2 \rightarrow Co_3O_4$) was used. In the present work, the reduced catalyst was oxidized to Co₃O₄ at 400 °C with pulses of O₂ in He flow. Using calibration peaks of O₂ at the same flow conditions, the total O₂ consumption was calculated. Given the oxidation stoichiometry, the amount of the reduced Co and hence the extent of reduction of the initial Co₃O₄, was quantified.

Figure 4.6 shows the re-oxidation profile of the reduced A series 12%Co-SiO₂ catalyst at 400 °C. In Figure 4.6 each arrow corresponds to one pulse of O₂ injection. O₂ injected by the first five pulses was completely consumed by the reduced Co catalyst. A portion of the

sixth pulse completed re-oxidation of the reduced Co. Due to completion of the Co re-oxidation reaction, O₂ consumption from the last two pulses was negligible. Extent of reduction calculated from Co oxidation does not have the limitations of the TPR technique discussed in Section 4.3. High temperature oxidation ensures a fast and complete oxidation of all the reduced Co to Co₃O₄. PXRD characterization of the catalysts after Co oxidation confirmed that Co₃O₄ was the only detectable phase in the catalyst.

In Table 4.6 the extent of reduction of the catalysts, based on Co oxidation, is reported. The trend of extent of reduction of the cobalt oxides with change in catalyst metal loading shows that by decreasing the metal loading, the extent of reduction decreased. This result is an indication of the presence of strong metal support interactions on low metal loading catalysts. Most probably with low metal loading catalysts, the size of catalyst precursor particles before calcination is smaller and the relative particle-support interface is larger. Under the high temperature calcination conditions the low loading catalysts generate more cobalt silicate compounds (Rosynek and Polansky, 1991; Coulter and Sault, 1995). Cobalt silicates are non-reducible under the reduction conditions of this work. Consequently the low loading catalysts have lower extents of reduction.

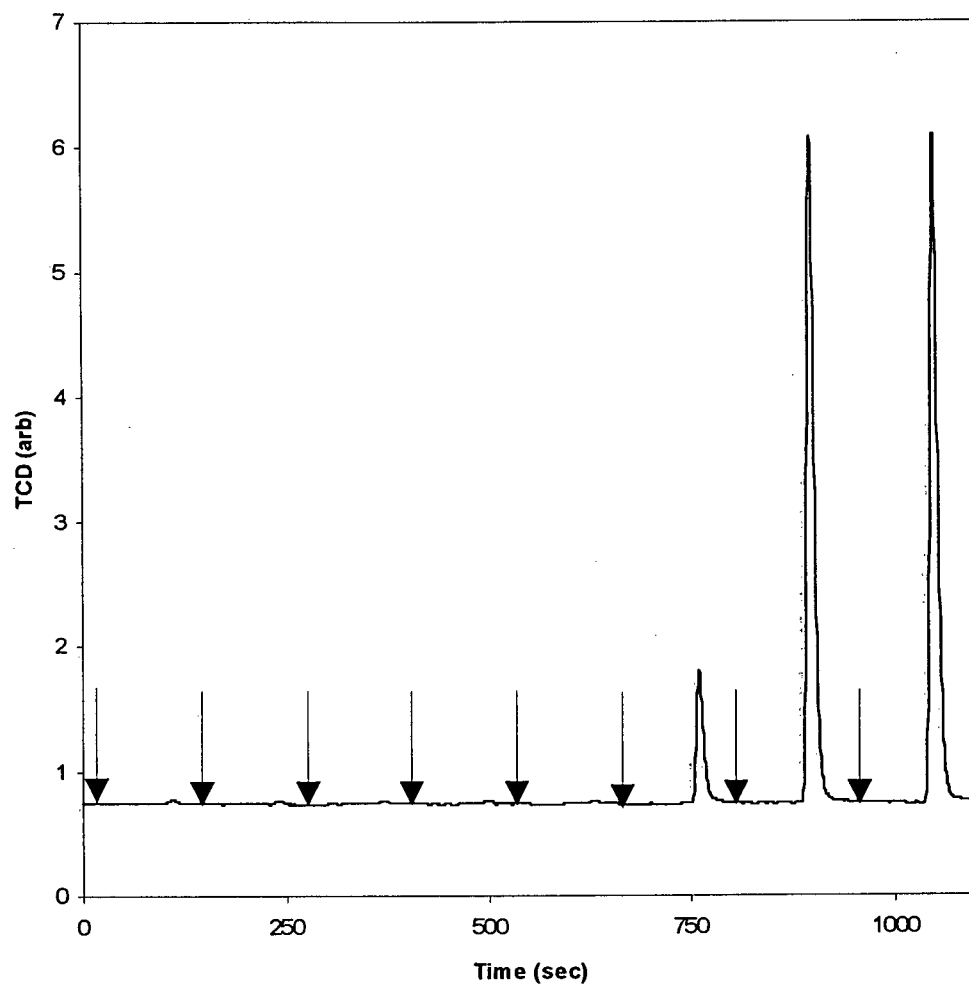


Figure 4.6. O₂ uptake profile from pulses of 1.0 ml O₂ in 15 ml/min of He flow by the reduced A series 12%Co-SiO₂ catalyst during the Co oxidation step. (Arrows indicate injection of an O₂ pulse.)

Table 4.6. Extent of reduction of Co catalyst based on re-oxidation of the reduced Co.

<i>Catalyst</i>	<i>Extent of Reduction</i> (%)
A-12% Co-SiO ₂	85
A-5% Co-SiO ₂	76
A-2% Co-SiO ₂	42
A-0.6% Co-SiO ₂	26

4.7. DRIFTS Study

Diffuse reflectance infra-red Fourier transform spectroscopy (DRIFTS) was used to characterize the catalyst in a cycle of two-step reaction under very similar operating conditions to the actual kinetic studies. Figure 4.7 shows the DRIFTS spectrum of a 16 wt% mixture of passivated A series 12% Co-SiO₂ catalyst and KBr with respect to pure KBr powder background at 50 °C. Absorption bands due to Si-O-Si bonds below 1100 cm⁻¹ and OH vibrations above 3500 cm⁻¹ due to isolated, paired and hydrogen-bonded hydroxyl groups, were observed (Unger, 1979; Iler, 1979).

To detect very small changes in the catalyst structure, the reduced catalyst/KBr mixture was used as a background to study the effect of activation and hydrogenation conditions on the catalyst. CH₄ was activated on the reduced catalyst at 450 °C for 7 min. The reaction cell was then closed and evacuated while cooling to 100 °C. H₂ was then admitted

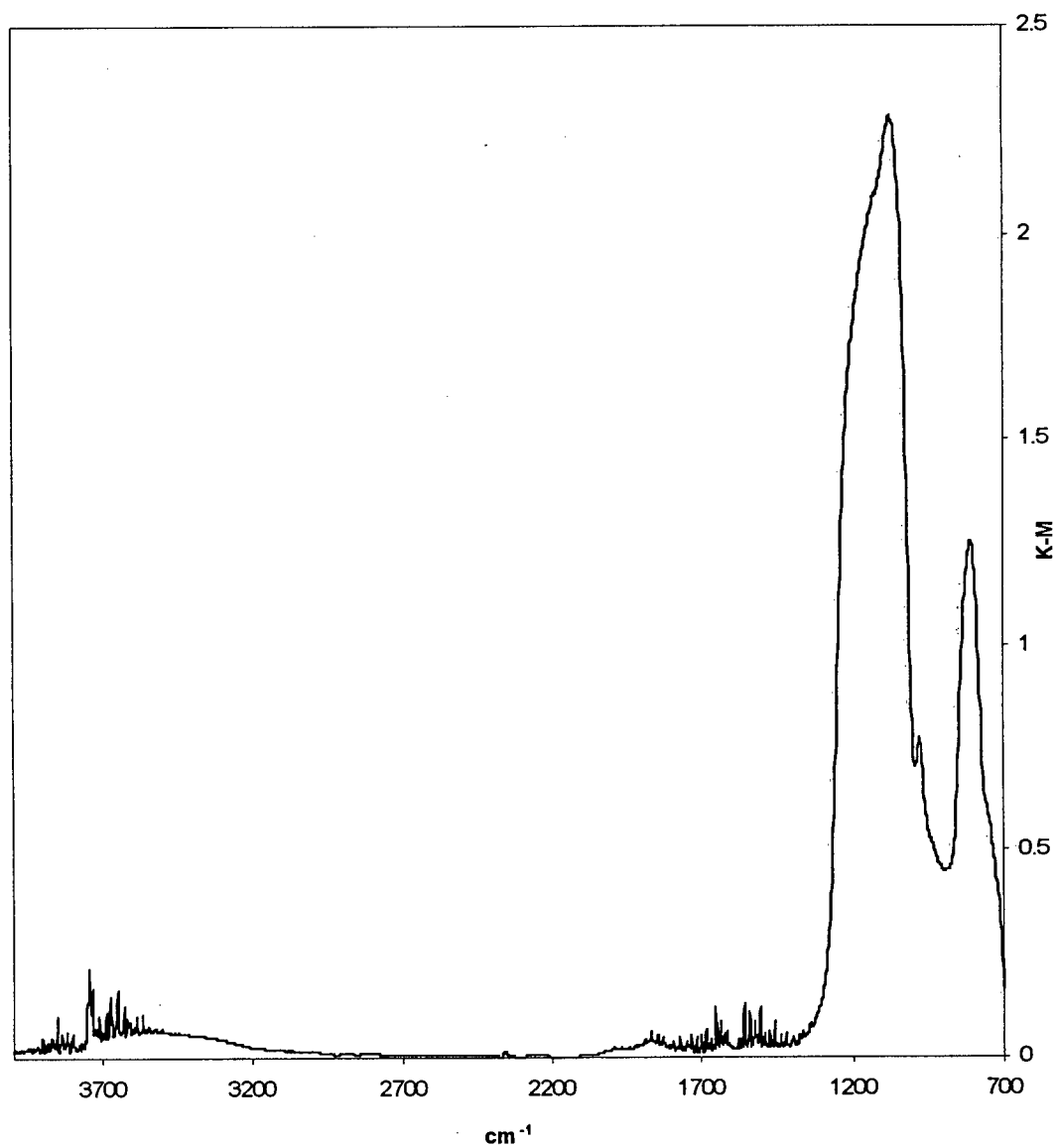


Figure 4.7. Diffuse reflectance infra-red Fourier transform spectrum of the dilute passivated A series 12%Co-SiO₂ catalyst, with respect to pure KBr background.
(K-M is the Kubelca-Munk unit.)

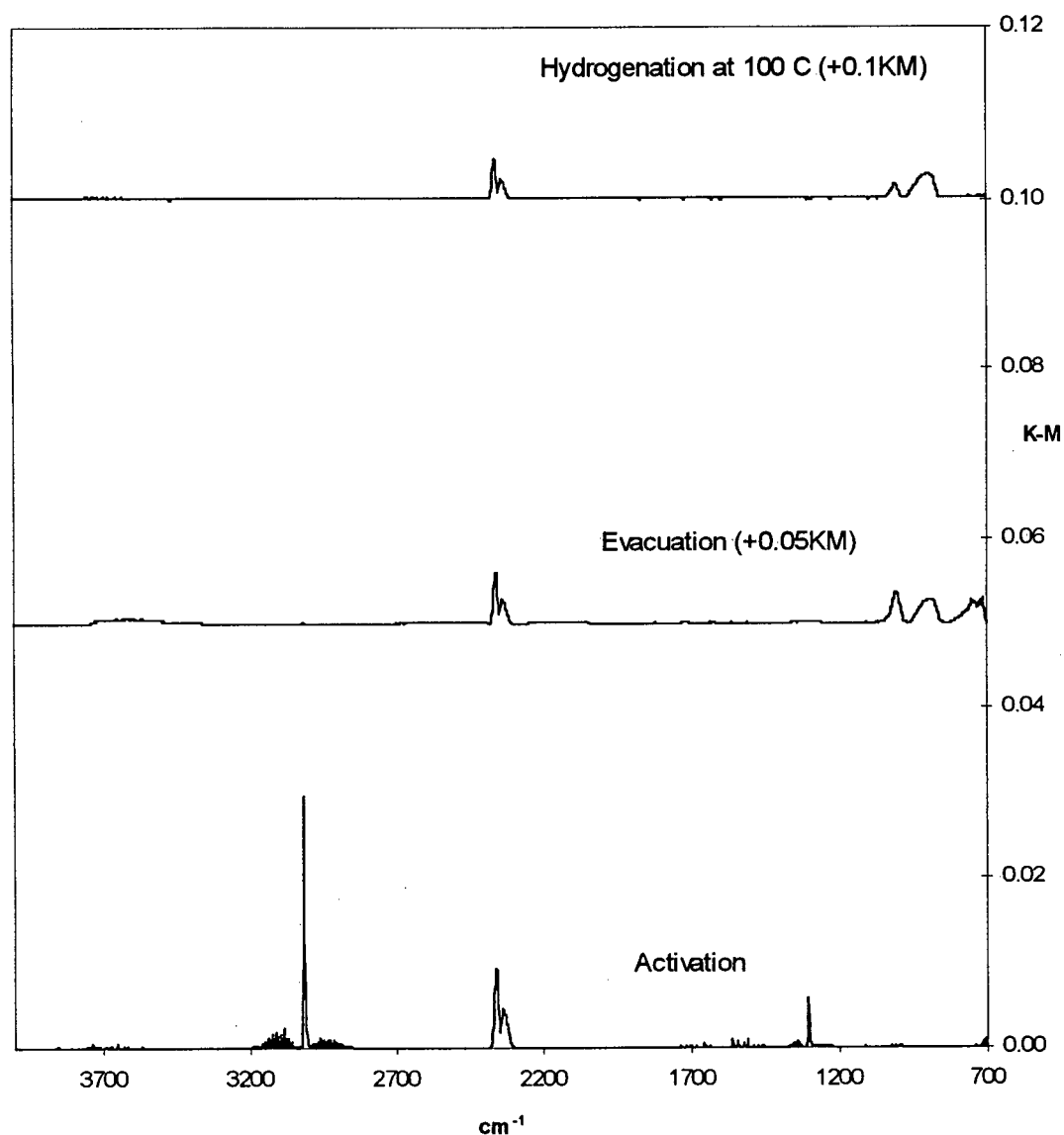


Figure 4.8. Diffuse reflectance infra-red Fourier transform spectra of the diluted A series 12%Co-SiO₂ reduced catalyst after activation, subsequent evacuation and hydrogenation with respect to the reduced diluted catalyst background.

Activation: 7 min activation of 5% CH₄/Ar at 450 °C

Evacuation: 30 min evacuation to 99.97 kPa.

Hydrogenation: 10 ml/min H₂ at 100 °C.

(Evacuation and Hydrogenation spectra have been shifted by 0.05 and 0.1 K-M units, respectively.)

4.8. Discussion

Table 4.7 summarizes the catalyst characterization data for the series A and B catalysts in which the nominal metal loading was varied from 0.6 wt% to 12 wt% Co on SiO₂. By decreasing the nominal metal loading, the degree of reduction based on the O₂ uptake measurement decreased from 85% to 26%. Previous studies (Coulter and Sault, 1995; Rosynek and Polansky, 1991; Reuel and Bartholomew, 1984) have reported somewhat lower levels of reduction for Co catalysts than those reported here. The higher values obtained in the present study are most likely due to the longer drying time and shorter calcination times used in the preparation of the catalysts. Generally, a low degree of reduction has been interpreted as evidence for the presence of cobalt silicates or a strong metal support interaction (MSI) that result in cobalt species that are difficult to reduce (Coulter and Sault, 1995; Rosynek and Polansky, 1991; Reuel and Bartholomew, 1984).

The Co dispersions, reported as a percentage of reduced Co and measured by H₂ desorption, did not show any strong dependence on metal loading. Of more significance, however, was the observation that the Co dispersions estimated by PXRD line broadening were approximately twice the value measured by H₂ desorption. Previous studies (Rosynek and Polansky, 1991; Reuel and Bartholomew, 1984; Bartholomew and Pannell, 1980) have shown that metal dispersions measured by PXRD line broadening and H₂ chemisorption agree within approximately 30%. Since the repeat analyses showed the experimental error for each method to be less than $\pm 10\%$, it was concluded that the differences in dispersions estimated by PXRD and chemisorption as shown in Table 4.7 were significant.

The data of Table 4.7 suggest that not all of the Co detected by PXRD was exposed to H₂ in the chemisorption measurement. This observation was interpreted as evidence for an additional MSI effect, namely migration of the SiO₂ support onto the reduced Co (Raupp, et al., 1987). A comparison of the difference between the PXRD and chemisorption measurements for the 12 wt% and 5 wt% Co catalysts (Table 4.7), suggests that this decoration of Co by SiO₂ became more significant as the metal loading decreased. Although SiO₂ is generally regarded as an inert support with weak MSI (Yoshitake and Iwasawa, 1992), other studies have shown the importance of MSI with Co, including the effect of incomplete metal reduction (Coulter and Sault, 1995; Rosynek and Polansky, 1991; Reuel and Bartholomew, 1984) and alloy formation (Potoczna-Petru and Kepinski, 1993).

Table 4.7. Summary of the Co-SiO₂ catalyst characteristics.

Series	Co loading	Extent of Reduction by		Co Dispersion Measured by	
		TPR in H ₂	O ₂ uptake	H ₂ desorption	PXRD of Co ₃ O ₄
	wt %	mol %	mol %	reduced catalyst	calcined catalyst
				%	%
A	12	91	85	5.6	10.0
A	5	84	76	5.1	11.0
A	2	(90) ⁺	42	5.3	-
B	8	78	-	4.6	8.8

⁺ Degree of reduction based on the TPR is not reliable.

Note that the presence of cobalt silicates or other unreduced Co species, as deduced from the incomplete cobalt reduction, cannot explain the difference in metal dispersions obtained by PXRD and H_2 . The difference between Co dispersion measured by PXRD and H_2 desorption suggests that almost 50% of the reduced Co surface is covered by SiO_2 .

Possible penetration of Co below the SiO_2 support surface cannot explain the difference between the Co dispersion measured by PXRD and H_2 desorption. Such a phenomenon can happen at the edges of Co particles where thin Co would be neither detectable by PXRD nor available for H_2 chemisorption. On the relatively large Co particles (about 20 nm) the contribution of such an effect would be small.

Figure 4.9 shows a schematic visualization of the state of Co- SiO_2 catalyst after reduction. In Figure 4.9 regions ① and ② are the SiO_2 and metallic Co phases, respectively. Regions ③ and ④ illustrate the two forms of metal-support interaction (MSI) in the Co- SiO_2 system. In region ③ cobalt silicate formation gives rise to incomplete reduction of the cobalt oxide phase during the TPR. Region ③ is not detected by PXRD, and H_2 adsorption does not occur in this region. Cobalt under the SiO_2 decoration in region ④ is reducible. Cobalt in region ④ can be observed by the PXRD, but not by H_2 chemisorption. As a result due to the effect of MSI in region ④, the PXRD measures a higher Co dispersion than the H_2 desorption method.

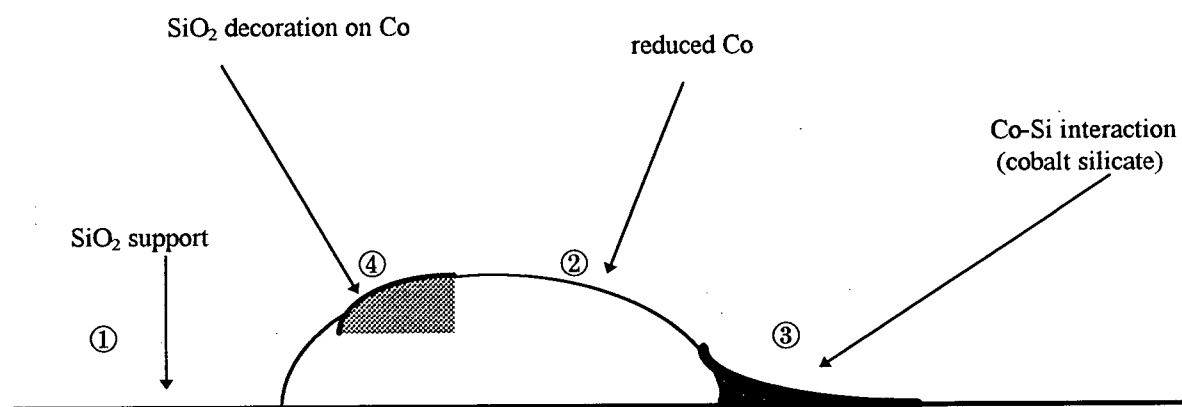


Figure 4.9. Schematic diagram of the two types of metal support interaction (MSI) on Co-SiO₂ catalyst.

Chapter 5

Activation of CH₄

5.1. Overview

In the two-step cycle, CH₄ reacts on the catalyst in the activation step to generate H₂ and deposit carbon species on the catalyst surface. The deposited carbon species are converted in the subsequent hydrogenation step to produce CH₄ and C₂₊ products. The amount and properties of the carbonaceous species deposited in the activation step have a major effect on the two-step cycle performance. In this chapter, results from the present study of the activation step are presented. For the first time, both the H₂ generation and CH₄ consumption profiles as a function of exposure time have been quantified.

Based on the experimental observations from this work, and published computational and experimental results, a semi-empirical model of CH₄ activation kinetics has also been developed. In the proposed model, gas phase CH₄ reacts with the active metal of the catalyst to produce adsorbed H and CH₃ species. Then, the adsorbed CH₃ species either dehydrogenate or migrate from the metal site to the support site to liberate the occupied metal site for further reaction of CH₄. Dehydrogenation of CH₃ on the support sites, combination of surface H species and desorption generate H₂.

The kinetic model has been used to quantify the effect of various parameters on the CH₄ activation reaction. The kinetic model, the parametric studies and the results of the

application of the kinetic model to the analysis of the activation step, are presented in this chapter.

5.2. Activation of CH₄

The QMS was used to monitor the reactor effluent stream during CH₄ activation on the Co-SiO₂ catalyst. Figure 5.1 shows a typical profile of the CH₄ consumption and H₂ generation per minute, during a 2 minute period of flow of a 5% CH₄/95% Ar gas mixture at 450 °C using the A series 12% Co-SiO₂ catalyst. The CH₄ consumption profile showed a short period of high reaction rate followed by a longer period of lower reaction rate. However, the rate of CH₄ consumption did not decrease to zero during the 2 minute reaction period. By numerical integration of the CH₄ consumption and H₂ production molar rate profiles, the cumulative CH₄ consumption and H₂ generation were calculated as functions of the reaction time. Hence, the cumulative CH₄ consumption per mole of surface Co on the reduced catalyst (the CH₄/Co ratio taken as a measure of the metal coverage) and the average value of x for the CH _{x} surface species, could be calculated and are presented in Figure 5.2.

A decrease in the slope of the cumulative CH₄ consumption curve is indicative of a decrease in the CH₄ consumption rate. As shown in Figure 5.2, the slope decreased over a period of time and then remained constant after approximately 1 min, corresponding to coverage of the Co by about a monolayer of CH _{x} (Boskovic and Smith, 1997).

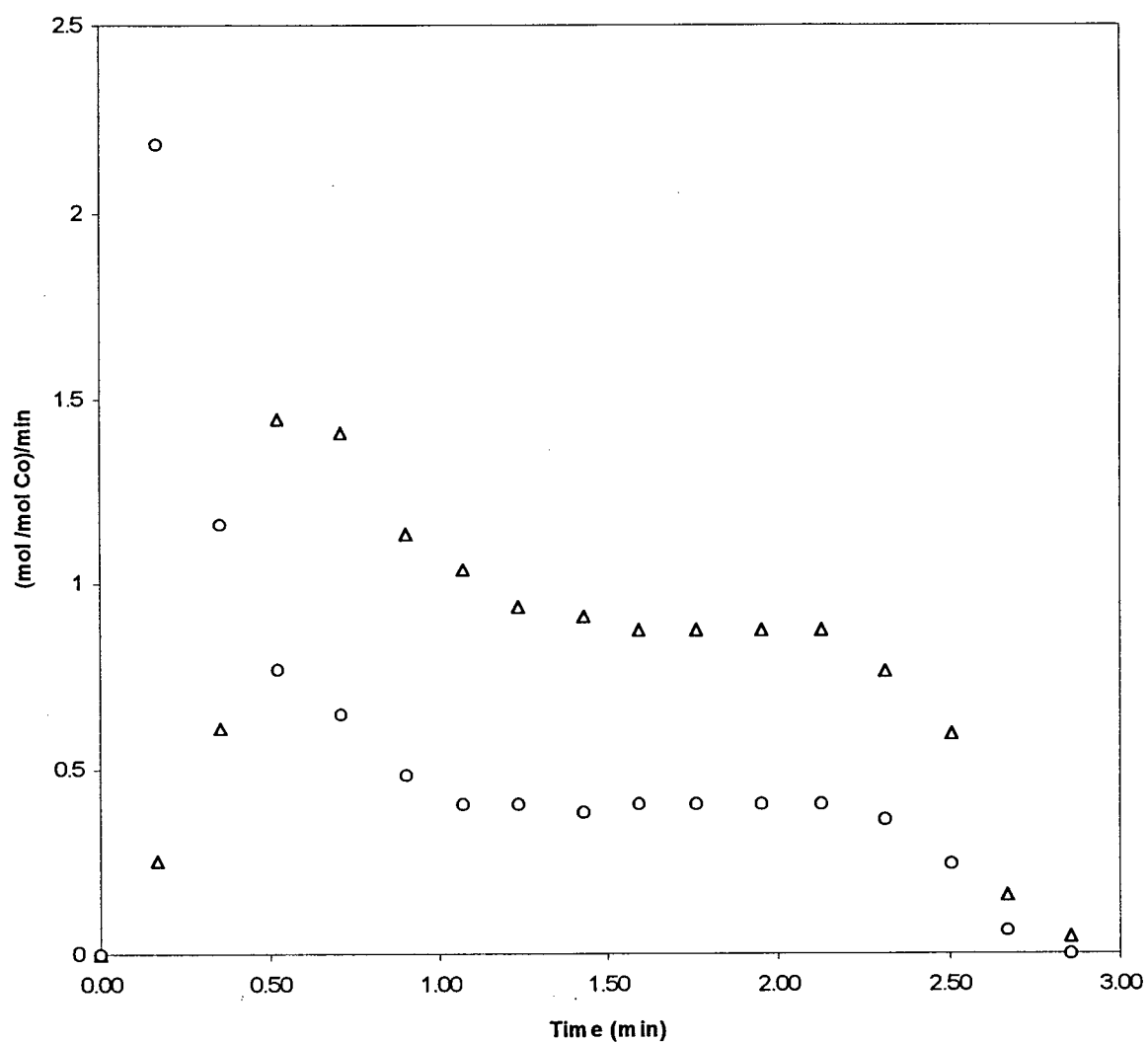


Figure 5.1. Rate of CH₄ consumption (O) and H₂ generation (Δ) per mole of Co during 2 min flow of 5%CH₄/95%Ar gas mixture at 54 ml/min and 450 °C over A series 12%Co-SiO₂ catalyst.

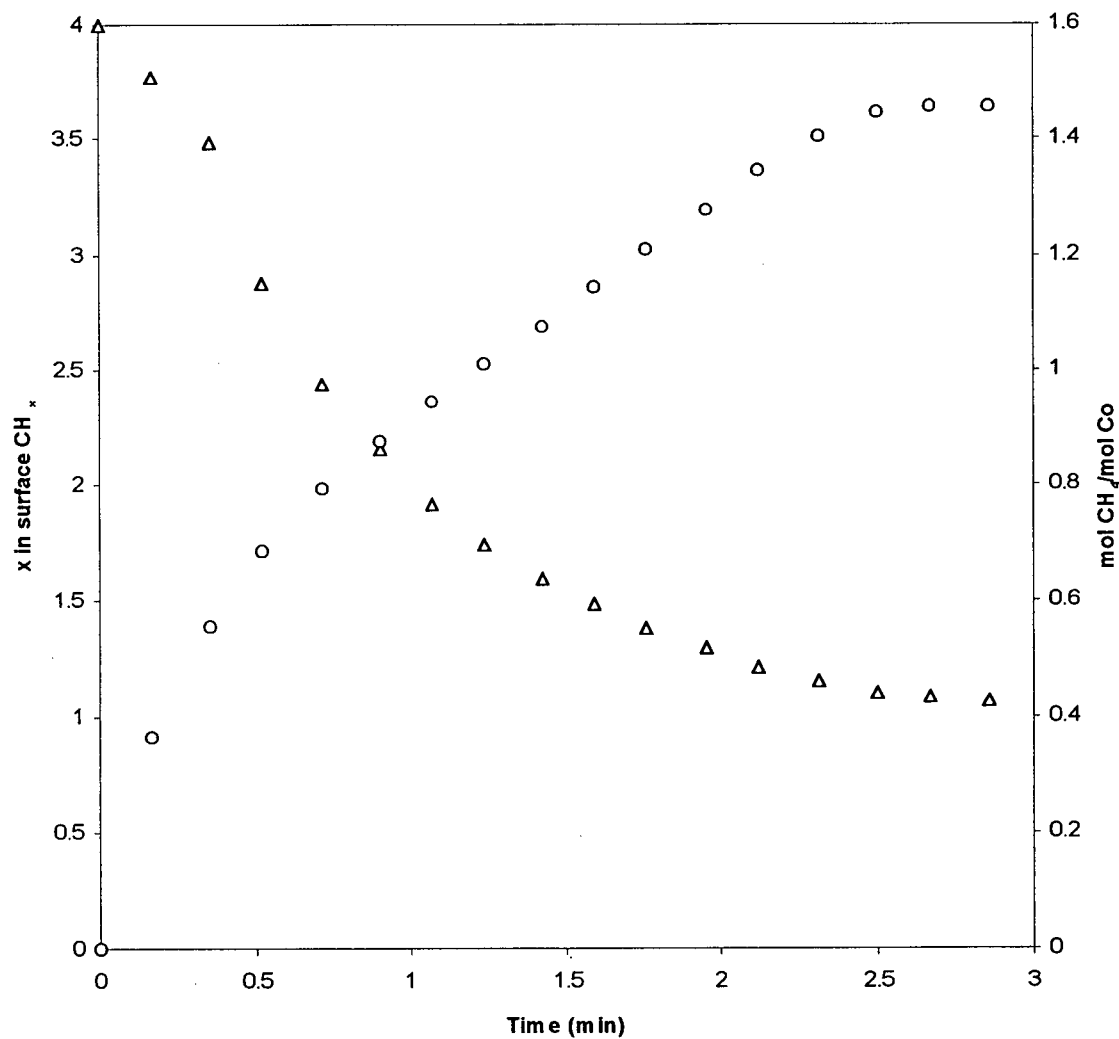


Figure 5.2. Cumulative moles of CH₄ consumed per mole of surface Co (O) and the value of x in the CH_x surface species (Δ) during 2 min flow of 5%CH₄/95%Ar gas mixture at 54 ml/min and 450 °C over A series 12%Co-SiO₂ catalyst.

The data of Figure 5.2 also show that the H content of the carbonaceous deposit decreased as the reaction time increased. Similar trends of decreasing x in CH_x surface species with increasing reaction time have been reported previously (Koerts et al., 1992).

5.3. Kinetics of CH_4 Activation

The data of Figure 5.2 clearly show that CH_4 consumption continued well beyond a nominal monolayer coverage of the metal sites. In addition, the data show that the species on the surface continued to lose hydrogen as time proceeded. To quantify these observations, a kinetic model of CH_4 activation was developed, based on the experimental observations from this work and published experimental and computational studies relevant to CH_4 activation kinetics.

Previous studies, reviewed recently by Guzzi et al. (1996), have shown that CH_4 interacts with metal surfaces to produce H_2 and some form of carbon species on the surface (Koerts and van Santen, 1991; Koerts et al., 1992; Solymosi et al. 1992; Belgued et al. 1996; Boskovic et al. 1996; Ferriera-Aparicio, 1997). Since the activation energy for the activation of gas phase CH_4 ($\text{CH}_{4(g)} + 2\text{S} \rightarrow \text{CH}_3\text{S} + \text{HS}$ where S represents an active catalyst site) is less than that of adsorbed CH_4 ($\text{CH}_4\text{S} + \text{S} \rightarrow \text{CH}_3\text{S} + \text{HS}$) over Group VIII metal catalysts (Shustorovich and Bell, 1991), it is reasonable to assume that the first step of the CH_4 activation reaction can be written according to reaction (5.1). Furthermore, estimates of the activation energies for the subsequent dehydrogenation of CH_3S to CH_xS ($x=2,1,0$) are 40 - 60 kJ/mol larger than those for the initial adsorption step (Shustorovich and Bell, 1991). Hence it is reasonable to assume that subsequent dehydrogenation of surface CH_3 species

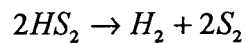
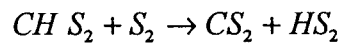
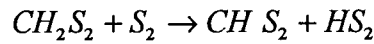
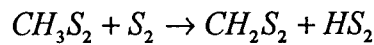
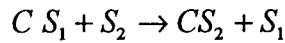
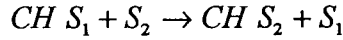
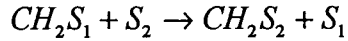
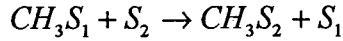
generates H_2 and various carbon fragments CH_x ($x=2,1,0$). Few studies on the structure of the carbonaceous fragments are available, although, vinylidene and methyldiyne species have been identified on Ru (Koranne and Goodman, 1995; Lenz-Solomun, et al., 1994). Detection of small amounts of C_2H_6 and H_2 during the activation of CH_4 on Ru supported catalysts has been taken as evidence for the presence of surface CH_3 species (Erdohelyi et al., 1993), the combination of which would yield C_2H_6 . Based on these observations, but neglecting the combination reaction of surface carbon species since in the present work production of higher hydrocarbons during the activation step was negligible, one can approximate the surface reactions by the following sequence of steps:



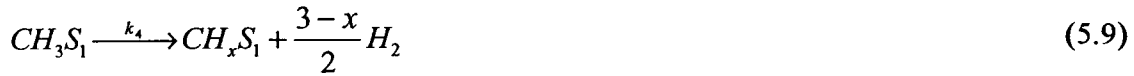
where XS refers to an adsorbed surface species and S is the active metal site.

However, these steps imply that the rate of CH_4 activation will decrease with time due to the occupation of vacant sites and finally cease upon complete coverage of the metal sites by the carbonaceous species. Since experimental observations have shown that the supported metal catalysts activate more CH_4 than that corresponding to a monolayer coverage (Lenz Solomun et al., 1994; Boskovic et al., 1996; Boskovic and Smith, 1997; Tsipourariet et al., 1996), possible migration or spillover of the carbon species from the metal site to the support (Driessen and Grassian, 1996) was included in the kinetic model. Incorporating migration of

all CH_x ($x=1, 2, 3$) surface species together with the dehydrogenation reactions, requires an additional eight equations to describe the reaction mechanism.



Here S_1 represents a metal active site while S_2 represents a support site. Since the present work is concerned primarily with CH_4 activation kinetics, the reaction mechanism was simplified further to reduce the number of rate constants in the kinetic model. Semi-empirical calculations (Koerts and van Santen, 1991) indicate that highly hydrogenated CH_x fragments such as CH_3 are more mobile than for example, CH_2 or CH , due to the weaker metal-adsorbate interaction of the CH_3 species. Consequently migration from the metal site to the support site was assumed to be dominated by adsorbed CH_3 species. Furthermore, it was assumed that CH_3 adsorbed on both the metal and support is dehydrogenated to produce H_2 and a less hydrogenated carbon species CH_x ($x < 3$). Since only carbon species were considered in the modeling, the possibility of migration of H from the metal site to the support site has been neglected. The simplified reaction mechanism is then as follows:



PXRD characterization of the catalysts before and after reaction (not reported here) has shown that under the reaction conditions of the two-step cycle, catalyst metal particle size did not change. Since the surface area of the support is much larger than the metal and since in the absence of sintering the metal-support interface does not change, it is safe to assume that the coverage of support sites is relatively constant during CH₄ activation. Given the small amount of CH₄ consumption, the change in CH₄ concentration in the gas phase is neglected.

Simplifying the rate constants k'_1 and k'_2 :

$$\begin{aligned} k_1 &= k'_1 P_{CH_4} \\ k_2 &= k'_2 \theta_{S_2} \end{aligned} \quad (5.11)$$

the rate of change of coverage of different surface species (Θ) follows directly from equations (5.6)-(5.10):

$$\frac{d\theta_{S_1}}{dt} = -2k_1\theta_{S_1}^2 + k_2\theta_{CH_3S_1} + k_3\theta_{HS_1}^2 \quad (5.12)$$

$$\frac{d\theta_{CH_3S_1}}{dt} = k_1\theta_{S_1}^2 - k_2\theta_{CH_3S_1} - k_4\theta_{CH_3S_1} \quad (5.13)$$

$$\frac{d\theta_{HS_1}}{dt} = k_1\theta_{S_1}^2 - 2k_3\theta_{HS_1}^2 \quad (5.14)$$

$$\frac{d\theta_{CH_xS_1}}{dt} = k_4\theta_{CH_3S_1} \quad (5.15)$$

$$\frac{d\theta_{CH_xS_2}}{dt} = k_5\theta_{CH_3S_2} \quad (5.16)$$

The set of first order differential equations is subject to the initial condition:

$$at\ t = 0 \quad \theta_{S_1} = 1, \quad \theta_{CH_3S_1} = \theta_{HS_1} = \theta_{CH_xS_1} = \theta_{CH_xS_2} = 0 \quad (5.17)$$

Using eq. (5.6) and (5.8)-(5.10) the cumulative CH_4 consumption and H_2 production as a function of exposure time are given by:

$$n_{CH_4} = -\int_0^t (mc_0) k_1 \theta_{S_1}^2 dt \quad (5.18)$$

$$n_{H_2} = \int_0^t (mc_0) \left\{ k_3 \theta_{HS_1}^2 + \frac{3-x}{2} [k_4 \theta_{CH_3S_1} + k_5 \theta_{CH_3S_2}] \right\} dt \quad (5.19)$$

The simplified reaction mechanism proposed herein represents the carbon surface species as CH_x . Experimental data have shown that the value of x changes with exposure to high temperature, and Figure 5.2 shows that x decreased from about 4 to approximately 1 after 2 min reaction. To avoid the complicated problem of describing the transformation kinetics for CH_x species and the change in x (Lenz-Solomun, et al., 1994), only the CH_4 consumption equation (5.18) together with equations (5.12)-(5.15) were used to estimate the rate constants k_1 , k_2 , k_3 and k_4 .

The rate constants were estimated using a combined pattern search and steepest descent optimization algorithm, with an initial guess of the rate constants. By means of a 4-th order Runge-Kutta method, the set of initial value first order differential equations was solved

and the CH₄ consumption was calculated as a function of time. Using the sum of squares of the difference between the actual and calculated CH₄ consumption profiles as an objective function, the optimization routine improved the estimate of the rate constants until the minimum of the objective function corresponding to the optimum rate constants k_1 , k_2 , k_3 and k_4 , was obtained. The computer code used to perform these numerical calculations is listed in Appendix 3.1.

Figure 5.3 is a typical comparison of the actual and calculated cumulative CH₄ consumption to surface Co molar ratio as a function of time, during CH₄ activation on the series A 12% Co-SiO₂ catalyst at 450 °C for a 2 min reaction period. The estimated rate constants and their corresponding standard deviations were $k_1 = 3.9 \pm 0.2 \text{ min}^{-1}$, $k_2 = 40.0 \pm 12.0 \text{ min}^{-1}$, $k_3 = 0.5 \pm 0.1 \text{ min}^{-1}$ and $k_4 = 1.1 \pm 0.3 \text{ min}^{-1}$, and the agreement between the measured and calculated values was excellent ($R^2 = 99.9\%$).

Note that without the migration step ($k_2 = 0$) the cumulative CH₄/Co molar ratio would approach on asymptote of 1, while the activation rate would approach on asymptote of zero (Kristyan, 1997). Clearly, the kinetic data are in accord with the proposed migration or spillover of CH₃ species from the Co to the support.

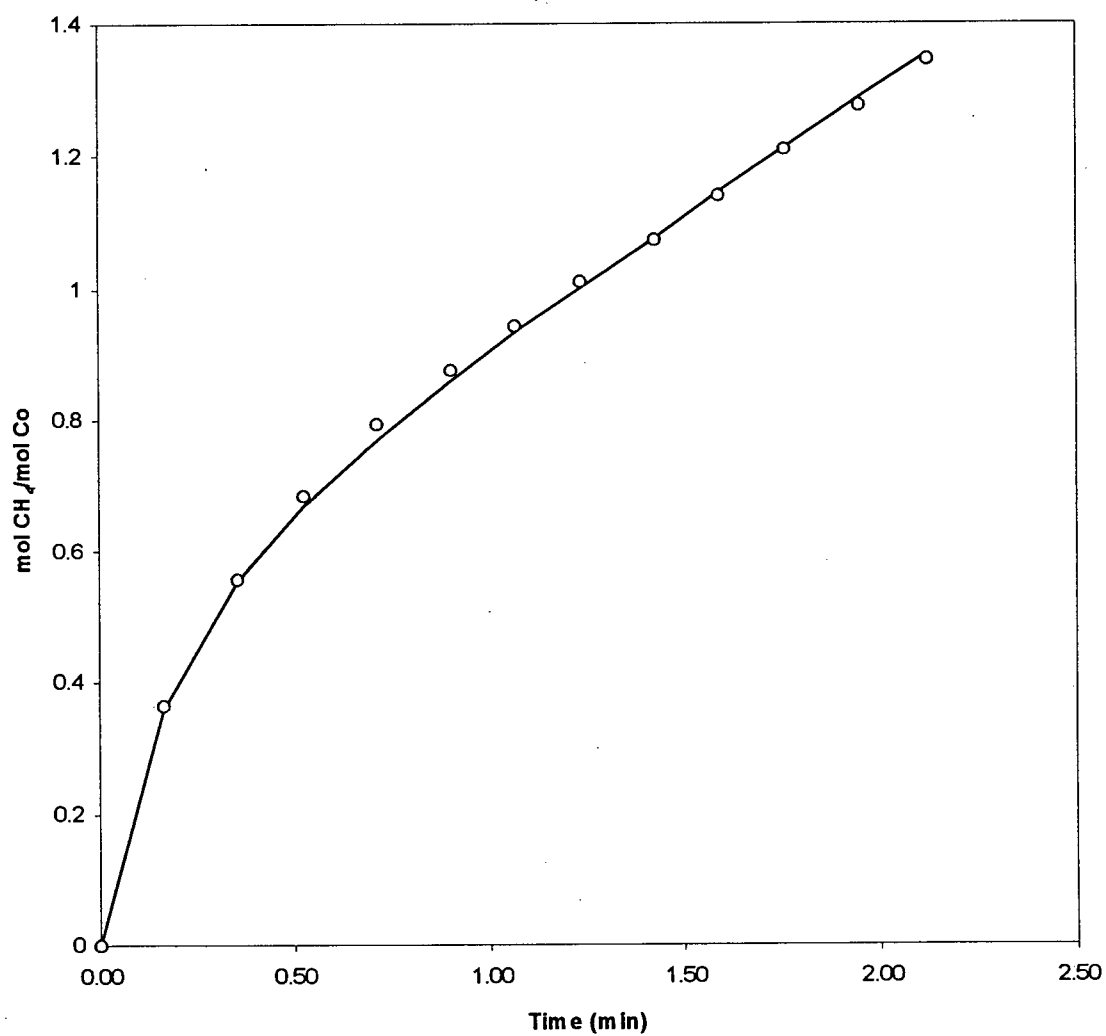


Figure 5.3. Cumulative moles of CH₄ consumed per mole of surface Co (O) measured during 2 min flow of 5%CH₄/95%Ar gas mixture and 54 ml/min at 450 °C over A series 12%Co-SiO₂ catalyst, compared to model fit (—). Model parameter estimates are given in the text.

5.3.1. Coverage of Surface Species

By applying the kinetic model to the experimental data, the optimum rate constants for reactions (5.6) to (5.9) were determined. Using these optimum reaction rate constants, the surface coverage Θ of different species, the rate of CH_4 activation on Co (eq. 5.6) and CH_3 migration from the metal to the support site (eq. 5.7) were calculated.

In Figure 5.4, the rate of CH_4 activation on Co ($\text{CH}_4 + 2\text{S}_1 \xrightarrow{k_1} \text{CH}_3\text{S}_1 + \text{HS}_1$, eq. 5.6) and CH_3 migration from Co to SiO_2 sites ($\text{CH}_3\text{S}_1 + \text{S}_2 \xrightarrow{k_2} \text{CH}_3\text{S}_2 + \text{S}_1$, eq. 5.7) are presented. The nominal metal coverage by carbon (mol CH_4 reacted per mol Co, Θ_c) as a function of reaction time is also presented in Figure 5.4.

Figure 5.5 shows the profiles of surface coverage for catalyst metal vacant site (S_1), adsorbed CH_3 species (CH_3S_1), adsorbed hydrogen (HS_1) and the adsorbed lumped carbon species CH_x (CH_xS_1) as functions of time. In addition, the nominal metal coverage by carbon (Θ_c) as a function of reaction time is presented in Figure 5.5.

The relative rate of CH_4 activation on the metal site (eq. 5.6) and CH_3 migration (eq. 5.7) from metal (S_1) to support site (S_2) has a major effect on the rate of activation of CH_4 on the Co- SiO_2 catalyst. Initially, the number of vacant metal sites (S_1) is high and there are no carbon species on the catalyst. As a result, the initial rate of CH_3 migration is zero whereas the CH_4 activation reaction is fast. As reaction time proceeds, CH_4 reacts with more metal sites (S_1) to produce CH_3S_1 surface species.

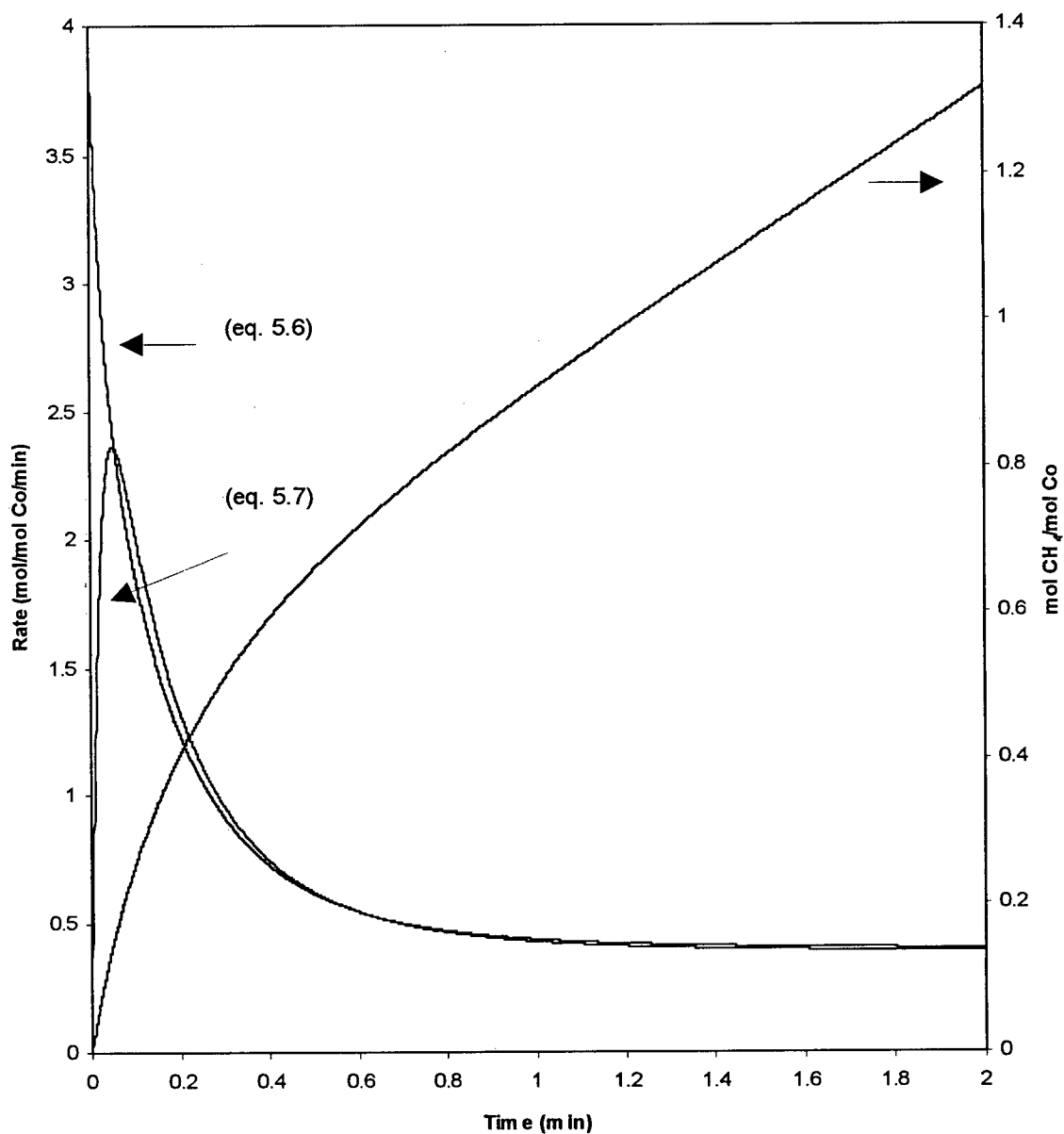
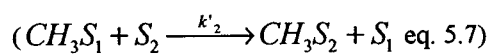


Figure 5.4. Results of simulation of reaction rates for 2 min activation of 5%CH₄/95%Ar gas mixture at 450 °C over A series 12%Co-SiO₂ catalyst.

Left y axis: Rate of Activation of CH₄ on metal ($CH_4 + 2S_1 \xrightarrow{k_1} CH_3S_1 + HS_1$, eq. 5.6) and migration of CH₃ from metal to support site



Right y axis: Nominal metal coverage (Θ_C) by carbon

Parameters: $k_1 = 3.9 \text{ min}^{-1}$, $k_2 = 40.0 \text{ min}^{-1}$, $k_3 = 0.5 \text{ min}^{-1}$ and $k_4 = 1.1 \text{ min}^{-1}$

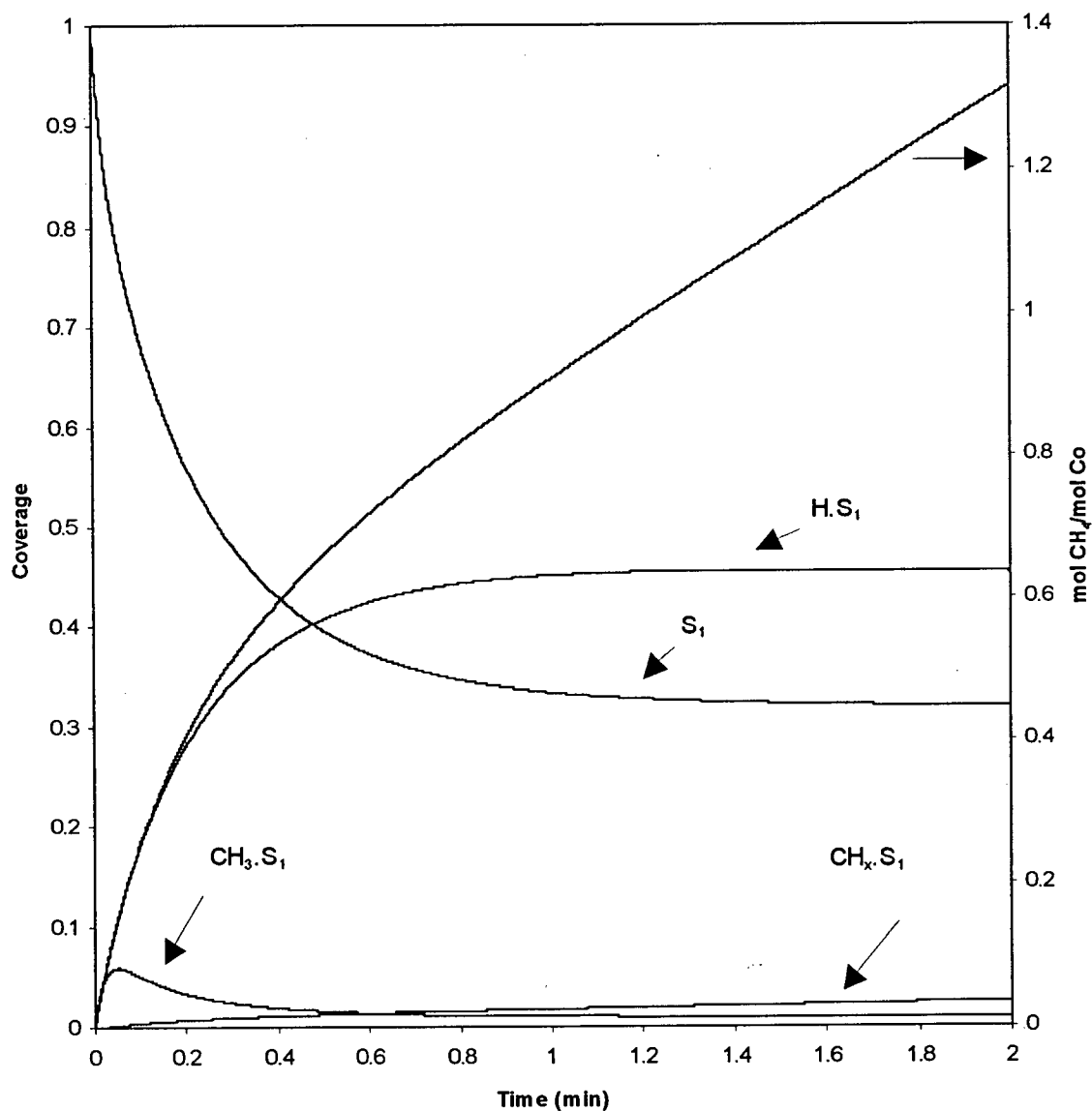


Figure 5.5. Results of simulation of surface coverage for 2 min activation of 5%CH₄/95%Ar gas mixture at 450 °C over A series 12%Co-SiO₂ catalyst.

Left y axis: Coverage (Θ) of catalyst vacant site S_1 , HS_1 , CH_3S_1 and CH_xS_1 surface species

Right y axis : Nominal metal coverage (Θ_C) by carbon

Parameters: $k_1 = 3.9 \text{ min}^{-1}$, $k_2 = 40.0 \text{ min}^{-1}$, $k_3 = 0.5 \text{ min}^{-1}$ and $k_4 = 1.1 \text{ min}^{-1}$

With deposition of these carbon species, the number of vacant sites S_1 , decreases, the rate of CH_4 activation decreases and the rate of CH_3 migration increases. At this initial stage, the rate of carbon deposition on the metal site is higher than the rate of carbon removal. This trend continues until the concentration of CH_3S_1 on the metal site reaches a maximum which corresponds to the maximum CH_3S_1 coverage (see Figure 5.5). Beyond this point, the rate of both the CH_4 activation on the metal site and the rate of CH_3 migration continue to decrease and approach asymptotic levels.

The rate of CH_xS_1 build-up on the catalyst is much smaller than the rate of CH_4 activation on the catalyst. Figure 5.5 shows that by increasing the exposure time and hence the nominal metal coverage (Θ_c) by carbon species, coverage of vacant sites S_1 decreases sharply at first then levels off as the rate of CH_4 activation and CH_3 migration reach a nearly constant value. With increasing activation time, the coverage of HS_1 species increases sharply at first and then levels off as the rate of initial CH_4 activation on the metal decreases and the rate of CH_3 migration from the metal to the support site increases. The coverage of CH_3S_1 species starts from zero at first, reaches a maximum and then decreases to a small nearly steady value. This is an indication of the initial build-up of CH_3S_1 species during the initial activation of CH_4 on the metal site with negligible carbon migration. By increasing the coverage of CH_3S_1 species, the rate of migration of CH_3S_1 becomes significant and the coverage of CH_3S_1 reaches an asymptotic level. By increasing the exposure time, the coverage of CH_xS_1 species increases slowly.

5.4. Parametric Study of the Kinetic Model

To examine the significance of different reactions and their rate constants on the performance of the reaction model a parametric study was performed. The 2 min activation of 5%CH₄/Ar on 0.5 g A series 12%Co-SiO₂ catalyst at 450 °C was analyzed by the kinetic model. The optimum rate constants (k_i) and the corresponding standard deviations (σ_i) were established above as $k_1 = 3.9 \pm 0.2 \text{ min}^{-1}$, $k_2 = 40.0 \pm 12.0 \text{ min}^{-1}$, $k_3 = 0.5 \pm 0.1 \text{ min}^{-1}$ and $k_4 = 1.1 \pm 0.3 \text{ min}^{-1}$. In the parametric study, the value of each reaction rate constant k_i was set as $k_i + 2\sigma_i$, $k_i - 2\sigma_i$ ($i=1$ to 4 with σ_i being the standard deviation of the corresponding rate constant) and zero, while the k_j ($j=1$ to 4, $j \neq i$) were set at their optimum values. The predicted nominal metal coverages Θ_c (mol CH₄ converted /mol surface Co atoms) were compared with the calculated Θ_c using the optimum rate constants and the experimental data.

Although the performance of the kinetic model depends on the complete set of the reactions (5.6 to 5.10), a study in which the reaction rate constants are varied one at a time provides qualitative insight into the physical significance of different steps of the kinetic model.

Reaction (5.6) represents the initial activation of CH₄ on the catalyst metal. A high value of k_1 indicates a more active catalyst for CH₄ activation and generation of surface CH₃S₁ species. Reaction (5.7) is responsible for transport of the adsorbed CH₃ species from the metal site to the support site and regeneration of the metal site S₁ for further activation of gas phase CH₄. A high k_2 increases the rate of regeneration of S₁ sites which leads to more CH₄ consumption. Reaction (5.8) generates H₂ by combination of two HS₁ species. This reaction

also liberates S_1 active sites. Reaction (5.9) does not directly affect the rate of CH_4 activation, but it transforms CH_3S_1 species to CH_xS_1 species and generates H_2 .

5.4.1. Initial Activation of CH_4

Initial activation of CH_4 is expressed by reaction (5.6) and the corresponding reaction rate constant k_1 . Figure 5.6 shows the results of the kinetic model prediction when k_1 is set at 4.3 min^{-1} ($k_1+2\sigma_1$) and 3.5 min^{-1} ($k_1-2\sigma_1$) with optimum k_2 , k_3 and k_4 values (40, 0.5 and 1.1 min^{-1} , respectively). For comparison the optimum nominal metal coverage and the experimental values are also included in Figure 5.6.

By increasing the initial CH_4 activation activity of the catalyst (increasing k_1), more CH_4 dissociates per unit of time on the catalyst to produce surface carbon species on the catalyst metal. This leads to higher initial activity of the catalyst. A more active catalyst metal with a high k_1 is more active for CH_4 activation only at low nominal metal coverage (Θ_c). With increasing exposure time and higher Θ_c the rate of CH_4 activation becomes nearly independent of the metal activity. This is due to the fact that at higher nominal metal coverage (Θ_c) the overall CH_4 consumption rate is governed by the carbon migration from the metal to the support site. Consequently, a more active metal is not as effective at high Θ_c as at low Θ_c .

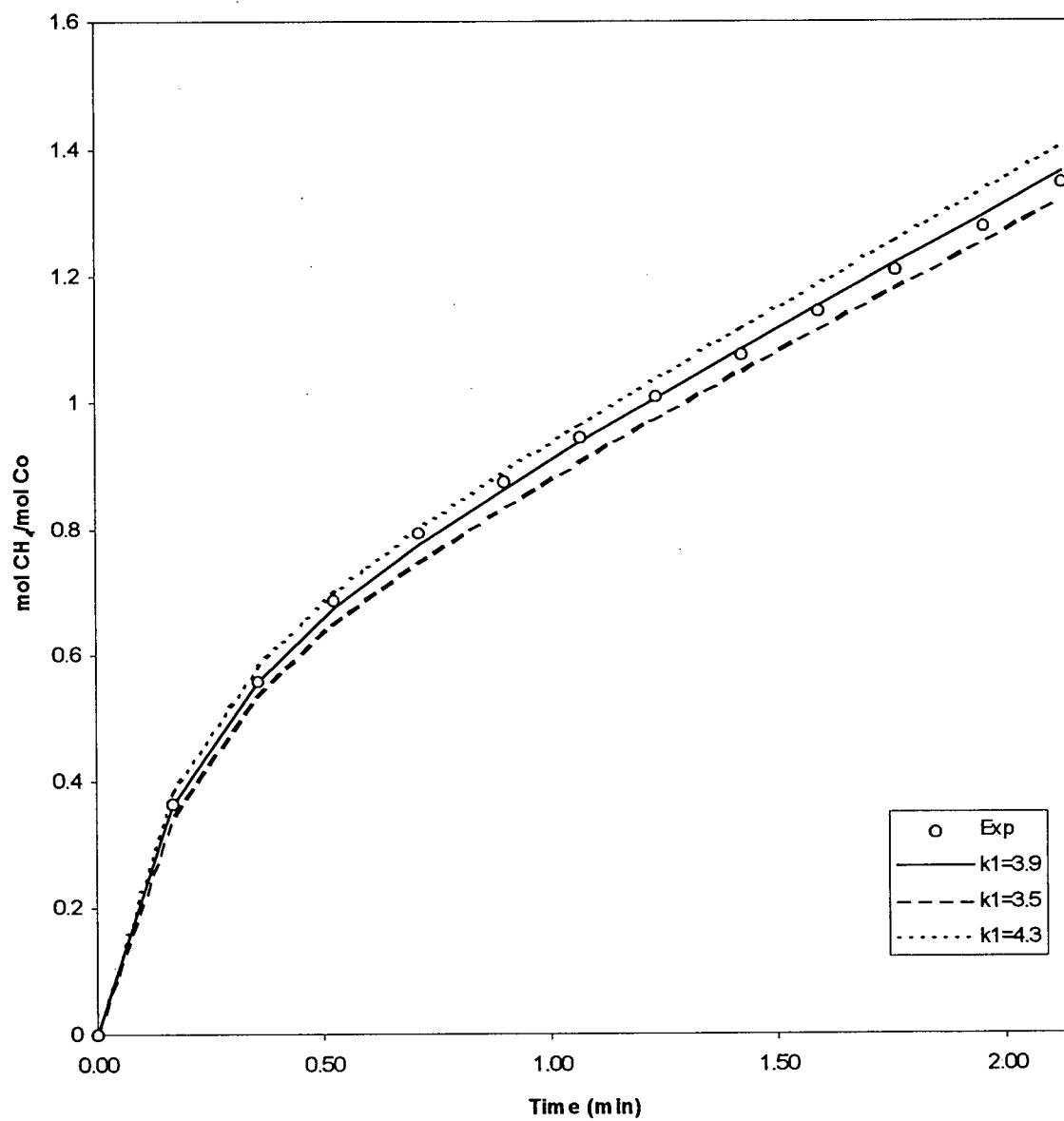


Figure 5.6. Effect of k_1 on nominal metal coverage, θ_c .

(O) Experimental θ_c , (—) and the best fit ($k_1=3.9 \text{ min}^{-1}$) compared to:

$k_1=3.5$ ($k_1-2\sigma_1$) and $k_1=4.3$ ($k_1+2\sigma_1$)

k_2 , k_3 and k_4 were the optimum values.

5.4.2. Carbon Migration

After initial activation of CH_4 on the catalyst metal site (reaction 5.6), the surface carbon species migrate from the active metal site to the support site (reaction 5.7). A high k_2 leads to a faster migration of the carbon species from the metal to the support site and hence faster regeneration of the active metal site for reaction with more CH_4 . The effect of migration of carbon species is initially low when Θ_c is small, whereas the effect of the migration step becomes significant at higher Θ_c .

In Figure 5.7 the kinetic model predictions for different k_2 values of 64 min^{-1} ($k_2+2\sigma_2$), 16 min^{-1} ($k_2-2\sigma_2$) and zero with optimum k_1 , k_3 and k_4 values (3.9 , 0.5 and 1.1 min^{-1} , respectively) are compared with the optimum Θ_c profile (with $k_2=40 \text{ cm}^{-1}$) and the experimental values. Figure 5.7 shows that Θ_c increases with increasing migration rate constant k_2 . The effect of varying k_2 is more pronounced at higher Θ_c . The $k_2 = 0$ profile corresponds to the case where the effect of migration of carbon species from the metal site to the support is neglected (Kristyan, 1997). In this case, the slope of Θ_c vs. time of reaction decreases with increasing exposure time. The slope of Θ_c versus exposure time approaches zero when Θ_c approaches unity.

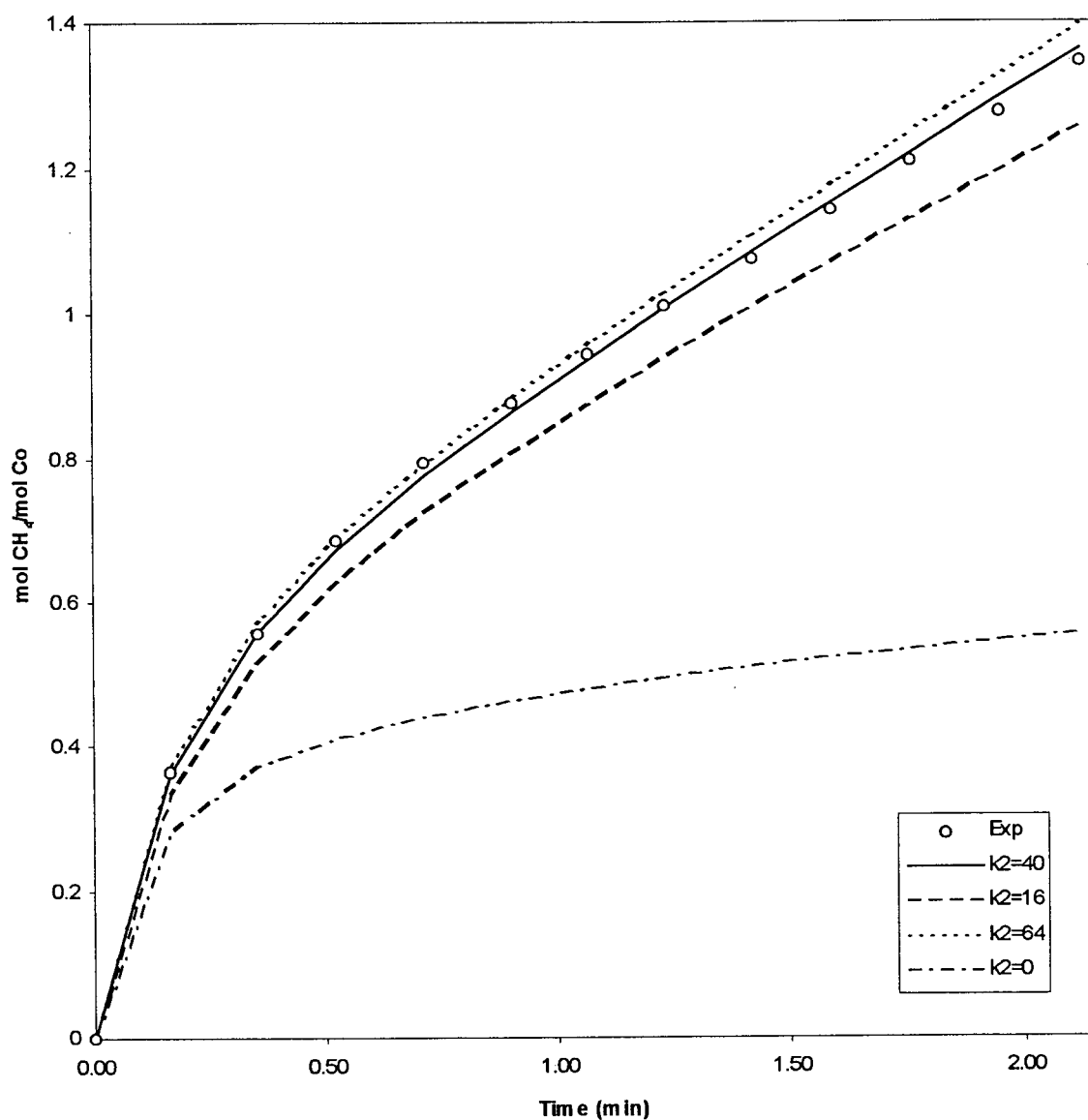


Figure 5.7. Effect of k_2 on nominal metal coverage, θ_c .

(O) Experimental θ_c , and (—) the best fit ($k_2 = 40 \text{ min}^{-1}$) compared to:

$k_2 = 0$, $k_2 = 16$ ($k_2 - 2\sigma_2$) and $k_2 = 64$ ($k_2 + 2\sigma_2$)

k_1 , k_3 and k_4 were the optimum values.

5.4.3. Hydrogen Desorption

Initial activation of CH_4 on the active metal site generates CH_3S_1 and HS_1 (reaction 5.6). Reaction (5.8) represents the combination of two HS_1 surface species to generate H_2 and liberate two active metal sites. A higher k_3 indicates a higher rate of H_2 evolution and faster regeneration of active metal sites which were occupied by adsorbed H. Hence, increasing k_3 leads to faster CH_4 activation.

Figure 5.8 shows the predicted Θ_c with rate constant k_3 set at 0.7 min^{-1} ($k_3+2\sigma_3$), 0.3 min^{-1} ($k_3-2\sigma_3$) and zero, while retaining optimum k_1 , k_2 and k_4 values of 3.9, 40 and 1.1 min^{-1} , respectively. For comparison, the experimental Θ_c values and the optimum profiles are included in Figure 5.8.

A higher k_3 gives rise to a higher nominal metal coverage (Θ_c) because the rate of H_2 desorption increases and the rate of regeneration of active metal sites increases making them available for further CH_4 activation. The Θ_c profile corresponding to $k_3=0$ represents the case where the adsorbed H does not desorb from the active metal site. In this case the rate of change of Θ_c with time decreases which corresponds to a very small rate of CH_4 activation. With $k_3=0$ (i.e. no desorption of the adsorbed H_2) as the exposure time increases, the metal active sites become occupied and the rate of CH_4 activation approaches zero. This is in accordance with the physical expectation that with $k_3=0$, once the active sites S_1 become occupied by CH_3 , CH_x and H species, the rate of CH_4 activation decreases to zero.

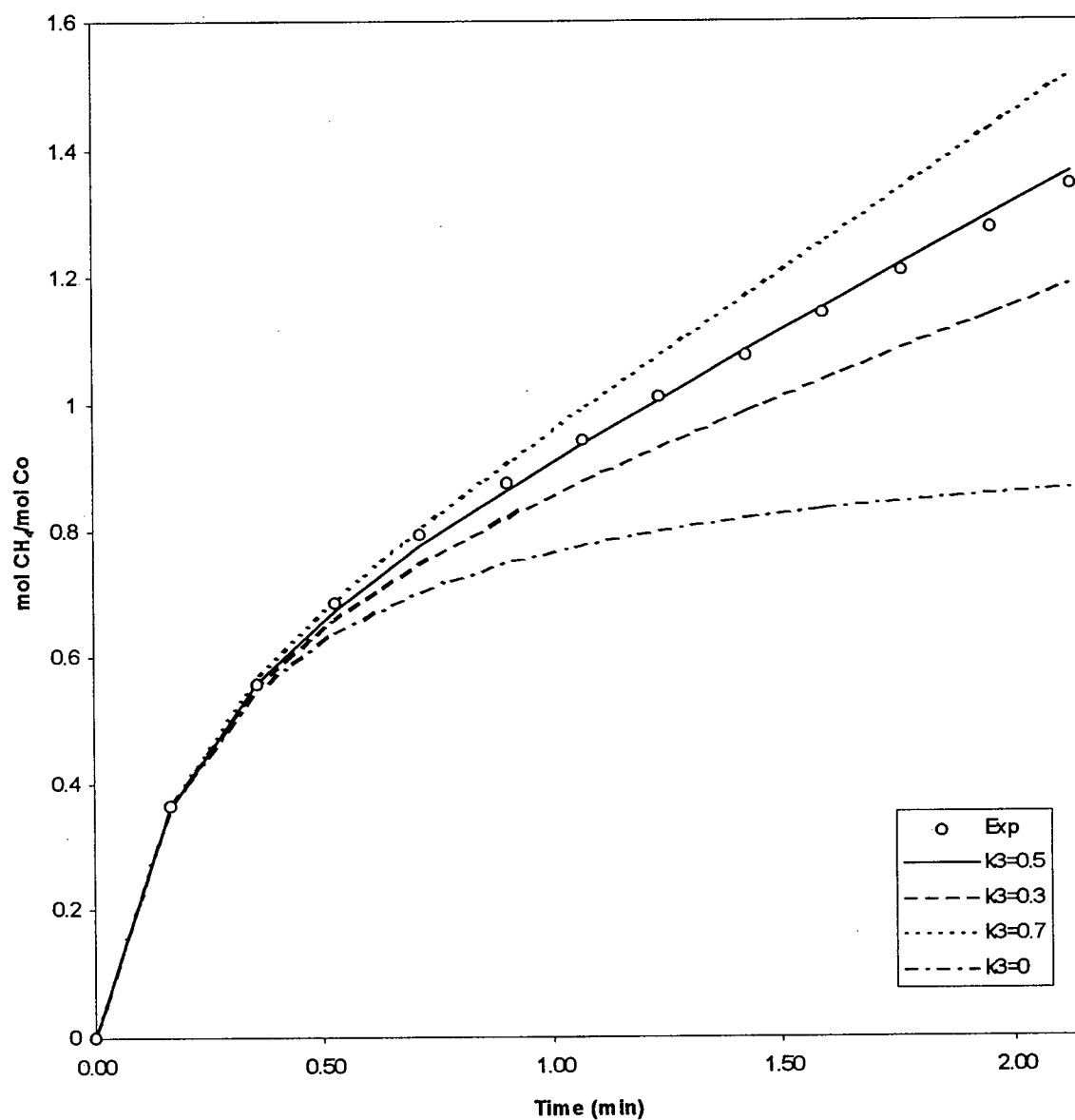


Figure 5.8. Effect of k_3 on nominal metal coverage, θ_c .

(O) Experimental θ_c , and (—) the best fit ($k_3=0.5 \text{ min}^{-1}$) compared to:

$k_3=0$, $k_3 = 0.3(k_3-2\sigma_3)$ and $k_3= 0.7(k_3+2\sigma_3)$

k_1 , k_2 and k_4 were the optimum values.

5.4.4. Dehydrogenation of Surface CH_3

Equation 5.9 is a representation of the lumped dehydrogenation of surface CH_3S_1 , CH_2S_1 and CHS_1 to the less hydrogenated species. Figure 5.9 compares the effect of changing k_4 to $k_4+2\sigma_4$ ($=1.7 \text{ min}^{-1}$), $k_4-2\sigma_4$ ($=0.5 \text{ min}^{-1}$) and zero while optimum k_1 , k_2 and k_3 values of 3.9, 40 and 0.5 min^{-1} respectively, are retained. Equation 5.9 has an important effect on the rate of H_2 generation in the CH_4 activation reaction, but its effect on CH_4 consumption kinetics is small. Hence k_4 has little effect on the performance of the present kinetic model.

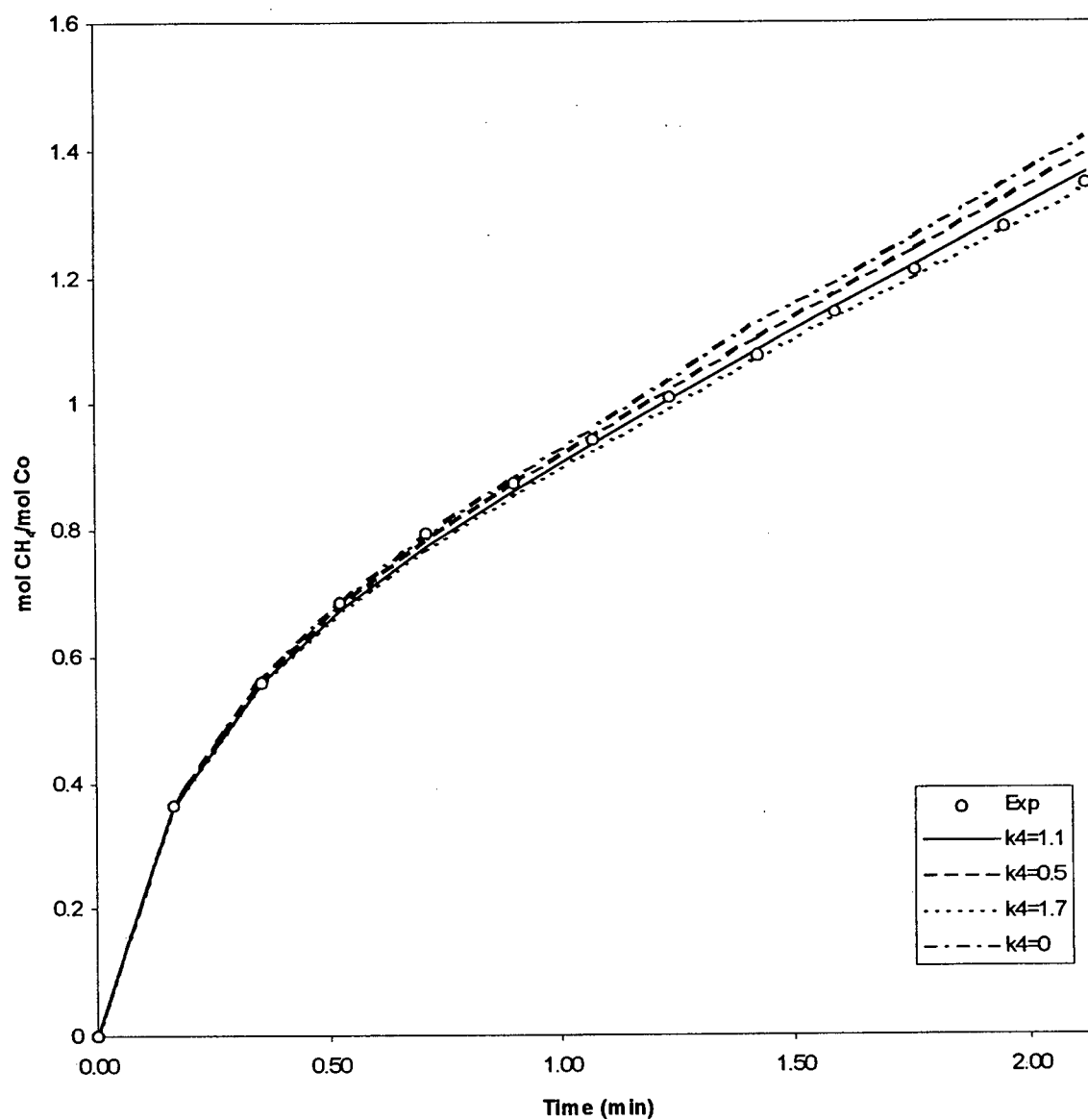


Figure 5.9. Effect of k_4 on nominal metal coverage, θ_c .

(O) Experimental θ_c , and (—) the best fit ($k_4=1.1 \text{ min}^{-1}$) compared to:

$k_4=0$, $k_4 = 0.5(k_4-2\sigma_4)$ and $k_4 = 1.7(k_4+2\sigma_4)$

k_1 , k_2 and k_3 were the optimum values.

5.5. Effect of Operating Variables

The kinetic model was used to assist in the interpretation of experimental data obtained to determine the effect of various operating conditions on the CH₄ activation step. The experimental data and calculation methods are provided in Appendix 2.2 and 2.3, respectively.

5.5.1. Effect of Reaction Time

In Figure 5.10, the cumulative CH₄ consumption per surface Co molar ratio as a function of time for the series A 12% Co-SiO₂ catalyst is shown for a total reaction time of 7 min. These data were also well described by the kinetic model ($R^2 = 99.4\%$) with the estimated parameter values of $k_1 = 4.3 \pm 0.8 \text{ min}^{-1}$, $k_2 = 54.3 \pm 12.3 \text{ min}^{-1}$, $k_3 = 0.6 \pm 0.1 \text{ min}^{-1}$ and $k_4 = 0.8 \pm 0.2 \text{ min}^{-1}$. Taking account of the standard deviation of the estimates, these values are in good agreement with the estimates obtained from the 2 min reaction time experiment (Figure 5.2). In Figure 5.10, the deviation in the model fit in the first 2 min activation time was greater than in the subsequent 5 min. This was due mostly to the fact that each data point carried equal weight in the fitting procedure.

Assuming that the carbon species on the surface can be represented as CH_x, the calculated value of x as a function of time is shown in Figure 5.11. Increasing exposure time decreased the hydrogen content of the CH_x surface species. In previous reports with less than a monolayer coverage (Koerts et al., 1992), x was reported to be close to 1.0.

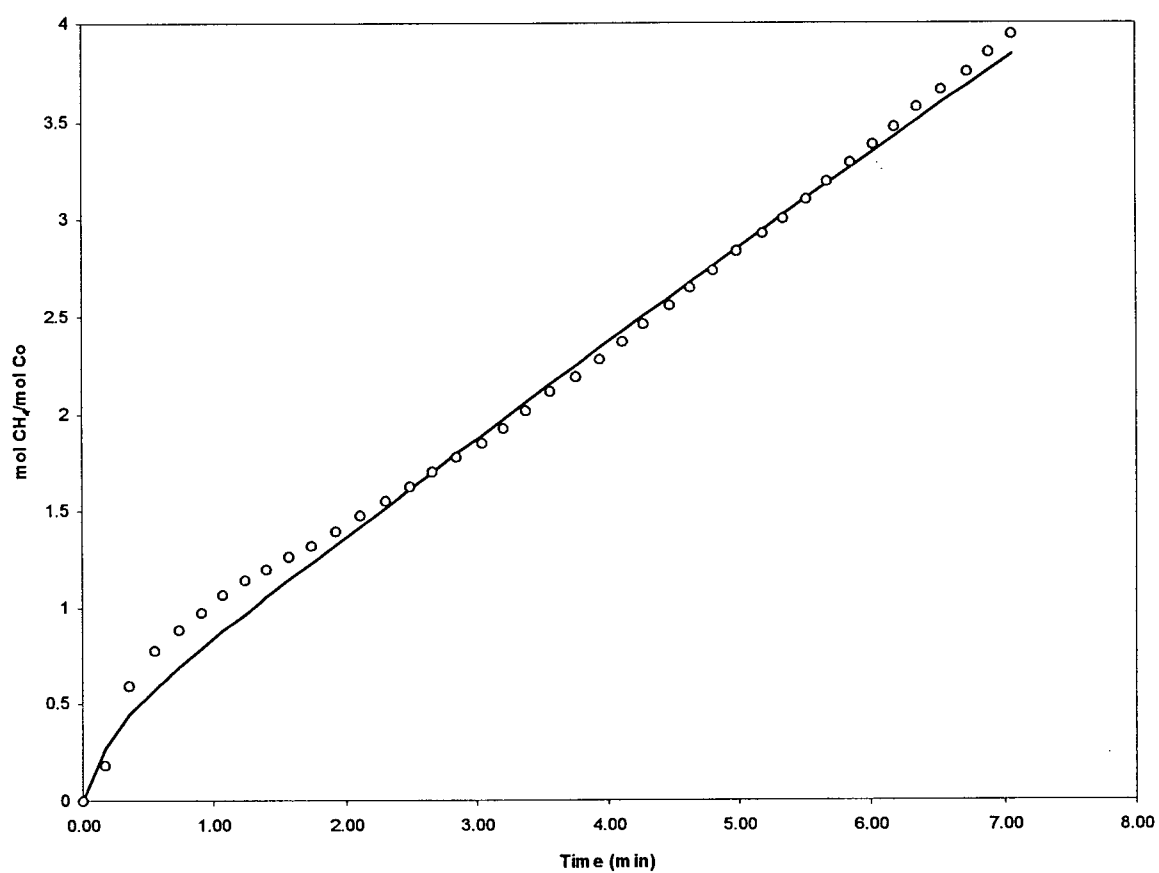


Figure 5.10. Cumulative moles of CH₄ consumed per mole of surface Co (O) measured during 7 min flow of 5%CH₄/95%Ar gas mixture at 54 ml/min and 450 °C over the A series 12%Co-SiO₂ catalyst, compared to model fit (—). Model parameter estimates given in the text.

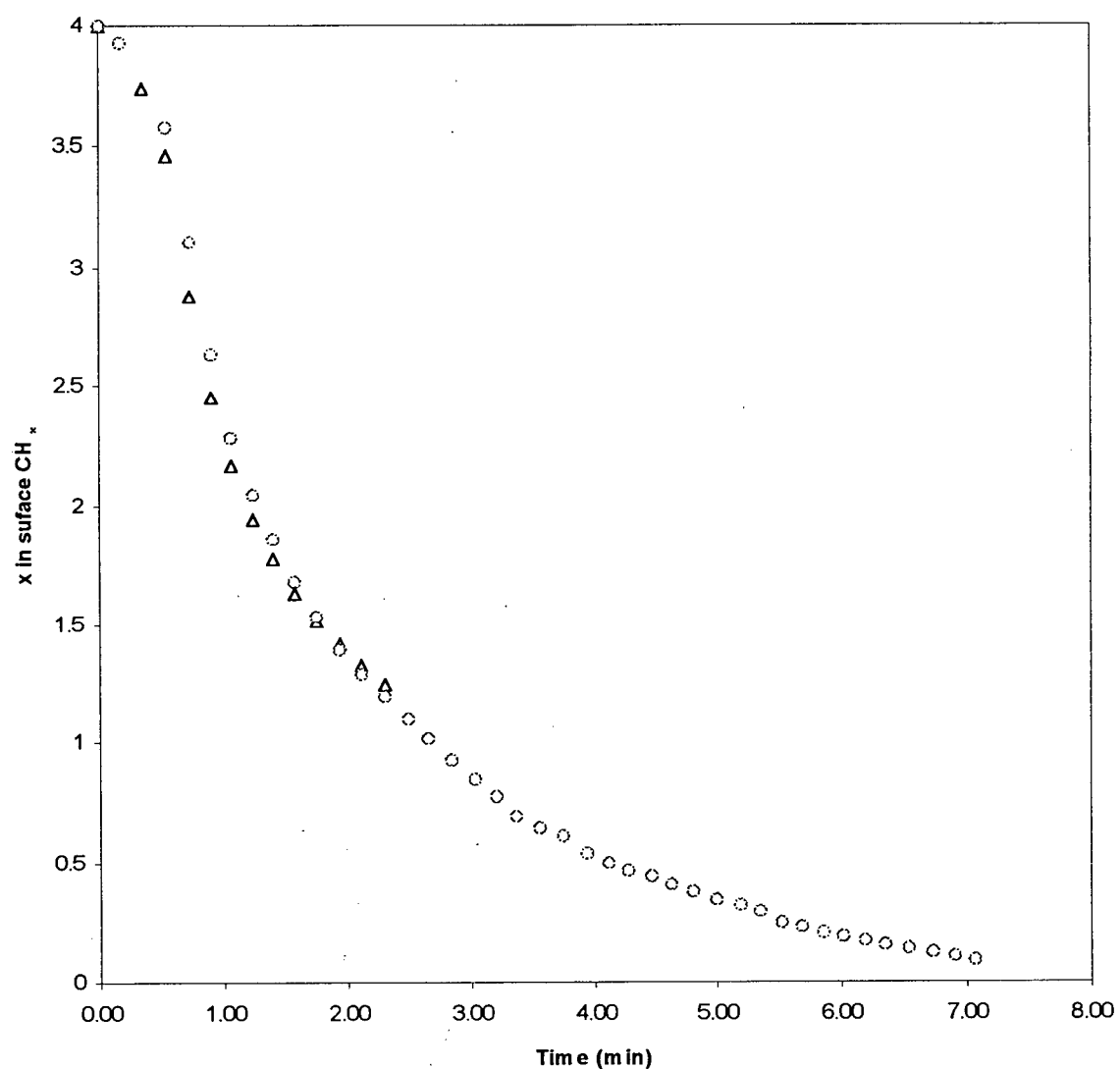


Figure 5.11. Value of x in the CH_x surface species during 2 min (Δ) and 7 min (O) flow of 5% CH_4 /95%Ar gas mixture at 54 ml/min and 450 °C over the A series 12%Co- SiO_2 catalyst.

In addition, the presence of CH and C₂H₄ species on Ru catalysts has been detected spectroscopically after activation (Lenz-Solomun, et al., 1994) and computational techniques (Koerts and van Santen, 1991) have shown that CH carbon species on a Pt catalyst can combine to form C₂₊ products more readily than CH_x species with $x > 1$. The data of Figure 5.11 suggest that to obtain $x = 1$, a reaction time of about 2.5 minutes is required at the conditions of the present study. The continuous dehydrogenation of carbon species with reaction time is an indication of production of less active carbon species. This is in accordance with previous reports of the transformation of more active carbon species to less active forms with increased reaction time (Koerts et al., 1992b).

5.5.2 Effect of Metal Loading

The A series Co-SiO₂ catalysts with 2, 5 and 12 wt% nominal Co were used to study the effect of catalyst loading on the CH₄ activation kinetics. Table 5.1 reflects the nominal metal coverage, reported as the moles of CH₄ reacted per mole of surface Co, and the estimated rate constants for CH₄ activation on the Co catalysts. At lower metal loadings the amount of activated CH₄ decreased and hence the relative error of measurement with QMS increased, leading to an increasing trend of R² with decreasing metal loading. The catalyst characterization data of Table 4.7 showed that by decreasing the Co loading, the extent of metal support interaction increased (i.e. there was a lower extent of reduction and increased silica decoration of the reduced Co).

Table 5.1 shows that an increased MSI not only increased the CH₄ activation activity (increased k_1), but also facilitated the migration of carbonaceous species from the metal to the

support (increased k_2). Expectedly, the rate constant of the hydrogen combination reaction was not influenced by the extent of the MSI. The electronic effect of supports on metal catalysts is mostly limited to a few atomic layers and is considered a short range effect (Raupp et al., 1987). The increased MSI at lower loadings observed in the present study suggests that the overall electronic effect of the support on the metal becomes significant and results in an increase in k_1 . In addition, as metal loading decreases, the metal-support contact surface area is expected to increase, resulting in an increases in the rate of migration (increased k_2).

Table 5.1. Effect of metal loading on reaction rate constants estimated at 450°C for a 2 minute reaction time with 5% CH₄ in Ar at 54 (STP)ml/min.

		Model Parameters				Std. Error	Regression
Catalyst		k_1	k_2	k_3	k_4	σ_e	Coefficient
Series A	CH ₄ Reacted						R^2
	mol CH ₄ /mol Co	min ⁻¹	min ⁻¹	min ⁻¹	min ⁻¹	mol CH ₄ /mol Co	%
12%Co-SiO ₂	1.81	5	23	0.7	1.8	0.02	99.7
5% Co-SiO ₂	2.01	117	153	0.5	12.0	0.06	98.5
2% Co-SiO ₂	2.3	121	346	0.6	10.9	0.37	93.1

5.5.3. Effect of Activation Temperature

The series A 12% Co-SiO₂ catalyst was also used to study the effect of temperature on the CH₄ activation kinetics. The metal coverage, the value of x of the CH_x carbon species after a reaction time of 2 minutes, and the rate constants are reported in Table 5.2 for

temperatures in the range 360-450 °C. In Appendix 2.4, the experimental kinetic data and kinetic model fit are compared.

Increasing temperature increased the CH₄ conversion and the metal coverage (total moles of CH₄ reacted per mole of surface Co), but decreased the H content of the resulting surface species. The activation energies for initial activation of CH₄ on Co (k_1), migration of the CH₃ species to the support (k_2) and H₂ evolution (k_3) were estimated from the data of Table 5.2 as 56, 48 and 171 kJ/mole, respectively.

Table 5.2. Effect of temperature on CH₄ activation over 12% Co-SiO₂ catalyst (Series A) measured with a 2 minute reaction time and 5% CH₄ in Ar at 54 (STP)ml/min.

Temperature	Total CH ₄ Reacted		x of CH _x	Model Parameters				σ_e	R ²
	Ratio	Conv.		k_1	k_2	k_3	k_4		
°C	mol CH ₄ /mol Co	%		min ⁻¹	min ⁻¹	min ⁻¹	min ⁻¹	ol CH ₄ /mol Co	%
360	0.5	7.2	2.1	1.4	5.9	0.01	0.87	0.01	90.6
390	0.6	9.8	1.4	2.0	5.1	0.24	1.13	0.03	99.2
450	1.3	20.8	0.9	5	16.8	0.56	1.24	0.01	99.7

The activation energy for k_1 was in reasonable agreement with the value of 42 kJ/mole reported for the activation of CH₄ on Co-SiO₂ catalysts at less than a monolayer coverage (Koerts et al., 1992a). Koerts et al. (1992a) reported the activation energy of CH₄ activation on Co based on cumulative H₂ production resulting from CH₄ activation. Extent of dehydrogenation of CH₄ on the catalyst and hence stoichiometry of the H₂ evolution during

CH₄ activation is a function of temperature (Koerts et al., 1992a). As a result the activation energy of 42 kJ/mole is considered an approximate value.

The apparent activation energy for the migration of CH_x species from Co to SiO₂ has not been reported. However, the activation energies for similar surface diffusion phenomena (e.g. surface diffusion of CO on Ni and H spillover onto Al₂O₃) have activation energies of similar magnitude (Conner and Pajonk, 1986; Roop et al., 1987). The activation energy of hydrogen desorption from silica-supported Co catalysts has not been reported either. However, the activation energy distribution for hydrogen desorption from silica-supported Ni catalysts has been reported to be in the range of 35 to 135 kJ/mole, depending on the preparation method, metal loading and surface coverage (Arai et al., 1995).

5.5.4. Effect of Support and K Promoter on the Activation of CH₄

Results of CH₄ activation on the 10% Co catalysts supported on SiO₂ and Al₂O₃, with and without 1 wt% K promoter (Boskovic et al., 1996) were also analyzed by the kinetic model. Catalyst characterization and details of experimental results for this section are reported by Boskovic et al. (1996). The experimental results and estimated rate constants are summarized in Table 5.3. Al₂O₃-supported Co catalysts showed a higher activity than SiO₂-supported catalysts (Boskovic and Smith, 1997; Boskovic et al., 1996, 1997) and this observation is reflected in the higher value of k_1 estimated for the 10%Co-Al₂O₃ catalyst compared to the 10%Co-SiO₂ catalyst. Previously it was suggested that the differences in total CH₄ activation obtained with the different supports may be due to differences in the rate of migration of the carbonaceous deposit from the metal to the support (Boskovic and Smith,

1997). The kinetic analysis shows, however, that the rate of CH₄ activation (k_1) was more important, being much greater on the Al₂O₃ supported catalyst than on the SiO₂ supported catalyst. Although differences in the estimated values of k_2 are shown in Table 5.3 for the two supports, the parameter estimates were based on a 1 minute activation time so the effect of migration did not dominate the kinetic analysis. Hence, the estimated values of the parameters k_2 , k_3 and k_4 have significant errors associated with them and definitive conclusions regarding changes in these parameters between the two supports were not possible.

The rate of migration (k_2) on the Al₂O₃ and SiO₂ supported catalysts increased significantly with addition of K promoter. The increase in k_2 may be due to the electron donor capability of the K promoter. The semi-empirical calculations referred to previously (Koerts and van Santen, 1991) show that increased d orbital filling decreases the adsorption energy of the CH₃ species to the metal. Hence, addition of K would be expected to weaken the Co-CH₃ bond and thereby increase the rate of migration or spillover to the support site, in agreement with the kinetic model parameters.

Table 5.3. Effect of support and K promoter on CH₄ activation at 450°C for a reaction time of 1 min.

Catalyst	Total CH ₄ Reacted		Model Parameters						σ_c	R^2
	Ratio	Conversion	k_1	k_2	k_3	k_4				
	mol CH ₄ /mol Co	%	min ⁻¹	min ⁻¹	min ⁻¹	min ⁻¹	mol CH ₄ /mol Co)	%		
10% Co-SiO ₂	1.15	37	5.8	18.6	74.1	11.0	0.05	98.5		
K-10%Co-SiO ₂	1.33	27	18.5	54.5	30.2	21.5	0.17	98.2		
Co-Al ₂ O ₃	1.92	32	17.7	11.5	57.4	5.6	0.08	99.1		
K-10%Co-Al ₂ O ₃	2.40	31	19.3	41.9	121.	8.9	0.21	99.1		

5.6. Conclusions

The initial high rate of CH_4 activation on supported Co catalysts at 450°C and 101 kPa, decreased rapidly but continued despite a nominal coverage of the surface Co by CH_x that was > 1 . The kinetic model developed to describe this observation assumed that activation of gas phase CH_4 on a Co site, was followed by migration of the resulting CH_x surface species from the Co to the support. Hence, the effects of reaction temperature, catalyst metal loading, support and promoter were interpreted in terms of the changes in the magnitudes of the activation and surface migration rate constants. The results indicate that metal-support interaction plays a key role in activation of CH_4 on the catalyst. Since the dispersion of the Co- SiO_2 catalysts were all about 5%, the possibility of strong effect of catalyst metal dispersion and particle size in this study can be ruled out.

Chapter 6

Hydrogenation

6.1. Overview

After deposition of the carbon species in the activation step, a low temperature (100 °C) isothermal hydrogenation was used to produce CH_4 and C_{2+} hydrocarbons. In the isothermal hydrogenation step, the most active surface species are hydrogenated. A temperature programmed surface reaction (TPSR) followed the isothermal hydrogenation step. In TPSR the temperature of the reactor was increased linearly, while pure H_2 flowed through the reactor. The reaction products were monitored by the calibrated quadrupole mass spectrometer (QMS). During TPSR the less active carbon species not hydrogenated in the isothermal hydrogenation step were hydrogenated at higher temperatures. Following TPSR a temperature programmed oxidation (TPO) was used to quantify the amount of inactive carbon species not removed in the TPSR step. In TPO, the temperature of the reactor was increased while pure O_2 flowed through the reactor. Any inactive carbon that had not been removed in TPSR reacted with O_2 to produce CO_2 at high temperature. The amount of CO_2 was quantified by the calibrated QMS.

Isothermal hydrogenation, TPSR and TPO comprised a complete set of carbon recovery experiments that could be compared to the initial carbon deposited in the activation step of the two-step CH_4 homologation cycle. A complete set of carbon recovery experiments was beneficial to establish a reasonable carbon balance in the experiments. In previous studies

of the two-step cycle, the quantitative analyses and results were based on either the CH_4 consumption in the activation step or hydrocarbon generation in the isothermal hydrogenation and TPSR. It was assumed that all the deposited carbon in the first step was recovered as hydrocarbons in the subsequent isothermal hydrogenation and TPSR (Koerts et al., 1992a; Pareja et al., 1994; Koranne et al., 1995; Guzzi, et al., 1997; Shen and Ichikawa, 1997). The complete carbon balance experiments of the present work showed that not all the carbon deposited in the first step was recovered by hydrogenation.

In this chapter the results of carbon recovery after CH_4 activation are presented in two sections. In the first section, the three carbon recovery steps of isothermal hydrogenation, temperature programmed surface reaction (TPSR) and temperature programmed oxidation (TPO) are discussed. The carbon recovered in the isothermal hydrogenation step, TPSR and TPO is compared to the carbon deposited in the activation step. The second section of this chapter is devoted to a discussion of the results of the effects of different operating variables on the two-step cycle.

6.2. Carbon Recovery

In this section, a typical set of isothermal hydrogenation, temperature programmed surface reaction and temperature programmed oxidation results are presented.

6.2.1 Isothermal Hydrogenation

A ten minute isothermal hydrogenation followed the activation step. During the isothermal hydrogenation, nine 0.25 μl samples of the reactor effluent were taken in 1 minute intervals, stored in the multi-loop valve of the GC and analyzed at the completion of the experiment. Figure 6.1 shows the profile of CH_4 , C_2H_4 and C_2H_6 production as a function of time in the isothermal hydrogenation of A series 12% Co-SiO₂ catalyst after 2 min activation of 5% CH_4/Ar at 450 °C. By numerical integration of the profiles, the number of moles of each hydrocarbon and carbon selectivity of C_{2+} products were determined.

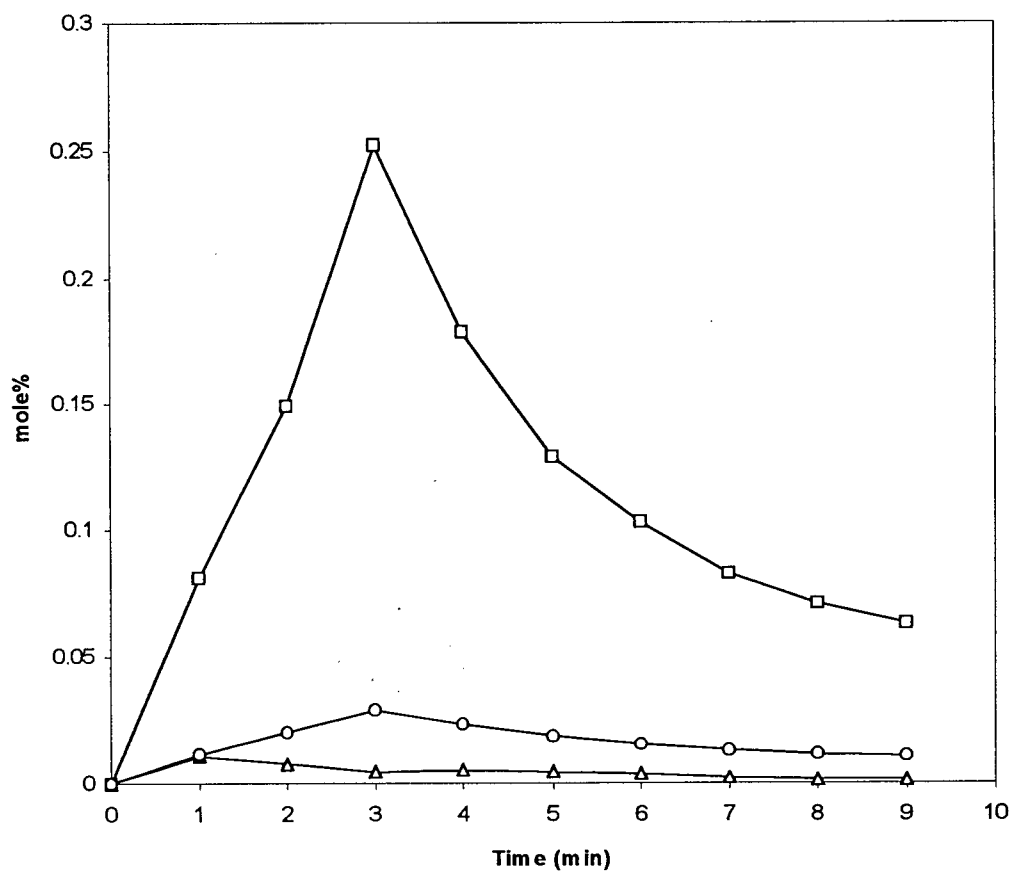


Figure 6.1. Profile of CH₄ (□), C₂H₄ (O) and C₂H₆ (Δ) production as a function of isothermal hydrogenation at 100 °C in 11 ml/min H₂ flow over the A series 12%Co-SiO₂ catalyst after 2 min activation with 5% CH₄/Ar mixture at 450 °C.

6.2.2. Temperature Programmed Surface Reaction

Temperature programmed surface reaction (TPSR) followed the isothermal hydrogenation step. The calibrated QMS was used to monitor the products in the TPSR. Figure 6.2 shows the TPSR profile of the A series 12% Co-SiO₂ catalyst after 2 min activation of 5%CH₄/Ar at 450 °C and 10 min isothermal hydrogenation. CH₄ was the only significant product in the TPSR.

Figure 6.2 shows two CH₄ production peaks at about 200 °C and 540 °C due to hydrogenation of C_β and C_γ carbon species. The 10 min isothermal hydrogenation at 100 °C removed the C_α active carbon form. The amount of inactive carbon in the TPSR was determined by numerical integration of the peak areas of C_β and C_γ carbon species.

Activation of CH₄ with transition metal catalysts generates H₂ and surface carbon species (see also section 2.2.1). In order of decreasing reactivity with H₂ in a TPSR, the carbon species have been classified as C_α, C_β and C_γ. C_α is the most active type of carbon that produces CH₄ and C₂₊ at low temperature (ca. 100 °C). C_β is less active and C_γ the least active carbon. These generate only CH₄ in the temperature range of 200 and 500 °C, respectively.

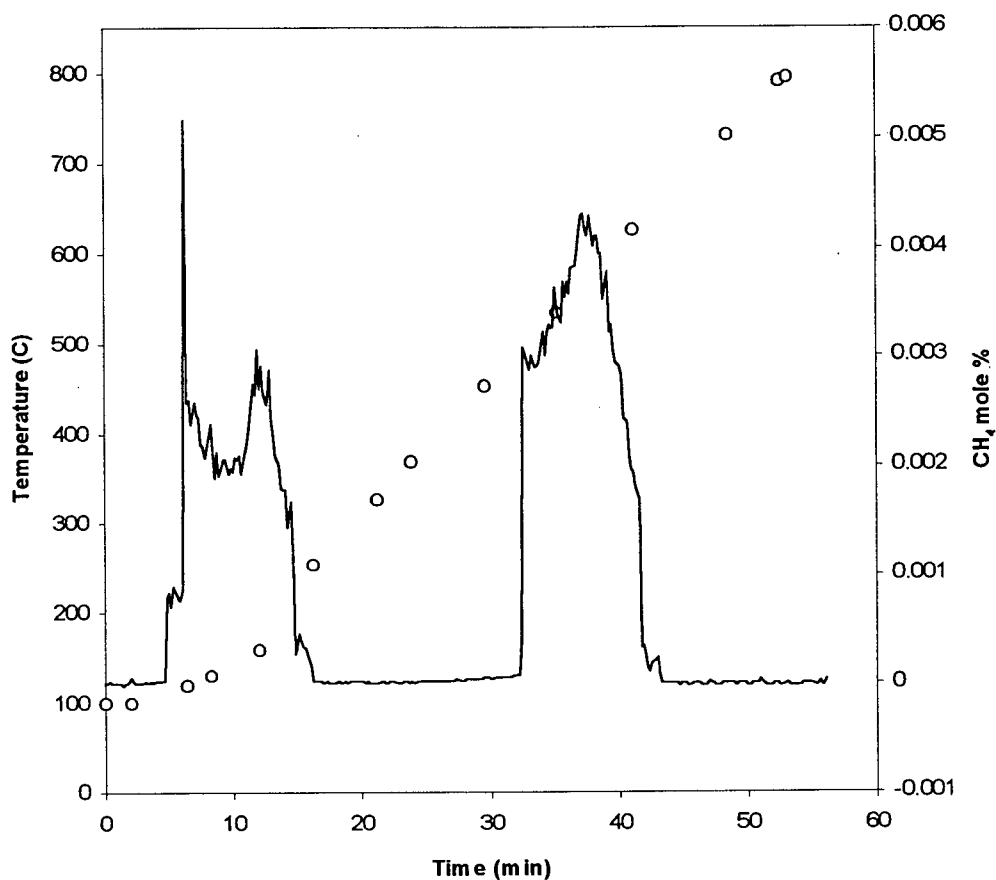


Figure 6.2. Profile of CH₄ production (—) and temperature (O) as a function of time in temperature programmed surface reaction (TPSR) in 11 ml/min of H₂ flow on A series 12%Co-SiO₂ catalyst.

Activation of CH₄ (2 min flow of 5% CH₄/Ar mixture at 450 °C) followed by 10 min isothermal hydrogenation at 100 °C.

6.2.3. Temperature Programmed Oxidation

Temperature programmed oxidation (TPO) was used to quantify the amount of carbon that was not removed by TPSR in H_2 . In TPO, the reactor temperature was increased in an O_2 flow and the reactor product was analyzed by the calibrated QMS. Figure 6.3 shows the CO_2 production profile and the reactor temperature as a function of time.

By numerical integration of the CO_2 production profile, the total amount of inactive carbon was determined. In the TPO step, in addition to CO_2 , the mass numbers 18, 31 and 28 corresponding to H_2O , CH_3OH (or C_2H_5OH), and CO were also monitored. H_2O mass number ($m/e=18$) showed a distinct peak due to H_2O production from oxidation of the adsorbed hydrogen in the catalyst. The trends of mass numbers 31 and 28 did not show any CH_3OH , C_2H_5OH or CO oxygenates production in the TPO step of the two-step cycle experiments.

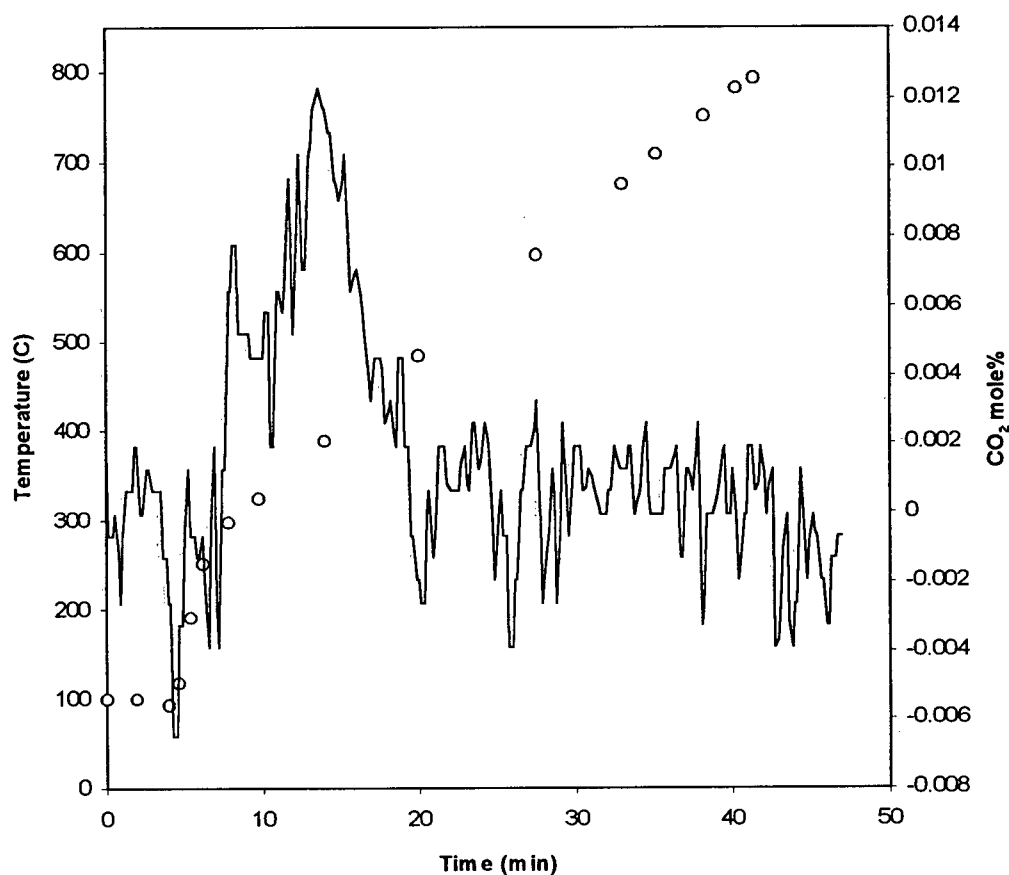


Figure 6.3. Profile of CO₂ production (—) and temperature (O) as a function of time during temperature programmed oxidation (TPO) in 11 ml/min of O₂ flow on A series 12%Co-SiO₂ catalyst.

(Activation: 2 min flow of 5% CH₄/Ar mixture at 450 °C)

6.2.4. Carbon Balance

To examine the reliability of the two-step cycle experiments, and to establish the fate of carbon generated from activation of CH_4 , the amount of carbon in the activation step was compared with that from hydrocarbons produced in the isothermal hydrogenation step, subsequent temperature programmed surface reaction (TPSR) in H_2 and finally temperature programmed oxidation (TPO). Since the activation, TPSR and TPO steps were monitored by the calibrated quadrupole mass spectrometer (QMS) and the isothermal step was monitored by both the gas chromatograph (GC) and QMS, a reasonable carbon balance was an indication of an accurate analysis of the complete set of reaction cycles.

Table 6.1 presents results from a series of experiments aimed at quantifying the carbon balance that could be achieved from each of the reaction steps. The first column of the table corresponds to an experiment in which the isothermal hydrogenation step was omitted. After activation the catalyst was exposed to TPSR and TPO only. In the second column, the results of an experiment without TPSR are shown. In this experiment, the catalyst was exposed to TPO after activation and isothermal hydrogenation. The third column summarizes the results of an experiment that had an activation and TPO step without exposure to hydrogen in isothermal hydrogenation or TPSR. The fourth column corresponds to a complete experiment with isothermal hydrogenation, TPSR and TPO after activation of CH_4 on the reduced catalyst.

Comparison of the relative magnitude of the deposited and recovered carbon in different steps of isothermal hydrogenation, TPSR and TPO showed that less than 10% of the deposited carbon was recovered in the isothermal hydrogenation step. Depending on the

experimental sequence 30-40% of the deposited carbon was recovered in the TPSR step and approximately 50% of the deposited carbon was recovered in the TPO step.

The last row in Table 6.1 represents the error in carbon balance which was calculated as: $\% \text{ error} = 100 \times [(\text{mol carbon deposited in activation step})/(\text{mol total carbon recovered}) - 1]$. The carbon balance error in a complete two-step cycle reaction was less than $\pm 20\%$.

Table 6.1. Summary of carbon balance calculations for A series 12% Co-SiO₂ catalyst.

<i>Steps</i>	<i>Ac, TPSR, TPO</i>	<i>Ac, Is, TPO</i>	<i>Ac, TPO</i>	<i>Ac, Is, TPSR, TPO</i>
Total $\mu\text{mol C}_{\text{in Ac}}$	61	60	63	57
$\mu\text{mol C}_{\text{out Is}}$	-	2	-	5
$\mu\text{mol C}_{\text{out TPSR}}$	27	-	-	19
$\mu\text{mol C}_{\text{out TPO}}$	33	62	65	25
Total $\mu\text{mol C}_{\text{out}}$	60	64	65	49
% error	+2	-7	-3	+14

Catalyst: 0.5 g reduced A series 12%Co-SiO₂

Activation (Ac): 2 minutes exposure to 5% CH₄/Ar at 450 °C

Isothermal hydrogenation (Is): 10 minutes exposure to 11 ml/min of H₂ at 100 °C

Temperature programmed surface reaction (TPSR): Exposure to 11 ml/min of H₂

Temperature programmed oxidation (TPO): Exposure to 11 ml/min of O₂

The results in Table 6.1 prove that a TPSR alone does not remove all of the inactive carbon from the catalyst. In previous studies (Koerts et al., 1992a; Pajero et al., 1994;

Koranne et al., 1995; Guzzi, et al., 1997; Shen and Ichikawa, 1997) the amount of carbon recovered from the isothermal hydrogenation and TPSR steps was assumed equal to the deposited carbon in the activation step. Based on the results of the present work in these studies, the presence of inactive carbon which can only be removed by TPO, has been overlooked. The data in Table 6.1 showed that inactive carbon (which is only removed by TPO) may account for as much as 50% of the deposited carbon. Product yield data reported based on the amount of carbon deposition in the activation step or the carbon recovered in the isothermal reaction and TPSR in H_2 , can be in error by a factor of 2.

6.3. Effect of Operating Variables

In this section the effect of different operating variables on the performance of the two-step cycle is discussed.

6.3.1. Effect of Loading

Using SiO_2 -supported catalysts with 2, 5 and 12% Co loading the effect of catalyst metal loading on the two-step cycle was studied. Table 6.2 shows a summary of the results from the hydrogenation step on these catalysts.

The data of Table 6.2 show that decreasing the catalyst metal loading from 12% to 2% increased the catalyst effectiveness for CH_4 activation. As discussed above, decreasing the metal loading increased the metal-support interaction, resulting in faster migration of carbon species from the primary activation site on the metal to the support (see section 5.4.2).

Table 6.2 also presents the hydrogen content (x) of the surface species CH_x generated in the activation step. Computational work based on semi-empirical quantum chemistry calculations of the reaction path for C-C bond formation (Koerts and van Santen, 1991) has shown that the activation energy for the combination of three-fold bonded carbon with a CH_2 species to form a vinylidene surface species was the lowest of all possible combinations.

Table 6.2. Effect of the catalyst metal loading on its hydrogenation performance.

<i>Catalyst</i>	<i>12% Co-SiO₂</i>	<i>5% Co-SiO₂</i>	<i>2% Co-SiO₂</i>
$\mu\text{mol CH}_4/\mu\text{mol Co (Ac)}$	1.8	2.0	2.3
x of CH_x	1.1	1.3	1.6
C_{2+} selectivity (Is)	17	5	2
C_{2+} yield/site, mol C_{2+} /mol Co(Is)	0.01	0.004	0.001
%C recovery (Is+TPSR)	43	21	12

Catalyst: 0.5 g reduced A series 12%Co-SiO₂, 5%Co-SiO₂ or 2%Co-SiO₂

Activation (Ac): 2 minutes exposure to 5% CH₄/Ar at 450 °C

Isothermal hydrogenation (Is): 10 minutes exposure to 11 ml/min of H₂ at 100 °C

Temperature programmed surface reaction (TPSR): Exposure to 11 ml/min of H₂

Experimental results (Koerts et al., 1992a) have also confirmed that on silica supported Rh, Co and Ru catalysts, the C-C bond formation was favorable for CH_x species in which the average value of x was about one. The trend of increasing hydrogen content of CH_x surface

species with decreasing metal loading of the catalysts, indicate that the C-C bond formation tendency of the surface species decreases with decreasing metal loading. Hence the C_{2+} carbon selectivity would be expected to decrease with decreasing metal loading and the experimental data of Table 6.2 confirm this observation.

C_{2+} hydrocarbons are generated in the isothermal hydrogenation of species adsorbed on the metal surface only in the isothermal hydrogenation step. The decreasing trends of C_{2+} selectivity and C_{2+} yield per site (number of moles of C_{2+} generated/ number of moles of surface Co) with metal loading indicate that although lower loading catalysts have higher CH_4 activation capability, they have lower C-C bond formation capability.

The final set of data presented in Table 6.2 shows the total percent recovery of initially deposited carbon by the isothermal and TPSR hydrogenation steps. The carbon recovery also decreases with decreased metal loading of the catalyst.

With reference to the previous discussion (section 5.4.2), by decreasing the metal loading of the catalyst, the metal-support interactions increased. In the activation step, increased metal-support interactions give rise to a higher rate of migration of carbon species from the initial activation metal site to the support site. Carbonaceous species residing on the support are not only inactive for C-C bond formation in isothermal hydrogenation, but they are not easily hydrogenated in TPSR. Hence, although a lower loading metal catalyst performs better in the activation step, it generates more inactive carbon on the support and less C_{2+} product in the isothermal hydrogenation step. Based on these results, to obtain a higher yield of C_{2+} products, a higher metal loading is recommended.

6.3.2. Activation Time

In the activation step of the two-step cycle, the carbonaceous species resulting from CH_4 activation on the metal not only migrate to the support site but also dehydrogenate and accumulate on the catalyst. As the duration of the activation step is increased, more carbon is deposited on the catalyst. In addition, a longer exposure to the high activation temperature can lead to a decrease in the amount of active carbon due to migration and aging of the carbon species. To examine these phenomena, 5% CH_4/Ar was activated for 1, 2 and 7 minutes on A series 12% Co-SiO_2 catalyst. The deposited carbon species were hydrogenated in the isothermal and TPSR steps, and then oxidized in TPO. Table 6.3 summarizes the results from these experiments.

The data of Table 6.3 show that longer reaction times of CH_4 at 450°C generate more carbon species on the catalyst and these species dehydrogenate on the surface resulting in decreased values of x in CH_x . In the subsequent isothermal hydrogenation step, selectivity to C_{2+} hydrocarbons and the total amount of carbon recovered, decreased in the isothermal hydrogenation step as the activation time increased. Finally the last row in the table corresponds to the total carbon recovery in the form of CH_4 in the TPSR step.

A longer CH_4 activation time generates more carbon deposits on the catalyst. Longer exposure to high temperature has two effects on the deposited carbon species. First, more carbon species migrate from the metal site to the support site. Second, the surface carbon species undergo more dehydrogenation. This effect is reflected in the x value of the CH_x shown in Table 6.3. The combined effect of temperature and time is loss of activity of surface carbon species and lower selectivity and carbon recovery in the isothermal hydrogenation step.

Table 6.3. Effect of activation time on the hydrogenation step.

<i>activation time (min)</i>	<i>7</i>	<i>2</i>	<i>1</i>
$\mu\text{mol CH}_4$ consumed (Ac)	177	71	45
$\mu\text{mol H}_2$ generated (Ac)	352	110	64
x of surface CH_x	0.0	0.9	1.1
$\mu\text{mol C}_{2+}$ generated (Is)	0.1	0.16	0.24
% C_{2+} selectivity (Is)	5	6	7
$\mu\text{mol C}$ produced (Is)	4	6	7
$\mu\text{mol C}$ produced (TPSR)	163	38	1

Catalyst: 0.5 g reduced A series 12%Co-SiO₂

Activation (Ac): 1, 2 or 7 minutes exposure to 5% CH₄/Ar at 450 °C

Isothermal hydrogenation (Is): 10 minutes exposure to 11 ml/min of H₂ at 100 °C

Temperature programmed surface reaction (TPSR): Exposure to 11 ml/min of H₂

Using the results of the kinetic model calculation of coverage of different species on the catalyst as a function of activation time (Figure 5.4 and Figure 5.5), one can safely assume that after approximately one minute of reaction, the coverages of different species reach their asymptotic values, and the difference between one and two minutes exposure on the coverage of different species on catalyst metal becomes negligible. As a result, the effect of migration of carbon species on the catalyst after one and two minutes reaction is the same. Consequently the only major difference between the carbon species in the three experiments of Table 6.3 is the activity of the surface carbon species which is reflected in the hydrogen content of the

surface species. Longer exposure of surface species to a high activation temperature of 450 °C generates dehydrogenated surface carbon species that are less active in C-C bond formation, resulting in less C₂₊ generation and lower C₂₊ selectivity. The low carbon reactivity in the isothermal hydrogenation step indicates that the carbon species are less active not only for C-C bond formation but also for hydrogenation to produce CH₄.

TPSR of the carbon species after the isothermal step, generated a larger amount of CH₄ on the catalyst as the exposure time to CH₄ increased. This is due to the larger amount of initial carbon deposited on the catalyst.

It is also worth noting that the 163 μmol CH₄, produced in the experiment with 7 minutes exposure, was more than the 48 μmol surface Co atoms available on the catalyst. This suggests that in TPSR, a large amount of carbon residing on the support can also be hydrogenated. The mechanism of this phenomenon is not clearly known, but may be related to a H spillover mechanism.

6.3.3. Activation Temperature

The effect of activation temperature on the two-step cycle was studied by activation of CH₄ in the temperature range of 360 to 450 °C. Table 6.4 summarizes the results of this study.

Data in Table 6.4 show that decreasing the activation temperature decreased the amount of both activated CH₄ and generated H₂. The x-value of CH_x carbon species also increased as a result of decreasing temperature of activation. Results of the kinetic model showed that in the temperature range of 360 to 450 °C, the coverage of adsorbed H atoms on

the surface was about 60% and it did not change appreciably with activation temperature. Consequently, the higher x value of CH_x species at low temperature indicates higher hydrogen content of the surface species. Data of C_{2+} generation and selectivity in the isothermal hydrogenation step showed that C_{2+} production dropped from 0.28 μmol for an activation temperature of 450 °C to 0.09 μmol for an activation temperature of 360 °C. C_{2+} selectivity also dropped by a factor of 3 by decreasing the temperature of activation from 450 °C to 360 °C.

Table 6.4. Effect of activation temperature on the hydrogenation step.

<i>Activation Temperature</i> (°C)	450	390	360
$\mu\text{mol CH}_4$ consumed (Ac)	57	37	27
$\mu\text{mol H}_2$ generated (Ac)	90	47	26
x of surface CH_x	0.9	1.4	2.1
$\mu\text{mol C}_{2+}$ generated (Is)	0.28	0.21	0.09
% C_{2+} selectivity (Is)	12	7	4
$\mu\text{mol C}$ produced (TPSR)	18.7	0.6	0.1

Catalyst: 0.5 g reduced A series 12%Co-SiO₂

Activation (Ac): 2 minutes exposure to 5% CH₄/Ar at 360, 390 or 450 °C

Isothermal hydrogenation (Is): 10 minutes exposure to 11 ml/min of H₂ at 100 °C

Temperature programmed surface reaction (TPSR): Exposure to 11 ml/min of H₂

The last row in Table 6.4 shows the total amount of CH_4 recovered in the TPSR step after isothermal hydrogenation. By decreasing the activation temperature from 450 °C to 360 °C a significant drop in carbon recovery in the TPSR step was observed.

Decreasing the activation temperature had a number of effects on the deposited carbon species. At lower activation temperature, the total amount of carbonaceous species deposited on the catalyst was lower. As a result, less carbon was available on the surface for combination. Activation temperature also affects the nature of the carbon species. A low activation temperature generated carbon species with higher hydrogen content. As has been demonstrated by computational methods (Koerts and van Santen, 1991), carbon species with high hydrogen content have lower tendency for C-C bond formation. This result has also been demonstrated by experimental observations (Koerts and van Santen, 1991; Koerts et al., 1992a) that a CH_x with x close to 1 is the most active type of carbon species for C-C bond formation. Higher mobility of carbon species at high temperature contributes to the migration of more carbon from the metal site to the support site, resulting in production of more inactive carbon on the support at high temperature.

6.3.4. Carbon Aging

Carbon species generated by CH_4 activation transform to less active forms by exposure to high temperature. The extent of this transformation depends on the exposure period (Koerts et al., 1992a; Carstens and Bell, 1996). In the present study, experiments were performed with different time delays between the activation and the isothermal hydrogenation steps in an attempt to quantify the carbon aging effect.

In these experiments, the A series 12% Co-SiO₂ catalyst was exposed to a 5% CH₄/Ar mixture at 450 °C for 2 minutes. The deposited carbon species were then aged in Ar atmosphere for 5, 10 and 20 minutes at 100 °C and hydrogenated isothermally at 100 °C for 10 minutes. A TPSR and TPO followed the isothermal hydrogenation step. A summary of the results from this set of experiments is given in Table 6.5.

The operating conditions for the activation step of this set of experiments were approximately the same. In the activation step, more than a nominal monolayer of carbon was deposited on the catalyst. Increasing the age of the carbonaceous deposits (by increasing the time delay between the activation and the isothermal step) decreased the production of both CH₄ and C₂₊ hydrocarbons in the isothermal hydrogenation step. A decreasing trend of C₂₊ selectivity with increased deposit age indicates that the effect of aging was more important for C-C bond formation than hydrogenation of carbon species to CH₄. Interestingly, there was some C₂H₄ production for the shorter aging times which decreased to zero at longer aging times. A small amount of C₃₊ hydrocarbons generated in the five minutes aging experiment and its absence in the longer aged experiments, indicates that the most active carbon which is capable of multiple C-C bond formation either undergoes C-C bond breakage to generate C₂₊ and eventually CH₄ or further C-C bond formation to produce inactive polycarbon species.

The total amount of carbon recovered in the isothermal hydrogenation is reported as C_α in Table 6.5.

Table 6.5. Effect of carbon aging on the hydrogenation step.

<i>Carbon Aging</i> <i>(min)</i>	<i>5</i>	<i>10</i>	<i>20</i>
$\mu\text{mol CH}_4$ consumed (Ac)	52	51	55
$\mu\text{mol H}_2$ generated (Ac)	79	78	81
x of surface CH_x	0.95	0.95	1.04
CH_4 production (μmol)	4.8	3.9	2.8
C_{2+} production (μmol)	0.84	0.74	0.21
% C_{2+} selectivity (Is)	29*	27	13
$\text{C}_2\text{H}_4/\text{C}_2\text{H}_6$ product	0.28	0.29	0
C_α production (μmol)	6.6	5.4	3.2
C_β production (μmol)	6.2	4.3	0.1
C_γ production (μmol)	18.6	19.5	N/A ⁺
$\mu\text{mol C}$ produced (TPSR)	24.8	23.8	N/A ⁺
CO_2 production in TPO (μmol)	11	15.3	26.9

* Selectivity includes both the C_2 and C_3 products.

+ Because of mass spectrometer failure this data point was not available.

Catalyst: 0.5 g reduced A series 12%Co-SiO₂

Activation (Ac): 2 minutes exposure to 5% CH₄/Ar at 450 °C

Isothermal hydrogenation (Is): 10 minutes exposure to 11 ml/min of H₂ at 100 °C

Temperature programmed surface reaction (TPSR): Exposure to 11 ml/min of H₂

Temperature programmed oxidation (TPO): Exposure to 11 ml/min of O₂

TPSR after isothermal hydrogenation showed that the amount of C_β decreased with aging time while the least active form carbon C_γ increased with aging time (for the first ten minutes). This indicates that aging decreased not only the amount of the most active carbon C_α , but also the amount of less active carbon C_β . The increasing trend of CO_2 production (in the TPO step) with aging indicated that the least active C_γ deactivated to a less active carbon that could only be recovered by TPO.

The effect of aging on the carbon species with more than a monolayer nominal coverage proved to be somewhat similar to the case with less than a monolayer coverage in the sense that the activity of carbon species decreases with aging. The fact that even at 100 °C aging can have significant effects on the activity and distribution of the carbon species and can generate inactive carbon has not been reported in the literature. In previous work (Koerts et al., 1992a; Koranne et al., 1995; Carstens and Bell, 1996), it was assumed that fast cooling of the carbon species after activation, to about 100 °C (the temperature of the isothermal hydrogenation step) prevented deactivation of the carbon species. The results of the present study proved that at a temperature of 100 °C there were significant deactivation effects due to aging of the carbon species.

6.3.5. Reaction Cycle

To study the effect of the number of two-step cycles on the catalyst, the A series 12% Co-SiO₂ catalyst was exposed to a series of three CH₄ activation, isothermal hydrogenation

and TPSR cycles without the TPO step. Only at the end of the third cycle was TPO performed. The results of this study are summarized in Table 6.6.

Table 6.6. Effect of reaction cycle on the hydrogenation step.

<i>Cycles of Operation</i>	<i>1st</i>	<i>2nd</i>	<i>3rd</i>
$\mu\text{mol CH}_4$ consumed (Ac)	66	53	48
$\mu\text{mol H}_2$ generated (Ac)	95	51	42
x of surface CH_x	1.1	2.1	2.2
CH_4 production (μmol)	7.7	2.1	1.83
C_{2+} production (μmol)	0.30	0.04	0.01
% C_{2+} selectivity (Is)	7.2	3.7	1.0
C recovered in TPSR (μmol)	10	38	36
C recovered in TPO (μmol)	-	-	6

Catalyst: 0.5 g reduced A series 12%Co-SiO₂

Activation (Ac): 2 minutes exposure to 5% CH₄/Ar at 450 °C

Isothermal hydrogenation (Is): 10 minutes exposure to 11 ml/min of H₂ at 100 °C

Temperature programmed surface reaction (TPSR): Exposure to 11 ml/min of H₂

Temperature programmed oxidation (TPO): Exposure to 11 ml/min of O₂

In the activation step, increasing the number of cycles decreased the amount of generated H₂ and activated CH₄, indicative of a gradual loss of activity of the catalyst as the

number of operating cycles increased. However, by increasing the number of cycles, the extent of dehydrogenation of surface carbon species decreased. As discussed in section 6.2.1, a higher H content of the surface carbon species decreased the activity of the carbon species in the C-C bond formation reaction. As has been discussed previously, activation of CH_4 with more than a monolayer metal coverage generates some inactive carbon species which cannot be removed by TPSR.

The build-up of inactive carbon on the catalyst not only reduced the activity of the catalyst, but also affected the activity of the generated surface species. Surface CH_x species with x close to one are most active for C-C bond formation. Carbon species with $x > 1$ are less active in the isothermal hydrogenation step. By increasing the number of cycles, not only did the amount of CH_4 and C_2H_6 products decrease, but the C_{2+} selectivity also decreased by a factor of seven.

TPSR after the isothermal hydrogenation showed that except for the first cycle, about $40\text{ }\mu\text{mol}$ of carbon was recovered in TPSR. This is due to stronger interaction of inactive carbon species with the catalyst in the first cycle. Inactive carbon species in the second and the third cycles have a weaker interaction with the support and are more easily removed by the TPSR.

6.3.6. Isothermal Medium

In the two-step CH_4 homologation on supported metal catalysts, the question of whether the C-C bond formation occurs during isothermal hydrogenation or if the carbon

species combine before hydrogenation, needs to be answered. In an attempt to address this question, different gases were used in place of H_2 in the isothermal step.

B series 8% Co-SiO₂ catalysts were exposed to 5% CH₄/Ar gas at 450 °C for 2 min to activate CH₄ and generate carbon deposits on the catalyst. After purging the reactor while cooling, the catalyst was exposed to either H₂, Ar, CO₂ or O₂ at 100 °C for ten minutes. In each experiment, nine samples were taken and stored for later analysis by GC. After purging the isothermal medium, TPSR in H₂ and TPO were performed to determine the amount of less active carbon species in each case. The results of these experiments are summarized in Table 6.7.

Table 6.7 shows that the activation conditions were practically the same for all experiments. The isothermal hydrogenation data show that small amounts of C₂₊ and CH₄ with a C₂₊ carbon selectivity of 13% were generated on the catalyst. A large part of the deposited carbon species were removed as less active and inactive carbon in the TPSR and TPO steps.

The isothermal reaction with Ar generated some CH₄ and almost the same amount of C₂H₆ as the isothermal hydrogenation. The carbon selectivity of C₂₊ in the isothermal Ar experiment was about 39%. The carbon recovery in the isothermal Ar experiment was almost half that of the isothermal hydrogen experiment. Comparing with the isothermal hydrogenation, in Ar medium more carbon was recovered in TPSR and less inactive carbon was recovered in TPO.

The presence of chemisorbed H in the isothermal step proves that either the Ar purge after CH₄ activation did not remove the chemisorbed H, or surface carbon species underwent

further dehydrogenation to generate chemisorbed H on the Co catalyst. The first possibility can be ruled out because H chemisorption at temperatures above 100 °C is negligible (Reuel and Bartholomew, 1984).

Table 6.7. Effect of the isothermal medium on the product distribution.

<i>Isothermal Medium</i>	<i>H₂</i>	<i>Ar</i>	<i>CO₂</i>	<i>O₂</i>
μmol CH ₄ consumed (Ac)	55	51	60	55
μmol H ₂ generated (Ac)	81	76	86	78
x of surface CH _x	1.0	1.0	1.1	1.1
CH ₄ production (μmol)	2.76	0.87	0.90	0.63
C ₂₊ production (μmol)	0.21	0.28	0.04	0.04
% C ₂₊ selectivity (Is)	13	39	8	11
C recovered in isothermal (μmol)	3.20	1.43	0.98	0.71
C recovered in TPSR (μmol)	14.3	24.7	58.5	-
C recovered in TPO (μmol)	26.9	9.9	7.2	8.6

Catalyst: 0.5 g reduced B series 8%Co-SiO₂

Activation (Ac): 2 minutes exposure to 5% CH₄/Ar at 450 °C

Isothermal hydrogenation (Is): 10 min exposure to 11 ml/min of H₂, Ar, CO₂ or O₂ at 100 °C

Temperature programmed surface reaction (TPSR): Exposure to 11 ml/min of H₂

Temperature programmed oxidation (TPO): Exposure to 11 ml/min of O₂

It is possible that after CH_4 activation and Ar purge, surface carbon species undergo further dehydrogenation to produce chemisorbed H on the surface. Surface H then reacts with some surface carbon species and saturates some of the H deficient CH_4 and C_{2+} precursors which then desorb and are removed by the gas flow in isothermal step.

Isothermal reaction in CO_2 also generated some CH_4 and a small amount of C_2H_6 . The large amount of carbon recovered in TPSR was due to adsorption of CO_2 .

Isothermal O_2 generated the smallest amounts of CH_4 and almost the same quantity of C_2H_6 as was obtained for the isothermal CO_2 case. There was a 6.5°C temperature rise during the isothermal O_2 flow. Product analysis showed some H_2O production in the isothermal step. The amount of CO , CH_3OH or $\text{C}_2\text{H}_5\text{OH}$ was negligible.

Comparison of the results of the four different reaction media under isothermal conditions showed that H_2 generated the highest amount of CH_4 , while the amounts of CH_4 produced in the Ar, CO_2 and O_2 reaction media were approximately the same. Surprisingly, H_2 and Ar generated almost the same amount of C_2H_6 . This indicates not only that C-C bond formation occurs to some extent before the isothermal step but also that the homologation products can be released from the catalyst by an inert medium. In the activation step, carbon species with an overall H/C ratio of 1 to 1.1 were deposited on the catalyst. The fact that C_{2+} products with H/C ratio of 4 to 3 could be produced by Ar proves that there is C-C bond formation, together with breakage and hydrogen exchange on the catalyst after activation. The temperature rise of 6.5°C and H_2O production in the isothermal O_2 medium proves that there was chemisorbed H on the catalyst surface before the isothermal step. Since after activation the catalyst was purged with Ar the possibility of adsorbed hydrogen remaining on the surface

is ruled out. The adsorbed hydrogen must have come from the adsorbed CH_x species after activation.

These results show that as a result of C-C bond formation and breakage and hydrogen exchange between the surface species as well as the metal surface, some C_{2+} products are produced on the catalyst surface before the isothermal step. Some of the C_{2+} products are saturated and are readily desorbed, whereas some of the species need hydrogen to generate CH_4 and C_2H_6 . In isothermal hydrogenation, hydrogen acts partially as a physical desorbing medium and it furnishes H for production of CH_4 and C_2H_6 from adsorbed species. H can also facilitate hydrogenolysis of some of the C-C bonds which are already formed on the surface.

Possibly, CO_2 dissociated on the catalyst, generating some carbon species and adsorbed oxygen. The adsorbed oxygen reacts with active carbon species on the catalyst and reduces the production of CH_4 and C_2H_6 products dramatically.

6.4. Conclusion

Based on the results discussed in this chapter, the following sequence of steps in the surface reaction can be proposed. After the initial activation of CH_4 on the catalyst that produces surface carbon species, some of the carbon species migrate from the active metal site to the support. C-C bond formation and C-C bond breakage reactions start immediately after carbon deposition in the activation step. Longer exposure to high temperature leads to deactivation of the carbon species partially because of more migration of carbon species from the metal to the support site. Decreasing temperature from the high activation temperature to the lower isothermal hydrogenation temperature reduces the rate of the deactivation reactions.

Exposure to any gas medium at low temperature in the isothermal step liberates some of the CH_4 and C_{2+} products that result from reactions on the catalyst before the reaction with the isothermal medium. In addition, the nature of the isothermal gas medium and its reactions with the surface species affect the isothermal step product distribution. Exposure to hydrogen at high temperature during the TPSR removes most of the carbon species from the metal site and some of the carbon species residing on the support site. Only high temperature oxidation in the TPO step ensures complete removal of the inactive carbon species from the catalyst.

To increase the C_{2+} yield of CH_4 homologation with a two-step cycle it is better to use a high metal loading catalyst. A short activation time at about 450°C followed immediately by the isothermal hydrogenation at about 100°C gives a high yield of C_{2+} products and reduces the production of inactive carbon.

In the CH_4 activation step, deposition of more than a nominal monolayer carbon on the catalyst leads to more carbon recovery in the isothermal hydrogenation and TPSR. In this work, it was shown that by deposition of more carbon in the activation step a C_{2+} yield per site of about 2% can be obtained in the isothermal hydrogenation step. Although this is considered an improvement in comparison to the previous reports of 1% C_{2+} yield per site, one should note that more inactive carbon is also produced in this case. From a practical point of view, inactive carbons that are recovered only by high temperature hydrogenation or oxidation as CH_4 or CO_2 are considered a serious drawback. Based on the present operating conditions, one cannot devise an economically feasible process based on the two-step cycle for CH_4 homologation. Further improvements need to be made before a viable process based on this concept can be proposed.

Chapter 7

Conclusions and Recommendations for Future Work

7.1. Conclusions

Two-step homologation of CH_4 with SiO_2 supported Co catalysts was investigated in this work. SiO_2 supported Co catalysts were prepared by the wetness impregnation method. The catalysts were characterized by BET surface area and pore volume measurements, powder X-ray diffraction (PXRD), temperature programmed reduction (TPR), H_2 desorption and Co re-oxidation. The characterized catalysts were used in the two-step homologation of CH_4 . In the two-step homologation cycle, high temperature (ca 450 °C) activation of CH_4 on the reduced catalyst produced H_2 and surface carbon species. Lower temperature (ca 100 °C) hydrogenation of the active carbon species generated CH_4 and higher hydrocarbons. Less active carbon species were hydrogenated at high temperature in a temperature programmed surface reaction (TPSR) which followed the isothermal hydrogenation. After TPSR, the remaining inactive carbon species were removed by oxidation in a temperature programmed oxidation (TPO).

By complete analysis of the reactor effluent, comparison of the carbon deposited in the activation step and carbon recovered in the isothermal hydrogenation, TPSR and TPO steps, became possible.

Based on the results of this study, a kinetic model for CH_4 activation on SiO_2 -supported Co catalysts was developed. The kinetic model and its rate equations were used to interpret the effects of activation time, catalyst loading, activation temperature and catalyst support and promoter on CH_4 activation. In the isothermal hydrogenation step the effects of catalyst loading, activation time, activation temperature, carbon aging, reaction cycles and isothermal medium were studied. The principal observations and conclusions from the study are listed below:

1. Catalyst characterization results showed that there were two possible types of metal-support interaction (MSI) on SiO_2 supported Co catalysts. In the first case, cobalt-silicate compounds, which were not reducible under the reduction conditions of this work, were formed. In the second case, SiO_2 patches decorated the Co metal particles. The Co located below the SiO_2 decorations was detected by PXRD. It could be reduced and re-oxidized. However, it was not available for H_2 chemisorption or CH_4 activation.

2. Activation of CH_4 on reduced Co catalysts generated H_2 and surface carbon species. Experimental observations showed that the supported catalysts could activate more CH_4 than that corresponding to monolayer coverage of the surface Co by carbon species. It was suggested that migration of carbon species from the metal active site to the support site was responsible for liberation of metal active sites for further activation of gas phase CH_4 . Based on the initial activation of gas phase CH_4 on reduced Co and subsequent migration of carbon species from a metal site to a support site, a kinetic model was developed. By fitting the experimentally determined CH_4 consumption profile to the kinetic model, the rate constants of

the different steps of the CH₄ activation kinetic model were obtained. The rate constants were used to interpret the effect of different operating parameters on the CH₄ activation reaction.

3. Carbon deposited in the activation step was recovered by isothermal hydrogenation, temperature programmed surface reaction and temperature programmed oxidation. It was shown that not all the deposited carbon was recoverable by high temperature hydrogenation; only about 50% of the deposited carbon was removed by high temperature oxidation. The presence of this inactive carbon has not been reported by previous researchers.

4. Co-SiO₂ catalysts with nominal metal loadings of 2-12% were used for the two-step CH₄ homologation. 2% Co-SiO₂ catalyst proved to be about 30% more active in the CH₄ activation reaction, but its C₂₊ yield and selectivity were an order of magnitude lower than the 12% Co-SiO₂ catalyst. It was shown that lower loading catalysts had stronger metal-support interactions and produced carbon species with higher H content which led to lower tendency for C-C bond formation.

5. The effect of activation time on the two-step cycle was studied by activation of CH₄ for 1-7 minutes and hydrogenation of the resulting carbon species. Longer activation times produced carbon species with lower hydrogen content. As a result, C₂₊ selectivity and yield corresponding to 7 min activation time was about half that obtained after one minute activation, while about four times as much carbon was deposited in the 7 min activation time. It was shown that longer activation time produced mainly inactive carbon deposits.

6. CH₄ was activated in the temperature range of 360 to 450 °C, and the deposited carbon species were hydrogenated at 100 °C. The activation energies of CH₄ activation on Co, adsorbed CH₃ migration from metal to the support and H desorption were estimated as

56, 48 and 171 kJ/mole, respectively. It was shown that lower activation temperatures generated carbon species with higher H content leading to C_{2+} selectivities and yields which were about one third of those corresponding to a CH_4 activation temperature of 450 °C.

7. After CH_4 activation at 450 °C, carbon species were aged at 100 °C for different periods of time. Hydrogenation of aged carbon species showed that, by increasing the aging time from 5 min to 20 min, C_{2+} selectivity and yield decreased by a factor of 2 and 4, respectively. Despite the accepted notion that only aging at high temperature deactivates the active carbon, present study showed that aging at a low temperature (100 °C) could also have a significant effect on the amount of active carbon.

8. It was shown that after CH_4 activation on the Co-SiO₂ catalyst, some C-C bond formation occurs on the catalyst before the isothermal hydrogenation step. As a result of this C-C bond formation, some CH_4 and C_2H_6 could be released by Ar instead of H_2 at 100 °C.

7.2. Recommendations for Future Work

As a result of this study, answers to some of the questions in the two-step cycle for CH₄ homologation were obtained. In addition, the results of this work led to some new questions. For further expansion of this work, a list of recommended tasks is given below.

1. Preparation and characterization of Co-SiO₂ catalysts and understanding the nature and mechanism of metal-support interactions proved to be an important problem in the present study. A better understanding of the chemical transformations during impregnation, drying, calcination and reduction could make a significant contribution to the control of catalyst properties.

2. The chemical identity of carbon species on the metal and support site and the effect of time and temperature on these carbon species would be a significant extension of the present work. Such a study should include the kinetics of dehydrogenation of each carbon species on the catalyst. The results of such a study should be linked to the kinetic model of this work.

3. In the present kinetic model, only the rate of CH₄ consumption was considered in the rate equations. The kinetics of hydrogen combination, desorption and spillover has not been treated. By considering these steps with the kinetics of dehydrogenation of carbon species (see above item) a complete kinetic model could be developed.

4. The possibility of using molecular sieves supported and ion exchanged catalysts should be explored more systematically for the two-step cycle. Also the effect of different promoters and bimetallic catalysts should be examined for this reaction. The present study

suggests that any method that can modify the metal-support interactions will have a significant effect on the two-step CH_4 homologation cycle.

5. The kinetic model in this work was developed based on initial activation of CH_4 on Co and migration of carbon species from the metal to the support. The possibility of the reverse reaction in which carbon migrates from the support to the metal should also be examined. The results of such an study could be useful in the field of catalyst deactivation and regeneration.

References

- Amariglio, A.; Pajera, P.; Belgued, M.; Amariglio, H., "Possibility of Obtaining Appreciable Yield in Methane Homologation through a Two-Step Reaction at 250 °C on a Platinum Catalyst", *J. Chem. Soc., Chem. Commun.* 1994, 561-562.
- Amenomiya, Y.; Birss, V.I.; Goledzinowski, M.; Galuszka, J.; Sanger, A.R., "Conversion of Methane by Oxidative Coupling", *Cat. Rev.- Sci. Eng.* 1990, 32, 3, 163-227.
- Anderson, J.R., "Methane to Higher Hydrocarbons", *Appl. Catal.* 1989, 47, 177-196.
- Anderson, R.B., *The Fischer-Tropsch Synthesis*; Academic Press, New York, 1984.
- Arai, M.; Nishiyama, Y.; Masuda, T.; Hashimoto, K., "The Distribution of Activation Energy for Hydrogen Desorption Over Silica-Supported Nickel Catalysts Determined from Temperature-Programmed Desorption Spectra", *Appl. Surf. Sci.* 1995, 89, 11-19.
- Bartholomew, C.H.; Pannell, R.B., "The Stoichiometry of Hydrogen and Carbon Monoxide Chemisorption on Alumina- and Silica-Supported Nickel", *J. Catal.* 1980, 65, 390-401.
- Belgued, M.; Amariglio, H.; Pareja, P.; Amariglio, A.; Sain-Just, J., "Low Temperature Catalytic Homologation of Methane on Platinum, Ruthenium and Cobalt", *Catal. Today* 1992, 13, 437-445.
- Belgued, M.; Amariglio, A.; Pareja, P.; Amariglio, H., "Oxygen-Free Conversion of Methane to Higher Alkanes Through an Isothermal Two-Step Reaction on Platinum (EUROPT-1) I. Chemisorption of Methane", *J. Catal.* 1996 ^(a), 159, 441-448.
- Belgued, M.; Amariglio, A.; Pareja, P.; Amariglio, H., "Oxygen-Free Conversion of Methane to Higher Alkanes Through an Isothermal Two-Step Reaction on Platinum (EUROPT-1) I. Hydrogenation of the Adspecies Resulting from the Chemisorption of Methane", *J. Catal.* 1996 ^(b), 159, 449-457.
- Belgued, M.; Amariglio, A.; Lefort, L.; Pareja, P.; Amariglio, H., "Oxygen-Free Conversion of Methane to Higher Alkanes Through an Isothermal Two-Step Reaction on Ruthenium", *J. Catal.* 1996 ^(c), 161, 282-291.
- Blitz, J.P.; Augustine, S.M., "Characterization of Heterogeneous Catalysts by FT-IR Diffuse Reflectance Spectroscopy", *Spectroscopy* 1994, 9,8, 28-34.
- Boskovic, G.; Soltan Mohammad Zadeh, J.; Smith, K.J., "K Promotion of Co Catalysts for the Two-Step Methane Homologation Reaction", *Catal. Lett.* 1996, 39, 163-168.

Boskovic, G.; Soltan Mohammad Zadeh, J.; Smith, K.J., "Methane Homologation on Co Supported Catalyst", In *Studies in Surface Science and Catalysis, Vol. 107*, M. de Pontes, R.L. Espinoza, C.N. Nicolaides, J.H. Scholz and M.S. Scurrrell (Editors), Elsevier Science, New York, 1997, pp 263-268.

Boskovic, G.; Smith, K.J., "Methane homologation and Reactivity of Carbon Species on Supported Co Catalysts", *Catal. Today* 1997, 1017, 1-8.

Brunauer, S.; Emmett, P.H.; Teller, E., "Adsorption of Gases in Multimolecular Layers", *J. Am. Chem. Soc.* 1938, 60, 309-319.

Carstens, J.N.; Bell, A.T., "Methane Activation and Conversion to Higher Hydrocarbons on Supported Ruthenium", *J. Catal.* 1996, 161, 423-429.

Conner, W.C.; Pajonk, G.M.; Teichner, S.J., Spillover of Sorbed Species", *Adv. Catal.* 1986, 34, 1-79.

Coulter, E.K.; Sault, A.G., "Effects of Activation on the Surface Properties of Silica-Supported Cobalt Catalysts", *J. Catal.* 1995, 154, 56-64.

Delannay, F., *Characterization of Heterogeneous Catalysts*, Marcel Dekker, New York, 1984.

Driessen M.D.; Grassian, V.H., "Methyl Spillover on Silica-Supported Copper Catalysts from the Dissociative Adsorption of Methyl Halides", *J. Catal.* 1996, 161, 810-818.

Erdohelyi, A.; Cserenyi, J.; Solymosi, F., "Activation of CH₄ and Its Reaction with CO₂ Over Supported Rh Catalysts", *J. Catal.* 1993, 141, 287-299.

Ferreira-Aparicio, P.; Rodrigues-Ramos, I; Guerrero-Ruiz, A., "Methane Interaction with Silica and Alumina Supported Metal Catalysts", *Appl. Catal. A: General* 1997, 148, 343-356.

Fox III, J.M., "The different Catalytic Routes for Methane Valorization: An assessment of Processes for Liquid Fuels", *Catal. Rev.-Sci. Eng.* 1993, 35, 2, 169-212.

Fox III, J.M.; Chen, T; Degen, B.D., "An Evaluation of Direct Methane Conversion Processes", *Chem. Eng. Prog.* 1990, 42-50.

Garnier, O.; Shu, J.; Grandjean, B.P.A., "Membrane-Assisted Two-Step Process for Methane Conversion into Hydrogen and Higher Hydrocarbons", *Ind. Eng. Chem. Res.* 1997, 36, 553-558.

Guczi, L.; van Santen, R.A.; Sarma, K.V., "Low-Temperature Coupling of Methane", *Catal. Rev.-Sci. Eng.* 1996 ^(a), 38, 2, 249-296.

Guczi, L.; Sarma, K.V.; Borko, L., "Non-oxidative Methane Coupling over Co-Pt/NaY Bimetallic Catalysts", *Catal. Lett.* 1996 ^(b), 39, 43-47.

Guczi, L.; Sarma, K.V.; Borko, L., "Low-Temperature Methane Activation Under Nonoxidative Conditions Over Supported Ruthenium-Cobalt Bimetallic Catalysts", *J. Catal.* 1997, 167, 495-502.

He, H.; Nakamura, J.; Tanaka, K., "Formation of CH_x Species on a Ni(100) Surface by the Hydrogenation of Carbodic Carbon", *Surf. Sci.* 1993, 283, 117-120.

Ho, S.; Houalla, M.; Hercules, D.M., "Effect of Particle Size on Co Hydrogenation Activity of Silica Supported Cobalt Catalysts", *J. Phys. Chem.* 1990, 94, 6396-6399.

Ib, D.; Hansen, J.B., "Large-Scale Production of Alternative Synthetic Fuels from Natural Gas", In *Studies in Surface Science and Catalysis, Vol. 107*, M. de Pontes, R.L. Espinoza, C.N. Nicolaides, J.H. Scholz and M.S. Scurrrell (Editors), Elsevier Science, New York, 1997, pp 99-116.

ICDD, International Center for Diffraction Data, CD ROM, 1994, 12 Campus Boulevard, Newton Square, PA, 19073-3273 US.

Iler, R.K., *The Chemistry of Silica: Solubility, Polymerization, Colloid and Surface Properties and Biochemistry*; John Wiley & Sons, Toronto, 1979.

Imelik, B.; Vedrine, J.C. (Ed.), *Catalyst Characterization, Physical Techniques for Solid Materials*, Plenum, New York, 1994.

Jabiconski, J.M.; Potoczna-Petru, D.; Okal, J.; Krajczyk, L., "Effect of High-Temperature Reduction on Co/SiO₂ Catalysts, Activity in the Hydrogenation of Benzene", *React. Kinet. Catal. Lett.* 1995, 54, 1, 15-20.

Khodakov, A.Yu.; Lynch, J.; Bazin, D.; Rebours, B.; Zanier, N.; Moisson, B.; Chaumette, P., "Reducibility of Cobalt Species in Silica-Supported Fischer-Tropsch Catalysts", *J. Catal.* 1997, 168, 16-25.

Koerts, T.; van Santen, R.A., "The Reactivity of Adsorbed Carbon on Vanadium Promoted Rhodium Catalysts", *Catal. Lett.* 1990, 6, 49-58.

Koerts, T.; van Santen, R.A., "The Reaction Path for Recombination of Surface CH_x Species", *J. Mol. Catal.* 1991 ^(a), 70, 119-127.

Koerts, T.; van Santen, R.A., "A Low Temperature Reaction Sequence for Methane Conversion", *J. Chem. Soc., Chem. Commun.* 1991 ^(b), 1281-1283.

Koerts, T.; Deelen, M.J.A.G.; van Santen, R.A., "Hydrocarbon Formation from Methane by a Low-Temperature Two-Step Reaction Sequence", *J. Catal.* 1992 ^(a), 138, 101-114.

Koerts, T.; Leclercq, P.A.; van Santen, R.A., "Homologation of Olefins with Methane on Transition Metals", *J. Am. Chem. Soc.* 1992 ^(b), 114, 7272-7278.

Koranne, M.M.; Goodman, D.W.; Zajac, G.W., "Direct Conversion of Methane to Higher Hydrocarbons via an Oxygen Free, Low-Temperature Route", *Catal. Lett.* 1995, 30, 219-234.

Kristyan, S., "Kinetics of the Heterogeneous Catalytic Decomposition of Methane", *Canad. J. Chem. Eng.* 1997, 75, 229-237.

Lange, J.P.; Tijm, P.J.A., "Processes for Converting Methane to Liquid Fuels: Economic Screening Through Energy Management", *Chem. Eng. Sci.* 1996, 51, 10, 2379-2387.

Lange, J.P.; de Jong, K.P.; Ansorge, A.; Tijm, P.J.A., "Keys to Methane Conversion Technologies", In *Studies in Surface Science and Catalysis, Vol. 107*, M. de Pontes, R.L. Espinoza, C.N. Nicolaides, J.H. Scholz and M.S. Scurrell (Editors), Elsevier Science, New York, 1997, pp 81-86.

Lapidus, A.; Krylova, A.; Kazanskii, V.; Borovkov, V.; Zaitsev, A.; Rathousky, J.; Zukal, A.; Jancalkova, M., "Hydrocarbon Synthesis from Carbon Monoxide and Hydrogen on Impregnated Cobalt Catalysts. Part I. Physico-Chemical Properties of 10% Cobalt/Alumina and 10% Cobalt/Silica", *Appl. Catal.* 1991, 73, 65-82.

Lenz-Solomun, P.; Wu, M.; Goodman, D.W., "Methane Coupling at Low Temperature on Ru(0001) and Ru(1120) Catalyst", *Catal. Lett.* 1994, 25, 75-86.

Lowell, S., *Introduction to Powder Surface Area*; Wiley, New York, 1979, pp 13-39.

Lunsford, J.H., "The Catalytic Oxidative Coupling of Methane", *Angew. Chem. Int. Ed. Engl.* 1995, 34, 970-980.

Mc Carty, J.G., "Approaches to Higher Yield in Methane Conversion Processes", *Abstract of Papers*, Symposium on Natural Gas Upgrading II, Presented before The Division of Petroleum Chemistry, Inc., American Chemical Society, San Francisco Meeting, April 5-10, 1992, pp 153-160.

Ming, H.; Baker, B.G., "Characterization of Cobalt Fischer-Tropsch Catalysts. I. Unpromoted Cobalt-silica gel Catalysts", *Appl. Catal.* 1995, 123, 23-36.

Nakamura, J.; Tanaka, K.; Toyoshima, I., "Reactivity of Deposited Carbon on Co-Al₂O₃ Catalysts", *J. Catal.* 1987, 108, 55-62.

Ovalles, C.; Leon, V.; Reyes, S.; Rosa, F., "Homologation of Propene with Methane Using Nickel-Supported Catalysts: A Surface Characterization Study", *J. Catal.* **1991**, *129*, 368-382.

Pareja, P.; Amariglio, A.; Belgued, M.; Amariglio, H., "Increasing the Yield in Methane Homologation Through an Isothermal Two-Reaction Sequence at 250 °C on Platinum", *Catal. Today* **1994**, *21*, 423-430.

Pitchai, R.; Klier, K., "Partial Oxidation of Methane", *Catal. Rev.-Sci. Eng.* **1986**, *28*, 1, 13-88.

Poirier, M.G.; Sanger, A.R.; Smith, K.J., "Direct Catalytic Conversion of Methane", *Canad. J. Chem. Eng.* **1991**, *69*, 1027-1035.

Potoczna-Petru, D.; Kepinski, L., "Influence of Oxidation-Reduction Treatment on the Interaction of Cobalt Particles with Silica Support", *J. Mat. Sci.* **1993**, *1*, 28, 3501-3505.

Rathousky, J.; Zukal, A.; Lapidus, A.; Krylova, A., "Hydrocarbon Synthesis from Carbon Monoxide + Hydrogen on Impregnated Cobalt Catalysts. Part III. Cobalt (10%)/Silica-Alumina Catalysts", *Appl. Catal. A: General*, **1991**, *79*, 167-180.

Raupp, A.G.; Stevenson, S.A.; Dumesic, J.A.; Tauster, S.J.; Baker, R.T.K., in "Metal Support Interactions in Catalysis, Sintering and Redesorption", Stevenson, S.A.; Dumesic, J.A.; Baker, R.T.K.; Ruckenstein, E., Eds, Van Nostrand Reinhold, New York, N.Y., 1987.

Reuel, R.C.; Bartholomew, C.H., "The Stoichiometry of H₂ and CO Adsorption on Cobalt: Effects of Support and Preparation", *J. Catal.* **1984**, *85*, 63-77.

Roop, B.; Costello, S.A.; Mullins, D.R.; White, J.M., "Coverage-Dependent Diffusion of Co on Ni(100)", *J. Chem. Phys.* **1987**, *86*, 3003-3008.

Ross, J.R.H.; van Keulen, A.N.J.; Hagarty, M.E.S.; Seshen, K., "The Catalytic Conversion of Natural Gas to Useful Products", *Catal. Today* **1996**, *30*, 193-199.

Rostrup-Nielsen, J.R.; Aasberg-Petersen, K.; Schoubye, P.S., "The Role of Catalysis in the Conversion of Natural Gas for Power Generation", In *Studies in Surface Science and Catalysis, Vol. 107*, M. de Pontes, R.L. Espinoza, C.N. Nicolaidis, J.H. Scholz and M.S. Scurrall (Editors), Elsevier Science, New York, 1997, pp 473-488.

Rostrup-Nielsen, J.R., "Catalysis and Large-Scale Conversion of Natural Gas", *Catal. Today* **1994**, *21*, 257-267.

Rosynek, M.P.; Polansky, C.A., "Effect of Cobalt Source on the Reduction Properties of Silica-Supported Cobalt Catalysts", *Appl. Catal.* **1991**, *73*, 97-112.

Schanke, D.; Vada, S.; Blekka, E.A.; Hilmen, A.M.; Hoff, A.; Holmen, A., "Study of Pt-Promoted Cobalt CO Hydrogenation Catalysts", *J. Catal.* **1995**, 156, 85-95.

Shen, G.; Ichikawa, M., "Methane Hydrogenation and Confirmation of CH_x Intermediate Species on NaY Encapsulated Cobalt Clusters and Co/SiO₂ Catalysts: EXAFS, FTIR, UV Characterization and Catalytic Processes", *J. Chem. Soc., Faraday Trans.*, **1997**, 93, 6, 1185-1193.

Shustorovich, E.; Bell, A.T., "An Analysis of Fischer-Tropsch Synthesis by the Bond-Order-Conservation Morse-Potential Approach", *Surf. Sci.* **1991**, 248, 359-368.

Sie, S.T.; Senden, M.M.G.; van Wechen, H.M.H., "Conversion of Natural Gas to Transportation Fuels via the Shell Middle Distillate Synthesis Process (SMDS)", *Catal. Today* **1991**, 8, 371-394.

Socrates, G., *Infrared Characteristic Group Frequencies, Tables and Charts*; Wiley: New York, 1994.

Solymosi, F.; Erdohelyi, A.; Cserenyi, J., "A Comparative Study on the Activation and Reactions of CH_4 on Supported Metals", *Catal. Lett.* **1992**, 16, 399-405.

Solymosi, F.; Kovacs, I.; Revesz, K., "A Comparative Study of the Thermal Stability and Reactions of CH_2 , CH_3 and C_2H_5 Species on the Pd(100) Surface", *Catal. Lett.* **1994**^(a), 27, 53-60.

Solymosi, F.; Erdohelyi, A.; Cserenyi, J.; Felvegi, A., "Decomposition of CH_4 over Supported Pd Catalysts", *J. Catal.* **1994**^(b), 147, 272-278.

Solymosi, F.; Cserenyi, J., "Decomposition of CH_4 over Supported Ir Catalysts", *Catal. Today*, **1994**, 21, 561-569.

Somorjai, G.A., *Introduction to Surface Chemistry and Catalysis*; John Wiley & Sons: New York, 1994.

Sundset, T.; Sogge, J.; Strom, T., "Evaluation of Natural Gas Based Synthesis Gas Production Technologies", *Catal. Today*, **1994**, 21, 269-278.

Tsipouriari, V.A.; Efstathiou, A.M.; Verykios, X.E., "Transient Kinetic Study of the Oxidation and Hydrogenation of Carbon Species Formed during CH_4/He , CO_2/He and CH_4/CO_2 Reactions over Rh/Al₂O₃ Catalysts", *J. Catal.* **1996**, 161, 31-42.

Unger, U.V., *Porous Silica*; Elsevier: Amsterdam, 1979.

van Steen, E.; Sewell, G.S.; Makhothe, R.A.; Micklethwaite, C.; Manstein, H.; de Lange, Martijn; O'Connor, C.T., "TPR Study on the Preparation of Impregnated Co/SiO₂ Catalysts", *J. Catal.* **1996**, 162, 220-229.

Vora, B.V.; Marker, T.L.; Barger, P.T.; Nilsen, H.R.; Kvisle., S.; Fuglerud, T., "Economic Route for Natural Gas Conversion to Ethylene and propylene", In *Studies in Surface Science and Catalysis, Vol. 107*, M. de Pontes, R.L. Espinoza, C.N. Nicolaides, J.H. Scholz and M.S. Scurrrell (Editors), Elsevier Science, New York, 1997, pp 87-98.

Wachs, I.E., *Characterization of Catalytic Materials*; Butterworth-Heineman: London, 1992.

Wu, M.; Lenz-Solomun; Goodman, D.W., "Two-Step, Oxygen-Free Route to Higher Hydrocarbons from Methane over Ruthenium Catalysts", *J. Vac. Sci. Technol. A- Vac., Surf., Films* **1994**, 12,4, 2205-2209.

Yoshitake, H.; Iwasawa, Y., "Electronic Metal-Support Interaction in Pt Catalysts under Deuterium-Ethane Reaction Conditions and the Microscopic Nature of Active Sites", *J. Phys. Chem.* **1992**, 96, 1329-1334.

Appendices

Appendix 1

1.1. Calibration of Mass Flow Controllers

1.2. Conditions of BET Analysis

1.3. Analysis with Gas Chromatograph

1.4. Calibration of Quadrupole Mass Spectrometer

1.5. Analysis Conditions of Infra-Red Spectroscopy

Appendix 1.1. Calibration of Mass Flow Controllers

Two 4 way-flow selection valves and two Brooks 5850E mass flow control sensors (see section 3.2) were used to prepare different gas mixtures for flow experiments. Mass flow control sensor "A" and "B" was factory calibrated for 20 ml/min (STP) CH₄ and 200 ml/min (STP) of N₂, respectively.

To use these flow sensors for other gases, calibration charts and calibration factors were developed. Using a soap bubble flow meter, calibration factors were obtained for different gases in the two control cells. The calibration factors agreed very well with the flow correction procedure outlined in the instrument manual (1). Figure A1.1(a) is a typical calibration plot which was obtained for O₂ flow with control cell "A".

Based on the calibration plots, flow correlations in the form of $Y = m \cdot X$ were developed. In the flow correlation:

Y: Volumetric gas flow, ml/min STP

X: Percent reading of the controller ($0 \leq X \leq 100$)

m: Flow correlation factor, ml/min

In Table A1.1 flow correlation factors are given.

(1) Installation and Operating Instructions, Brooks Mass Flow Controller, Model 5850E
Brooks Instrument Division, Emerson Electric Co, Hatfield, Pennsylvania 19440

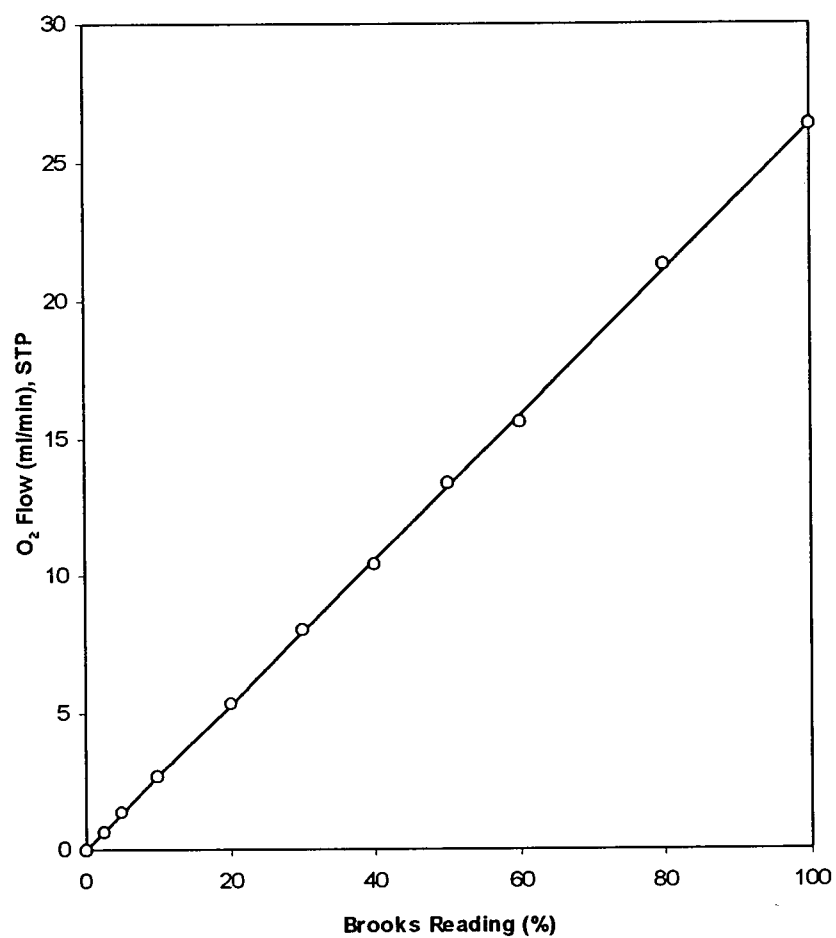


Figure A1.1. Measured (O) vs. best fit for calibration plot of O₂ with Brooks mass flow sensor (A).

Table A1.1. Flow correlation factor (m).

<i>Gas</i>	<i>Flow Cell</i>	<i>m, ml/min</i>
CO ₂	A	0.19
CH ₄	A	0.20
O ₂	A	0.24
H ₂	A	0.25
Ar	B	2.79
5.16% CH ₄ /Ar	A	0.33
5.16% CH ₄ /Ar	B	2.69

Appendix 1.2. Conditions of BET Analysis

Catalyst surface area and pore volume were determined using a Micromeritics (1) ASAP 2010 Accelerated Surface Area and Porosimetry System. ASAP 2010 is a computer controlled system which performs the analyses and calculations based on the user programmed parameters. The summary of the analysis options are given below.

Analysis Adsorptive: Nitrogen

Maximum manifold pressure: 925.00 mmHg

Non-ideality factor: 0.000066

Density conversion factor: 0.0015468

Therm. tran. hard-sphere diameter: 3.860 Å

Molecular cross-sectional area: 0.162 nm²

Fast evacuation: Yes

Crossover pressure: 5.0 mmHg

Leak test: No

Leak test duration: 120 secs

Evacuation time: 0.1 hours

Backfill Gas: Analysis

Equilibration interval: 5 secs

Maximum volume increment: No

Target tolerance: 5.0 % or 5.0 mmHg

Min. equil. delay at $P/P_o \geq 0.995$: 600 secs

(1) Micromeritics, One Micromeritics Drive, Norcross, GZ, 30093-1877

Free space group: Measured

Warm free space: 16.0000 cm³

Cold free space: 45.0000 cm³

Post-free space evacuation: No

Evacuation time: 0.1 hours

Leak test: Yes

Leak test duration: 180 secs

Low pressure dosing: No

Dose amount: 0.00 cm³/g STP

Minimum equilibration delay: 0.00 hours

Maximum equilibration delay: 999.00 hours

Po type: Measured

Po: 740.000 mmHg

Measurement interval: 120 minutes

Temperature type: Entered

Temperature: 77.35 K

Measurement gas: N2

Inside diameter of sample tube: 9.530 mm

Appendix 1.3. Analysis with Gas Chromatograph

A calibrated gas chromatograph (GC) with a flame ionization detector (FID) was used for sampling and analysis of the reaction products in the isothermal hydrogenation step.

For calibration, an analyzed gas mixture (Praxair) of 4.89% H₂, 10.60% CH₄, 2.01% C₂H₄, 3.95% C₂H₆ and 78.62% Ar was used. By repeat analyses, calibration factors (ratio of peak area of component "i" to mole% of component "i") were determined. Typical calibration factors and corresponding retention times are reported in Table A3.1.

Table A1.3. Calibration factors and retention time of different components.

<i>Component</i>	<i>Retention time</i>	<i>calibration factor (peak area/mole%)</i>
	<i>min</i>	<i>mol%⁻¹</i>
CH ₄	0.71	8.005 X 10 ⁷
C ₂ H ₄	3.16	1.511 X 10 ⁸
C ₂ H ₆	4.15	1.598 X 10 ⁸

During the sampling step, the sampling valve and the flow direction valve were programmed to direct the reactor effluent through the sampling valve and to take nine samples with an interval one minute. The GC operating program for sampling is provided in Figure A3.1(a)

After sampling, the GC column had to be purged completely before analyzing the samples. In Figure A.1.3(b), the GC program for pre-analysis purging is given.

Sequential analysis of the collected samples were performed according to the program provided in Figure A.1.3(c)

METHOD 1
TIME 11:11 15 AUG 97
REV 9609051640

INITIAL COLUMN TEMP 145°
INITIAL COL HOLD TIME 0.00

INJECTOR TEMP 145°

AUXILIARY TEMP 220°
INITIAL AUX HOLD TIME 0.00

DETECTOR TEMP 220°

FID B ATTN RANGE A/Z
8 9 YES

INITIAL RELAYS -12

RELAYS		
PRGM	TIME	STATE
1	1.00	1
2	1.10	-1
3	2.00	1
4	2.10	-1
5	3.00	1
6	3.10	-1
7	4.00	1
8	4.10	-1
9	5.00	1
10	5.10	-1
11	6.00	1
12	6.10	-1
13	7.00	1
14	7.10	-1
15	8.00	1
16	8.10	-1
17	9.00	1
18	9.10	-12
19	9.50	2

Figure A1.3. (a). List of program for sampling and storage of the reactor effluent in the sampling loops.

METHOD 2
TIME 11:12 15 AUG 97
REV 9605121724

INITIAL COLUMN TEMP 145°
INITIAL COL HOLD TIME 0.00

	FINAL		HOLD	TOTAL
PRGM	TEMP	RATE	TIME	TIME
1	195	6.0	5.00	13.33

INJECTOR TEMP 145°

AUXILIARY TEMP 220°
INITIAL AUX HOLD TIME 0.00

DETECTOR TEMP 220°

FID B ATTEN RANGE A/Z
8 9 YES

PLOT SPEED 0.0 CM/MIN
ZERO OFFSET 15 %
PLOT SIGNAL B
TIME TICKS NO
INSTR EVENT CODES NO
USER NUMBER 0-0
PRINT USER NUMBER NO
PRINT REPORT NO
PRINT RUN LOG NO

INITIAL RELAYS 1-2

Figure A1.3. (b). List of program for purging the GC column before sample analyses.

METHOD 3
TIME 11:12 15 AUG 97
REV 9609061711

INITIAL COLUMN TEMP 145°
INITIAL COL HOLD TIME 0.00

PRGM	FINAL TEMP	RATE	HOLD TIME	TOTAL TIME
1	195	6.0	5.00	13.33

INJECTOR TEMP 145°

AUXILIARY TEMP 220°
INITIAL AUX HOLD TIME 0.00

DETECTOR TEMP 220°

TCD A	ATTEN	RANGE	A/Z	SIG
	16	.5	YES	NEG

FILAMENT TEMP OFF°

FID B	ATTEN	RANGE	A/Z
	128	12	YES

PLOT SPEED 0.5 CM/MIN
ZERO OFFSET 15 %
PLOT SIGNAL B
TIME TICKS NO
INSTR EVENT CODES YES
USER NUMBER 0-0
PRINT USER NUMBER NO
PRINT REPORT YES
PRINT RUN LOG NO

INITIAL RELAYS 1-2

RELAYS PRGM	TIME	STATE
1	0.01	1
2	0.03	-1

Figure A1.3. (c). List of program for analysis if the stored samples.

Appendix 1.4. Calibration of Quadrupole Mass Spectrometer

A mass spectrometer operates based on ionization of components and determination of relative amounts of ionized species based on differing "mass/charge" ratio. If each molecule produced only one characteristic ion, it would be a relatively easy task to find the composition of the analyte stream by determining the peak intensity of the characteristic mass numbers. In practice, because of different effects of isotope abundance and fragmentation, most of the molecules produce more than one charged species. Each molecule has a characteristic cracking pattern and a mixture of gases produces a complicated spectrum of charged species with overlapping mass numbers. Analysis of partial pressure versus mass number of a mixture of gases to find the gas composition is difficult when more than one molecule produces charged species at the same mass number (overlapping spectrum).

For a system containing "n" gases and "m" mass number peaks, one can relate the measured mass number partial pressures to the actual partial pressures:

$$\overline{M} = \overline{A} \times (\overline{S} \times \overline{P})$$

Where \overline{M} is the peak intensity vector, \overline{A} is the cracking pattern matrix, \overline{S} is the sensitivity vector and \overline{P} is the actual partial pressure vector (1-5).

Calculation of partial pressure i.e. chemical composition from mass spectrometer mass numbers measurement involves a tedious experimental procedure and mathematical solution algorithm.

In this work the quadrupole mass spectrometer (QMS) was used to monitor the three steps of activation of CH₄, temperature programmed surface reaction (TPSR) and temperature programmed oxidation (TPO). One common feature of these three steps was the simplicity of

the reaction mixture. In CH₄ activation step, a mixture of 5.16% CH₄ and 94.84% Ar flowed through the reactor. Because of the CH₄ activation on the catalysts, the reactor effluent contained the unreacted CH₄ (less than the inlet stream), generated H₂ and Ar (the same amount as inlet stream). In TPSR, H₂ was admitted into the reactor and the effluent stream contained H₂ (approximately the same amount as inlet stream) and CH₄ which was produced by reaction. In TPO, O₂ was introduced into the reactor and the outlet stream contained O₂ (approximately the same amount as the inlet stream), CO₂ and H₂O which were produced by the oxidation reaction.

In all these systems the chemical components of the analysis stream were known and there was a main component with high concentration and negligible change in composition i.e. Ar in CH₄ activation, H₂ in TPSR and O₂ in TPO. Simplicity of the reaction mixture was a great advantage to avoid the difficult experimental and computation task and to devise a simple method of converting the mass number recordings to chemical composition.

In this simple method, the QMS was calibrated with mixtures of gases with a similar composition to the analysis gas. Calibration gas flows were established using the calibrated mass flow meters and UHP grade pure gas or analyzed premixed gas mixtures. With different concentrations of the calibration gas stream, the mass number and total pressure from the QMS were recorded. By plotting the known mole fraction of the calibration stream versus (atomic mass unit)/(total pressure) readings from the QMS a calibration plot was prepared. Figure A1.4(a) shows a typical calibration plot of CH₄/Ar mixture. From the least square best fit of the experimental points a calibration factor was extracted.

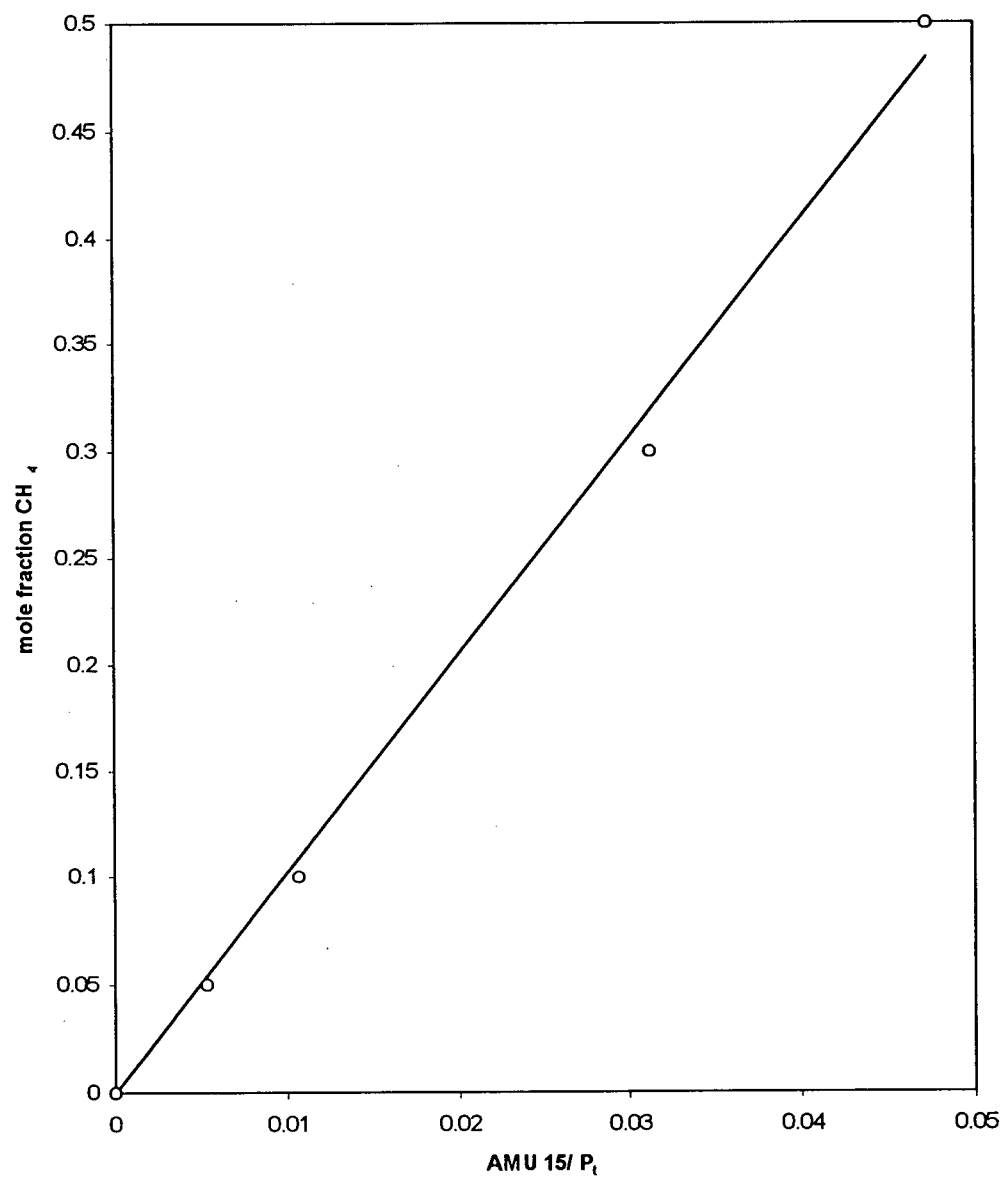


Figure A1.4(a). Calibration plot of CH₄ mole fraction (O) vs. AMU 15/P_t

(O) is the experimental data and (—) is the best fit.

In fact the calibration factor contained the effects of the cracking pattern, relative peak intensity and relative sensitivity of QMS for each component. Table A1.4 typical calibration factors for various gas mixtures are given.

Table A1.4. Calibration factors for different components.

<i>Component</i>	<i>Major Component</i>	<i>Mass Number</i>	<i>Calibration Factor</i>
H ₂	Ar	2	1.0
CH ₄	Ar	15	10.2
Ar	Ar	40	15.2
H ₂	H ₂	2	0.9
CH ₄	H ₂	15	3.5
C ₂ H ₄	H ₂	25	37.4
C ₂ H ₆	H ₂	30	13.1
CO ₂	O ₂	44	21.8
H ₂ O	O ₂	18	-
O ₂	O ₂	32	9.0

In the simple reaction mixture of this work the accuracy of the above method was better than 95% in most cases.

1. O'Hanlon J.F., "*A User's Guide to Vacuum Technology*", second ed., John Wiley & Sons, 1989.
2. Harris, N., "*Modern Vacuum Technology*", McGraw Hill Books Co., 1989.
3. Dobrozemsky R., "Experience with a computer program for residual gas analyzers", *The Journal of Vacuum Science and Technology*, vol. 9, No. 1, 220.
4. Easton D.S., Clausing R.E., "Outguessing of nuclear rocket fuel elements", *The Journal of Vacuum Science and Technology*, Vol. 7, No. 6, S116.
5. Raimondi D.L., et al., "Automation of a residual gas analyzer on a time-shared computer", *IBM J. Res. Dev.*, 1971, 307.

Appendix 1.5. Analysis Conditions of Infra-Red Spectroscopy

Diffuse reflectance Infra-red Fourier transform spectroscopy (DRIFTS) was used to study the catalyst and deposited carbon species during the two-step reactions. The analysis conditions and data manipulation parameters of the DRIFTS studies are listed in this appendix.

Requested_Scans_per_Scanset= 100

Number_of_Scansets= 60

Scan_type= K-Munk

Background_File= c:\win_ir\data\soltan\try2\kbr50.spc

Resolution= 4

Igram_Symmetry= Single Sided

Sampling= UDR-2

Gain_Range_Radius= 40

Scanning= Unidirectional

Aperture= Open

Detector= Back

Beam_Path= Internal

Source= MIR

Gain_Amplifier= 1

Velocity= 20 KHz

Low_Pass_Filter= 5 KHz

Apodization= Triangular

Zero_Filling_Factor= 1

Laser_Wavenumber= 15800.82

Starting_Wavenumber=4000

Ending_Wavenumber= 700

Experiment_type= Normal

Scans_per_scanset=100

Appendix 2

2.1. Temperature Programmed Reduction Profiles

2.2. Experimental Data

2.3. Equations for Calculations

2.4. Study of the Effect of Activation Temperature by the Kinetic Model

Appendix 2.1. Temperature Programmed Reduction Profiles

The calcined Co-SiO₂ catalysts were reduced by a temperature programmed reduction (TPR) procedure in H₂ (Section 3.4.1). The TPR profile for the A series 12% Co-SiO₂ catalyst is presented in Section 4.4. In this section, the TPR profiles of A series 5, 2 and 0.6% Co-SiO₂ catalysts are presented in Figure A.2.1.(a), A.2.1.(b) and A.2.1.(c), respectively.

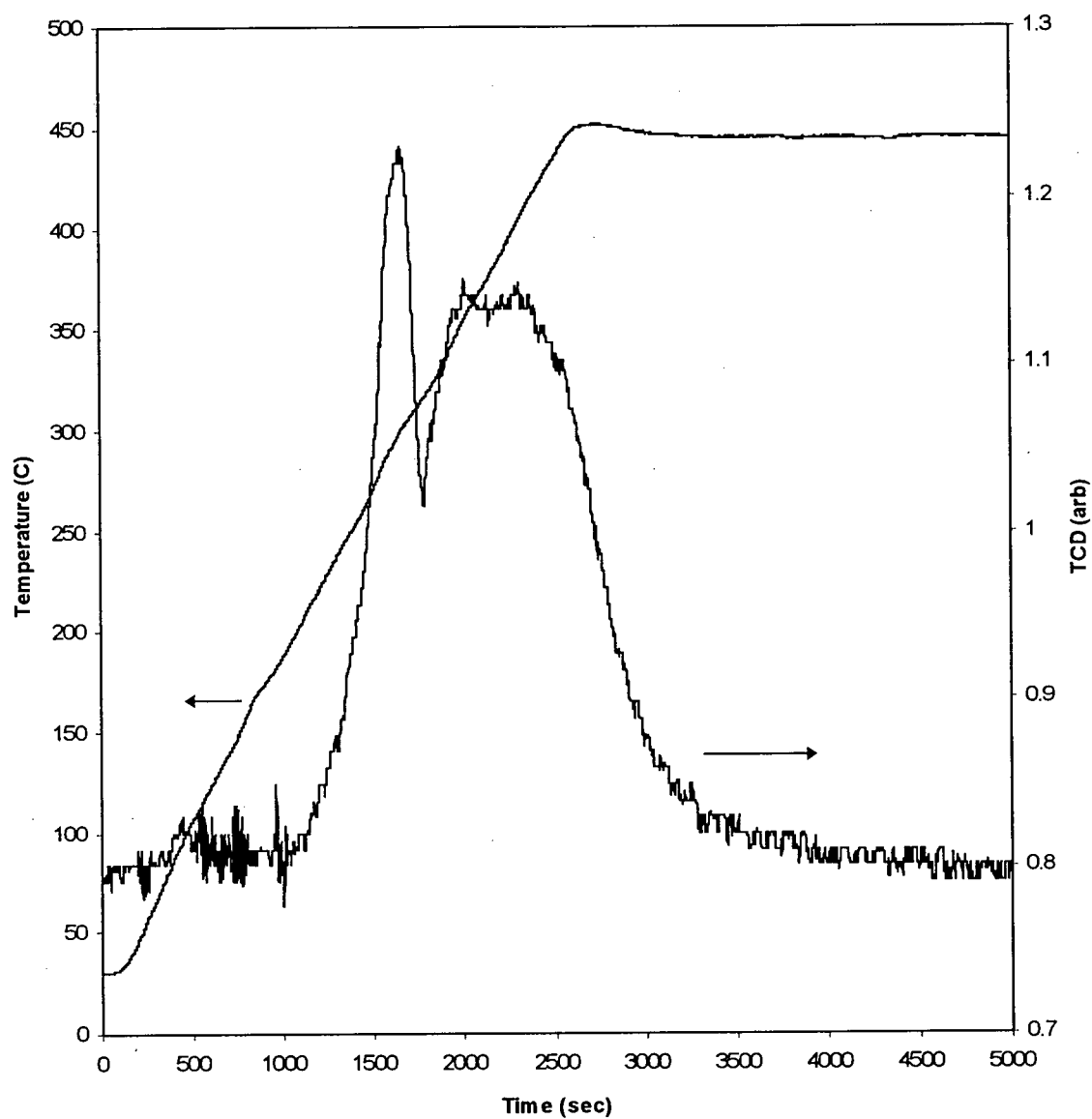


Figure A.2.1.(a). Profile of the temperature programmed reduction (TPR) of the A series 5%Co-SiO₂ catalyst with 54 ml/min of 20%H₂/Ar gas mixture.

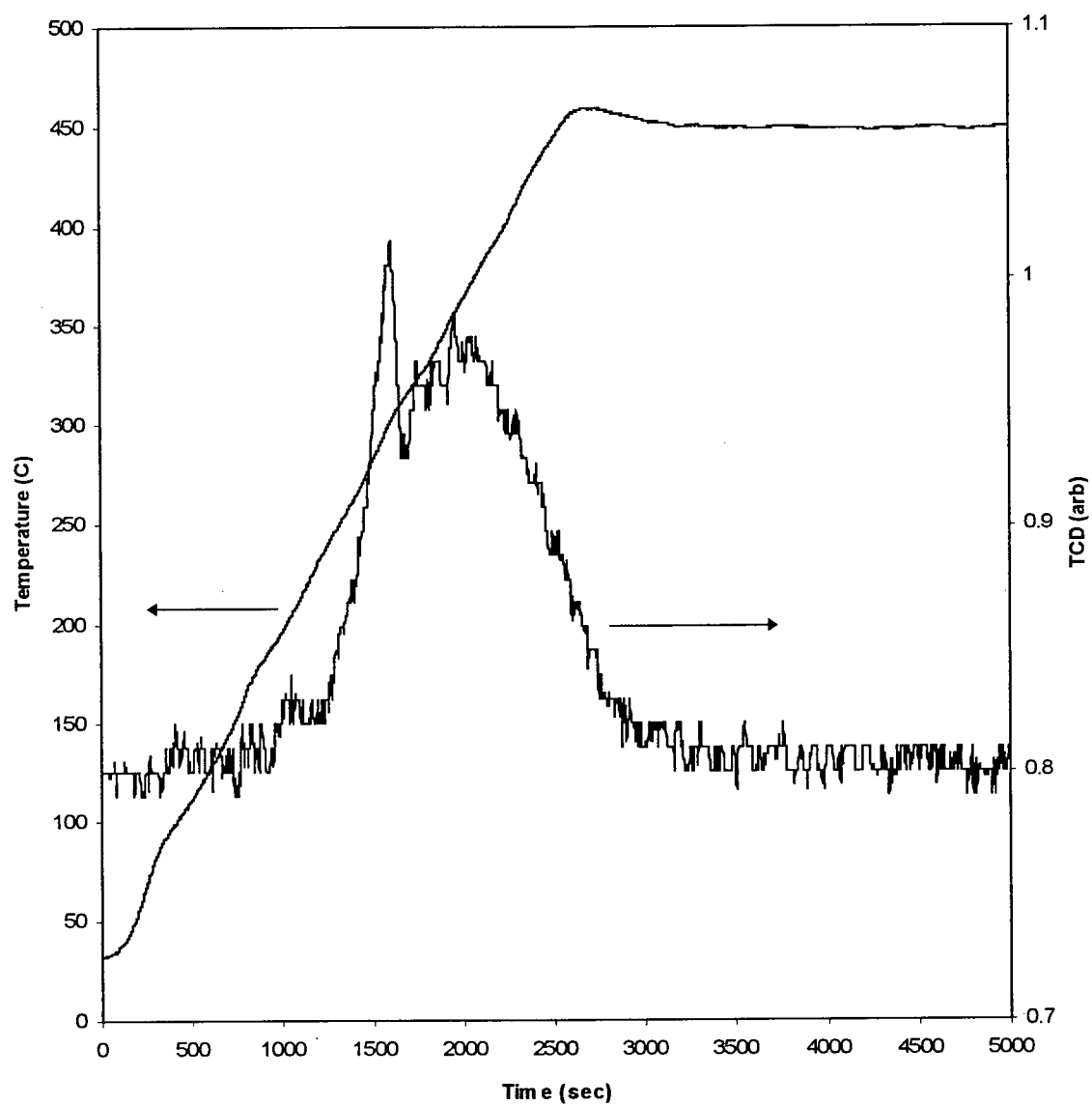


Figure A.2.1.(b). Profile of the temperature programmed reduction (TPR) of the A series 2%Co-SiO₂ catalyst with 54 ml/min of 20%H₂/Ar gas mixture.

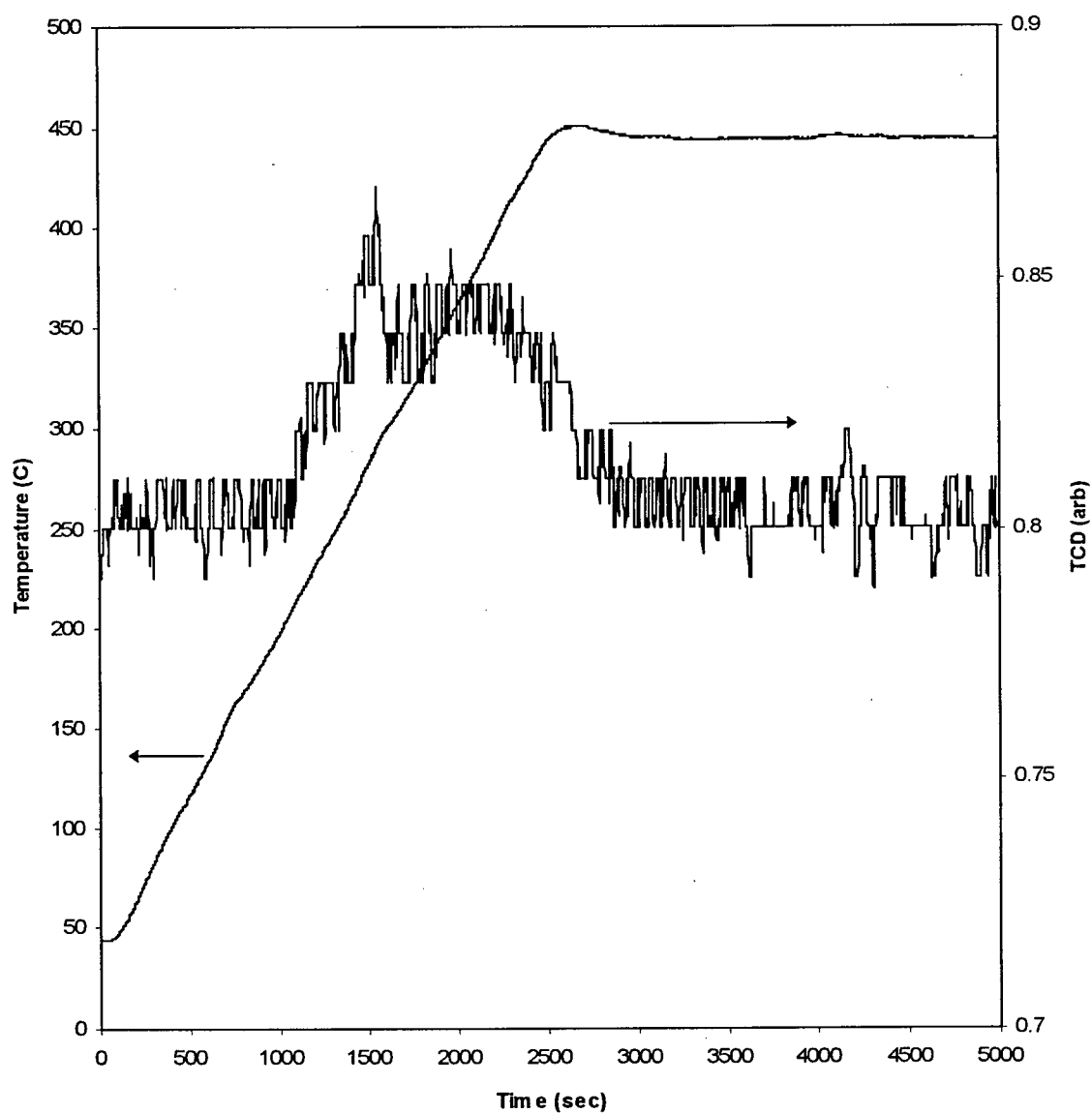


Figure A.2.1.(c). Profile of the temperature programmed reduction (TPR) of the A series 0.6%Co-SiO₂ catalyst with 54 ml/min of 20%H₂/Ar gas mixture.

Appendix 2.2. Experimental Data

Experimental reaction data of CH_4 in CH_4 activation step, production of hydrocarbons in the isothermal hydrogenation step, CH_4 formation in the TPSR step and CO_2 formation in the TPO step were used to evaluate the effect of operating variables on the two-step cycle. In this section the experimental data for each set of experiments are reported in Table A2.2.(a) through A2.2.(g).

Table A2.2(a). Effect of activation time.

Activation Time (min)	7	2	1
experiment series	P52	P48	P53
$\mu\text{mol CH}_4$ consumed (Ac)	176.9	71.3	44.5
$\mu\text{mol H}_2$ generated (Ac)	352.3	110.3	64
x of surface CH_x (Ac)	0	0.91	1.12
$\mu\text{mol CH}_4$ production (Is)	3.70	5.27	6.30
$\mu\text{mol C}_{2+}$ production (Is)	0.10	0.16	0.24
$\mu\text{mol C}$ production (TPSR)	163.0	38.0	1.0
$\mu\text{mol CO}_2$ production (TPO)	37.0	N/A	N/A

Catalyst: 0.5 g reduced A series 12%Co-SiO₂

Activation (Ac): exposure to 5% CH₄/Ar at 450 °C and atmospheric pressure

Isothermal hydrogenation (Is): 10 minutes exposure to 11 ml/min of H₂ at 100 °C

Temperature programmed surface reaction (TPSR): Exposure to 11 ml/min of H₂

Temperature programmed oxidation (TPO): Exposure to 11 ml/min of O₂

Table A2.2(b). Effect of catalyst metal loading.

Catalyst Metal Loading (%)	12	5	2
experiment series	P37	P38	P39
$\mu\text{mol CH}_4$ consumed (Ac)	85.1	43.6	36.7
$\mu\text{mol H}_2$ generated (Ac)	102.0	59.4	44.3
x of surface CH_x (Ac)	1.6	1.3	1.6
$\mu\text{mol CH}_4$ production (Is)	4.3	3.2	1.1
$\mu\text{mol C}_{2+}$ production (Is)	0.44	0.08	0.013
$\mu\text{mol C}$ production (TPSR)	31.1	5.8	1.4
$\mu\text{mol CO}_2$ production (TPO)	N/A	N/A	N/A

Catalyst: 0.5 g reduced A series 12%Co-SiO₂, 5%Co-SiO₂ and 2%Co-SiO₂

Activation (Ac): 2 minutes exposure to 5% CH₄/Ar at 450 °C and atmospheric pressure

Isothermal hydrogenation (Is): 10 minutes exposure to 11 ml/min of H₂ at 100 °C

Temperature programmed surface reaction (TPSR): Exposure to 11 ml/min of H₂

Temperature programmed oxidation (TPO): Exposure to 11 ml/min of O₂

Table A2.2(c). Effect of activation temperature.

Activation Temperature (°C)	450	390	360
experiment series	P60	P55	P56
μmol CH ₄ consumed (Ac)	56.8	36.7	27.0
μmol H ₂ generated (Ac)	89.5	47.2	26.3
x of surface CH _x (Ac)	0.90	1.43	2.06
μmol CH ₄ production (Is)	4.1	5.70	3.90
μmol C ₂₊ production (Is)	0.28	0.21	0.09
μmol C produced (TPSR)	18.7	0.2	0.1
μmol CO ₂ production (TPO)	25.0	N/A	29.4

Catalyst: 0.5 g reduced A series 12%Co-SiO₂

Activation (Ac): 2 minutes exposure to 5% CH₄/Ar at atmospheric pressure

Isothermal hydrogenation (Is): 10 minutes exposure to 11 ml/min of H₂ at 100 °C

Temperature programmed surface reaction (TPSR): Exposure to 11 ml/min of H₂

Temperature programmed oxidation (TPO): Exposure to 11 ml/min of O₂

Table A2.2(d). Effect of various steps on carbon balance.

Steps	Ac TPSR TPO	Ac Is TPO	Ac TPO	Ac Is TPSR TPO
experiment series	P57	P58	P59	P60
$\mu\text{mol CH}_4$ consumed (Ac)	61.0	60.0	63.0	56.8
$\mu\text{mol H}_2$ generated (Ac)	91.4	89.6	88.8	89.5
x of surface CH_x (Ac)	1.0	1.0	1.2	0.9
$\mu\text{mol CH}_4$ production (Is)	-	2.03	-	4.1
$\mu\text{mol C}_{2+}$ production (Is)	-	N/A	-	0.28
$\mu\text{mol C}$ produced (TPSR)	27.3	-	-	18.7
$\mu\text{mol CO}_2$ production (TPO)	33.0	61.5	64.9	25

Catalyst: 0.5 g reduced A series 12%Co-SiO₂

Activation (Ac): 2 minutes exposure to 5% CH₄/Ar at 450 °C and atmospheric pressure

Isothermal hydrogenation (Is): 10 minutes exposure to 11 ml/min of H₂ at 100 °C

Temperature programmed surface reaction (TPSR): Exposure to 11 ml/min of H₂

Temperature programmed oxidation (TPO): Exposure to 11 ml/min of O₂

Table A2.2(e). Effect of carbon aging.

Carbon Aging (min)	5	10	20
experiment series	P67	P68	P63
$\mu\text{mol CH}_4$ consumed (Ac)	52	51	55
$\mu\text{mol H}_2$ generated (Ac)	79	78	81
x of surface CH_x (Ac)	0.95	0.95	1.04
$\mu\text{mol CH}_4$ production (Is)	4.8	3.9	2.8
$\mu\text{mol C}_{2+}$ production (Is)	0.84	0.74	0.21
$\mu\text{mol C}_\beta$ production (TPSR)	6.2	4.3	0.1
$\mu\text{mol C}_\gamma$ production (TPSR)	18.6	19.5	N/A
$\mu\text{mol C}$ produced (TPSR)	18.7	0.6	0.1
$\mu\text{mol CO}_2$ production (TPO)	11	15.3	26.9

Catalyst: 0.5 g reduced A series 12%Co-SiO₂

Activation (Ac): 2 minutes exposure to 5% CH₄/Ar at 450 °C and atmospheric pressure

Isothermal hydrogenation (Is): 10 minutes exposure to 11 ml/min of H₂ at 100 °C

Temperature programmed surface reaction (TPSR): Exposure to 11 ml/min of H₂

Temperature programmed oxidation (TPO): Exposure to 11 ml/min of O₂

Table A2.2(f). Effect of cycles of operation.

Cycle	1	2	3
experiment series	P51a	P51b	P51c
$\mu\text{mol CH}_4$ consumed (Ac)	66	53.3	47.8
$\mu\text{mol H}_2$ generated (Ac)	95.0	50.5	41.6
x of surface CH_x (Ac)	1.1	2.1	2.2
$\mu\text{mol CH}_4$ production (Is)	7.7	2.1	1.8
$\mu\text{mol C}_{2+}$ production (Is)	0.3	0.04	0.01
$\mu\text{mol C}$ produced (TPSR)	10	38	36
$\mu\text{mol CO}_2$ production (TPO)	N/A	N/A	6.0

Catalyst: 0.5 g reduced A series 12%Co-SiO₂

Activation (Ac): 2 minutes exposure to 5% CH₄/Ar at 450 °C and atmospheric pressure

Isothermal hydrogenation (Is): 10 minutes exposure to 11 ml/min of H₂ at 100 °C

Temperature programmed surface reaction (TPSR): Exposure to 11 ml/min of H₂

Temperature programmed oxidation (TPO): Exposure to 11 ml/min of O₂

Table A2.2(g). Effect of isothermal medium.

Isothermal Medium	H ₂	Ar	CO ₂	O ₂
experiment series	P63	P64	P65	P66
μmol CH ₄ consumed (Ac)	54.6	51.3	59.8	54.8
μmol H ₂ generated (Ac)	80.6	75.9	85.6	78.1
x of surface CH _x (Ac)	1.0	1.0	1.1	1.1
μmol CH ₄ production (Is)	2.76	0.87	0.90	0.63
μmol C ₂₊ production (Is)	0.21	0.28	0.04	0.04
μmol C produced (TPSR)	14.3	24.7	58.5	N/A
μmol CO ₂ production (TPO)	26.9	9.9	7.2	8.6

Catalyst: 0.5 g reduced B series 8%Co-SiO₂

Activation (Ac): 2 minutes exposure to 5% CH₄/Ar at 450 °C and atmospheric pressure

Isothermal hydrogenation (Is): 10 minutes exposure to 11 ml/min of H₂ at 100 °C

Temperature programmed surface reaction (TPSR): Exposure to 11 ml/min of H₂

Temperature programmed oxidation (TPO): Exposure to 11 ml/min of O₂

Appendix 2.3. Equations for Calculations

In this section the definitions and equations for various parameters are presented.

CH₄ conversion: (number of moles of CH₄ activated)/(number of moles of CH₄ in the feed)

x of CH_x surface species: Hydrogen content (H/C) in the surface species.

$$x = 4 - 2 * (\text{number of moles of H}_2 \text{ generated}) / (\text{number of moles of activated CH}_4)$$

Θ_c, nominal metal coverage by carbon = (number of moles of CH₄ activated)/(number of moles of surface Co in the catalyst)

C₂₊ yield per site: (number of moles of C₂₊ generated in isothermal hydrogenation)/(number of moles of surface Co in the catalyst)

C₂₊ carbon selectivity in isothermal hydrogenation step: (number of moles of surface carbon converted to C₂₊ products in isothermal hydrogenation step)/(number of moles of recovered surface carbon in isothermal hydrogenation step)

$$\text{C}_{2+} \text{ carbon selectivity} = [(2 * \text{number of moles of C}_2\text{H}_6 \text{ and C}_2\text{H}_4) + (3 * \text{number of moles of C}_3 \text{ products})] / [(\text{number of moles of CH}_4) + (2 * \text{number of moles of C}_2\text{H}_6 \text{ and C}_2\text{H}_4) + (3 * \text{number of moles of C}_3 \text{ products})]$$

Appendix 2.4. Study of the Effect of Activation Temperature

by the Kinetic Model

In this section, experimental results of the effect of CH₄ activation temperature are compared with the kinetic model profiles. Figure A2.4(a), A2.4(b) and A2.4(c) show this comparison for the activation temperature of 450 °C, 390 °C and 360 °C, respectively.

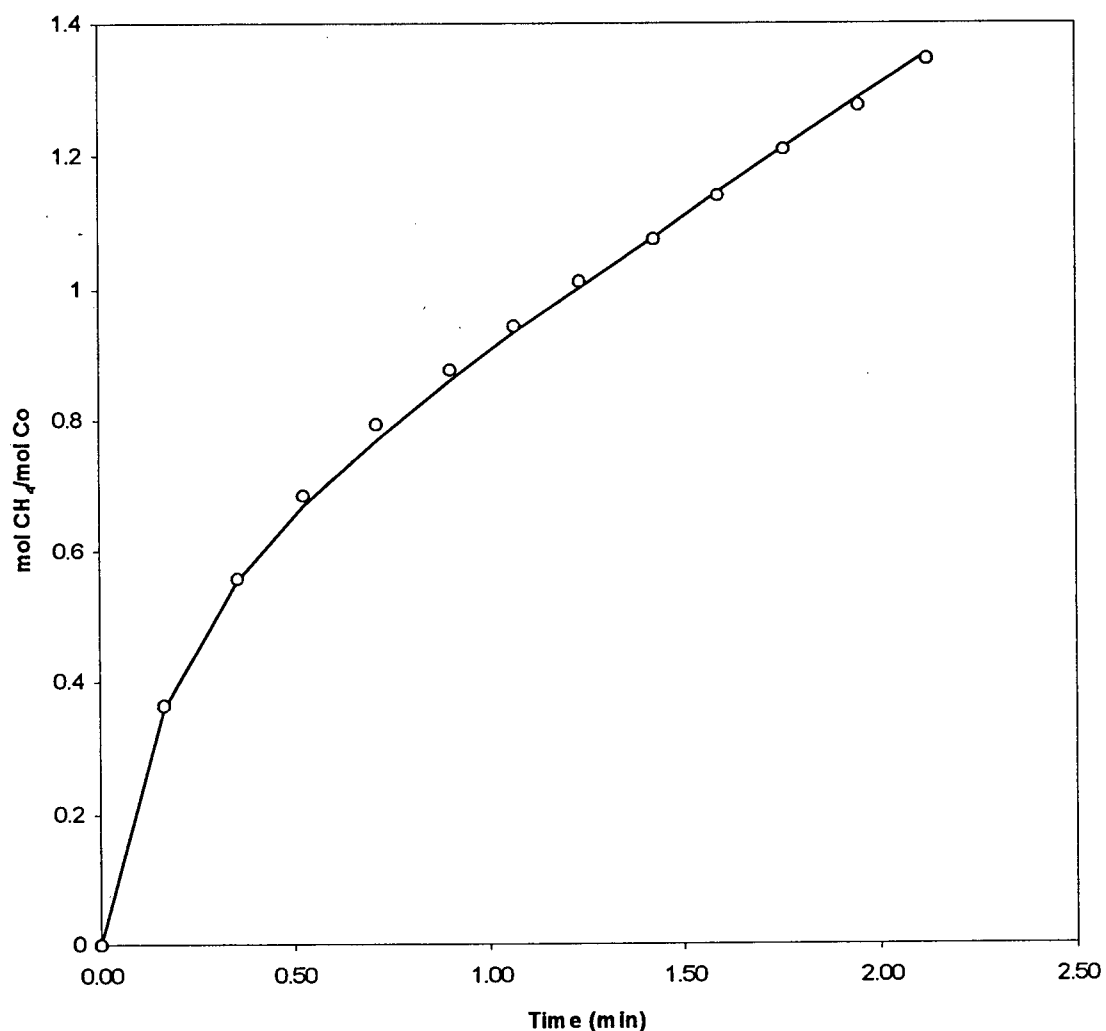


Figure A2.4(a). Cumulative moles of CH₄ consumed per mole of surface Co (O) measured during 2 min flow of 5%CH₄/95%Ar gas mixture and 54 ml/min at 450 °C over A series 12%Co-SiO₂ catalyst, compared to model fit (—).
 Model parameter estimates: $k_1=5 \text{ min}^{-1}$, $k_2=16.8 \text{ min}^{-1}$, $k_3=0.56 \text{ min}^{-1}$ and $k_4=1.24 \text{ min}^{-1}$
 ($R^2=.997$)

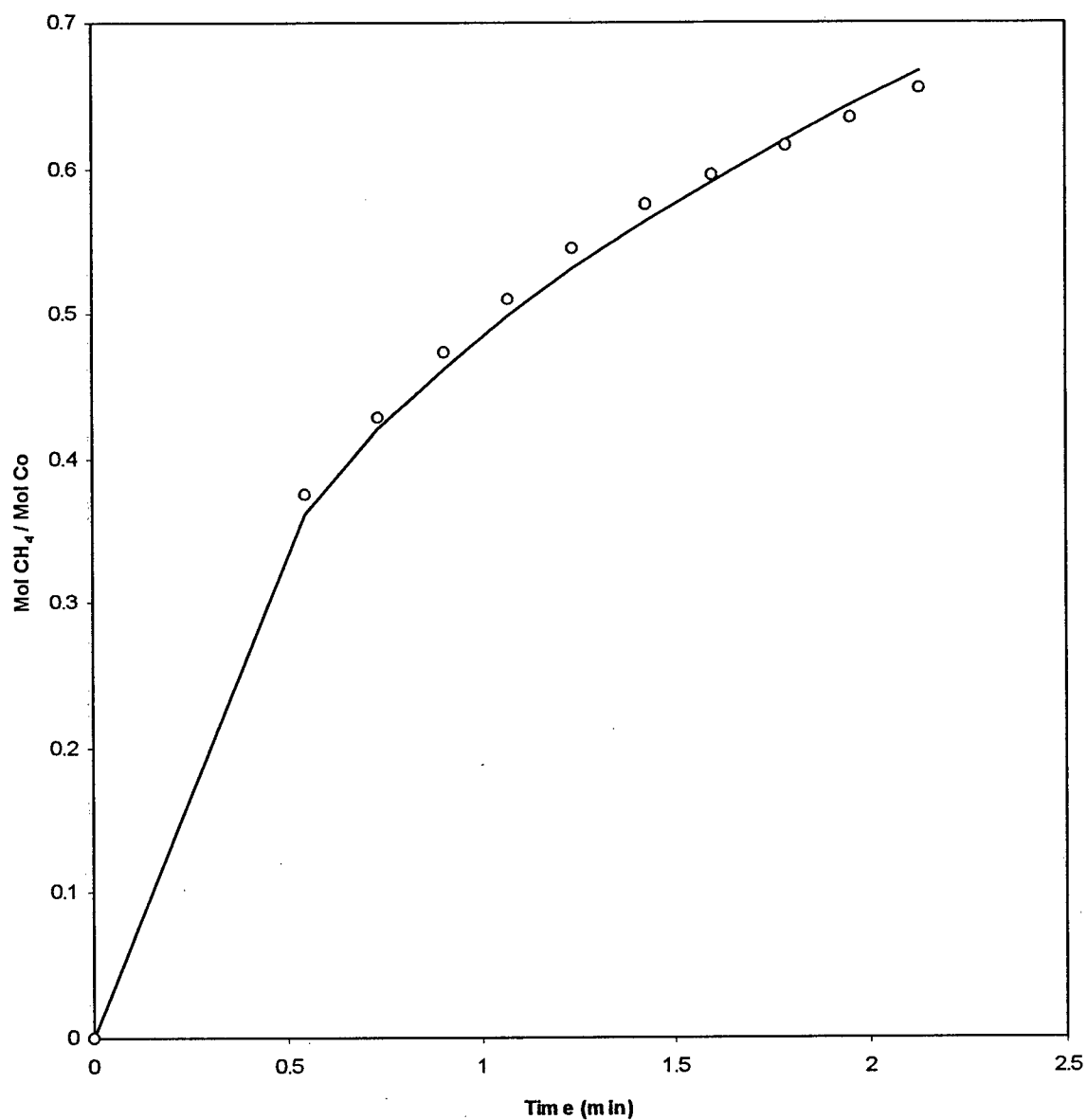


Figure A2.4(b). Cumulative moles of CH₄ consumed per mole of surface Co (O) measured during 2 min flow of 5%CH₄/95%Ar gas mixture and 54 ml/min at 390 °C over A series 12%Co-SiO₂ catalyst, compared to model fit (—).

Model parameter estimates: $k_1=2 \text{ min}^{-1}$, $k_2=5.1 \text{ min}^{-1}$, $k_3=0.24 \text{ min}^{-1}$ and $k_4=1.13 \text{ min}^{-1}$

($R^2=.992$)

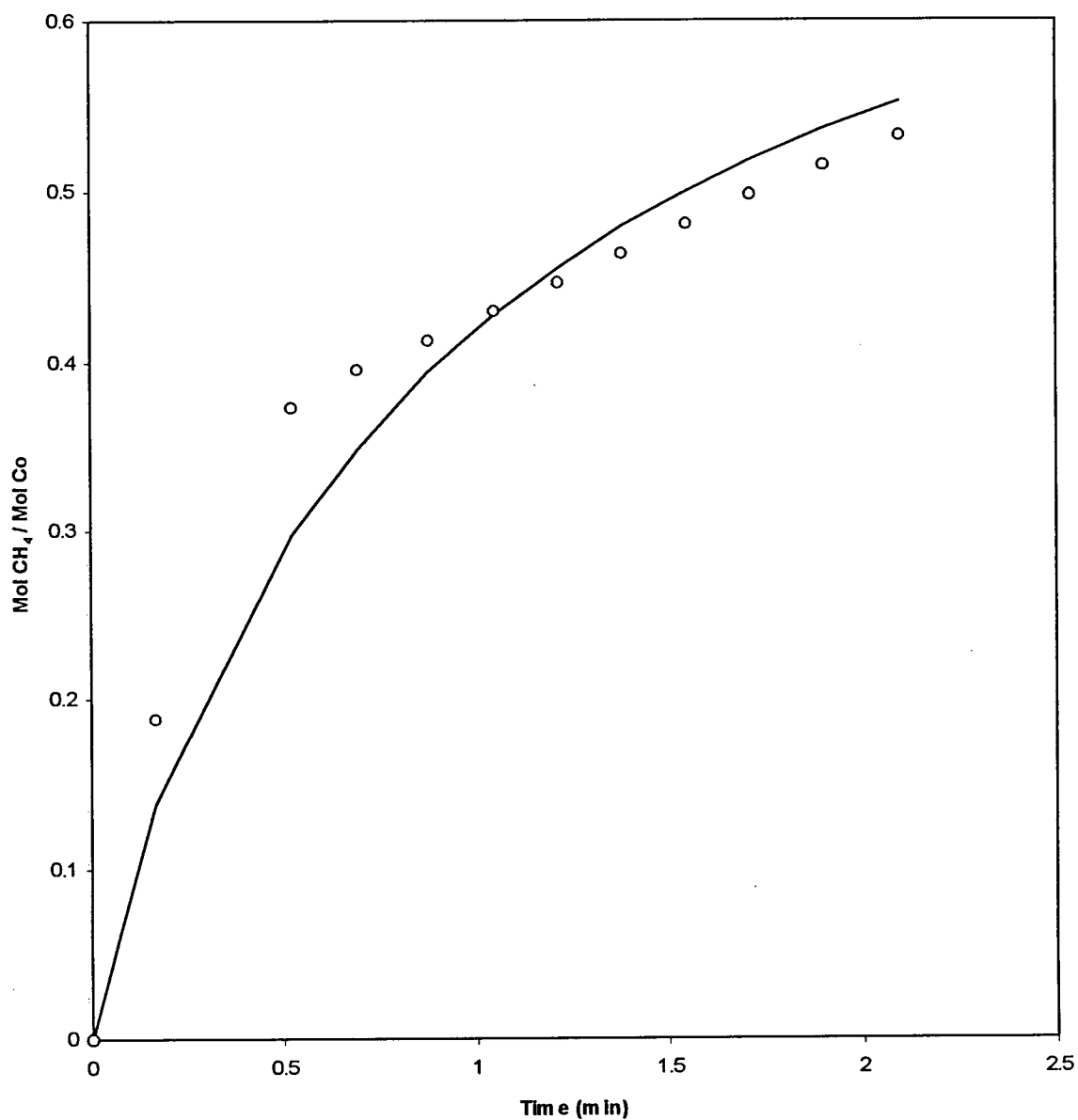


Figure A2.4(c). Cumulative moles of CH₄ consumed per mole of surface Co (O) measured during 2 min flow of 5%CH₄/95%Ar gas mixture and 54 ml/min at 360 °C over A series 12%Co-SiO₂ catalyst, compared to model fit (—).

Model parameter estimates: $k_1=1.4 \text{ min}^{-1}$, $k_2=5.9 \text{ min}^{-1}$, $k_3=0.01 \text{ min}^{-1}$ and $k_4=0.87 \text{ min}^{-1}$

($R^2=.906$)

Appendix 3

3.1. Computer Program Listing

Appendix 3.1. Computer Program Listing

REM COMBINED MODEL AND OPTIMIZATION

CLS

REM Dimensions

DIM Y1(100), FHOLD(100)

DIM TIME(100), CH2EXP(100), CH2CAL(100), CCH4EXP(100), CCH4CAL(100)

DIM RK1(5), RK2(5), RK3(5), RK4(5)

DIM RH2CAL(100), RCH4CAL(100), CUMXCAL(100), CUMXEXP(100)

DIM S(100), CH3S(100), HS(100), CHXS(100), S2(100), CH3S2(100), CHXS2(100)

REM Coverage Functions

DEF FNS (TS, TCH3S, THS, TCH3S2) = -2 * K1 * TS ^ 2 + K2 * TCH3S + 2 * K3 * THS ^ 2

DEF FNCH3S (TS, TCH3S, THS, TCH3S2) = K1 * TS ^ 2 - (K2 + K4) * TCH3S

DEF FNHS (TS, TCH3S, THS, TCH3S2) = K1 * TS ^ 2 - 2 * K3 * THS ^ 2

DEF FNCH3S2 (TS, TCH3S, THS, TCH3S2) = K2 * TCH3S1 - K5 * TCH3S2

DEF FNCHXS2 (TS, TCH3S, THS, TCH3S2) = K5 * TCH3S2

REM Read Data

H = .001

REM READ DATA FOR TIME(20), CH2EXP(20), CCH4EXP(20)

OPEN "C:\soltan\KINETICS\INPUT\SEVEN.PRN" FOR INPUT AS #1

INPUT #1, NDAT

FOR I = 1 TO NDAT

INPUT #1, TIME(I), CH2EXP(I), CCH4EXP(I)

NEXT I

CLOSE #1

REM Optimization conditions

CONS = 2410.7

```

MC0 = 40.75
TIMEMX = TIME(NDAT)
WH2 = 0
WCH4 = 1
NP = 4

TH(1) = 2.782
TH(2) = 12.67
TH(3) = 1
TH(4) = .228
TH(5) = 1
NOB = NDAT
FOR I = 1 TO NOB
Y1(I) = 0!
NEXT I

INPUT "Output data saved as"; A$
b$ = "C:\soltan\kinetics\STAT\" + A$ + ".pm"
OPEN "o", #1, b$

REM Optimization program
REM
REM .....MAIN ROUTINE FOR NON-LINEAR REGRESSION ANALYSIS
REM
60 REM
    REM calculate sel and conv
DIM signs(NP), DIFZ(NP)
    EPS1 = .000001
    EPS2 = .000001
    FLAM = .5: MIT = 6: XFNU = 5!
    FOR ks = 1 TO NP

```

```

DIFZ(ks) = .5: signs(ks) = 1!
PRINT #1, signs(ks)
NEXT ks
signs(1) = 0

IH = NOB * NP
DIM Q(NP), P(NP), E(NP), PHI(NP), TB(NP)
DIM F(1700), r(1700), A(8000), d(1700), DELZ(9000)
DIM XA(NP, NP), XB(NP, NP)
GOSUB 340
CLOSE #1
CLOSE #2
CLOSE #3
END
PRINT #1, "*****FINISHED*****"
340 DEF FNACOS (X) = ATN(SQR(1 / X / X - 1))
ERS2 = EPS2
NPSQ = NP * NP
IX$ = " TEST ONE"
PRINT #1, "NON-LINEAR REGRESSION ANALYSIS"; IX$: PRINT #1, "NUM OBS = "; NOB
PRINT #1, "NUM PARAMS = "; NP
PRINT "NON-LINEAR REGRESSION ANALYSIS"; IX$: PRINT #1, "NUM OBS = "; NOB
PRINT "NUM PARAMS = "; NP
GA = FLAM
nit = 1
LAOS = 0
IF EPS1 < 0 THEN EPS1 = 0
SSQ = 0
FOR I = 1 TO NP
XTH(I) = TH(I): NEXT I
GOSUB 7000
FOR I = 1 TO NOB

```



```

REM PRINT F(I)
r(I) = Y1(I) - F(I)
SSQ = SSQ + r(I) * r(I): NEXT I
PRINT #1, "INITIAL SUM OF SQUARES "; SSQ
PRINT "INITIAL SUM OF SQUARES "; SSQ
REM
REM .....BEGIN ITERATION
REM
550 GA = GA / XFNU
INCNT = 0: PRINT #1, : PRINT #1, : PRINT #1,
PRINT #1, "ITERATION NUMBER "; nit
PRINT "ITERATION NUMBER "; nit
580 JS = 1 - NOB
FOR J = 1 TO NP
TEMP = TH(J)
P(J) = DIFZ(J) * TH(J)
TH(J) = TH(J) + P(J)
Q(J) = 0: JS = JS + NOB
FOR ks = 1 TO NOB: FHOLD(ks) = F(ks): NEXT ks
FOR KX = 1 TO NP
XTH(KX) = TH(KX): NEXT KX
GOSUB 7000
ij = JS - 1
FOR I = 1 TO NOB
ij = ij + 1
DELZ(ij) = F(I): F(I) = FHOLD(I)
DELZ(ij) = DELZ(ij) - F(I): Q(J) = Q(J) + DELZ(ij) * r(I)
NEXT I
Q(J) = Q(J) / P(J): REM .....STEEPEST ASCENT
TH(J) = TEMP
NEXT J
IF LAOS > 0 GOTO 2410

```

```

FOR I = 1 TO NP
FOR J = 1 TO I
SUM = 0!
KJ = NOB * (J - 1)
KI = NOB * (I - 1)
FOR K = 1 TO NOB
KI = KI + 1
KJ = KJ + 1
SUM = SUM + DELZ(KI) * DELZ(KJ)
NEXT K
TEMP = SUM / (P(I) * P(J))
JI = J + NP * (I - 1)
d(JI) = TEMP
ij = I + NP * (J - 1)
d(ij) = TEMP
NEXT J
E(I) = SQR(d(JI))
NEXT I
REM
920 REM
FOR I = 1 TO NP
ij = I - NP
FOR J = 1 TO I
ij = ij + NP
A(ij) = d(ij) / (E(I) * E(J))
JI = J + NP * (I - 1)
A(JI) = A(ij): NEXT J
NEXT I
REM
REM .....A SCALED MOMENT MATRIX
REM
II = -NP

```

```

FOR I = 1 TO NP
P(I) = Q(I) / E(I): PHI(I) = P(I)
II = NP + 1 + II
A(II) = A(II) + GA
NEXT I
I = 1
FOR KX = 1 TO NP
FOR ks = 1 TO NP
KJS = ks + NP * (KX - 1)
XA(ks, KX) = A(KJS): XB(ks, 1) = P(ks): NEXT ks: NEXT KX
NB = I: NNVAR = NP
GOSUB 2770
DET = XDET
FOR ks = 1 TO NP: FOR KX = 1 TO NP
KJS = KX + NP * (ks - 1)
P(ks) = XB(ks, 1): A(KJS) = XA(KX, ks): NEXT KX: NEXT ks
REM
REM .....P/E CORRECTION FACTOR
REM
XSTEP = 1: SUM1 = 0: SUM2 = 0: SUM3 = 0
1250 FOR I = 1 TO NP
SUM1 = P(I) * PHI(I) + SUM1
SUM2 = P(I) * P(I) + SUM2
SUM3 = PHI(I) * PHI(I) + SUM3
PHI(I) = P(I): NEXT I
TEMP = SUM1 / SQR(SUM2 * SUM3)
IF TEMP >= 1! THEN TEMP = 1!
TEMP = 57.29 * FNACOS(TEMP)
PRINT #1, "DETERMINANT "; DET; " ANGLE IN SCALED COORDS "; TEMP
FOR I = 1 TO NP
P(I) = PHI(I) * XSTEP / E(I)
TB(I) = TH(I) + P(I)

```

```

NEXT I
PRINT #1, "TEST POINT PARAMS "
FOR I = 1 TO NP
PRINT #1, TB(I);
NEXT I
FOR I = 1 TO NP
IF signs(I) < 0 GOTO 1470
IF TH(I) < 0 THEN TH(I) = 1
IF TB(I) < 0 THEN TB(I) = 1
IF TH(I) * TB(I) < 0 GOTO 1560
1470 NEXT I
SUMB = 0
FOR ks = 1 TO NP: XTH(ks) = TB(ks): NEXT ks
GOSUB 7000
FOR I = 1 TO NOB
r(I) = Y1(I) - F(I)
SUMB = SUMB + r(I) * r(I): NEXT I
PRINT #1, : PRINT #1, "TEST POINT SUM OF SQUARES "; SUMB
IF SUMB - (1 + EPS1) * SSQ < 0 GOTO 1650
1560 IF TEMP - 30 < GA GOTO 1580 ELSE IF GA > 0 GOTO 1620
GOTO 1590
1580 IF TEMP - 30 > 0 GOTO 1620
1590 XSTEP = XSTEP / 2
INTCNT = INTCNT + 1
IF INTCNT - 36 < 0 GOTO 1250 ELSE GOTO 1870
1620 GA = GA * XFNU
INTCNT = INTCNT + 1
IF INTCNT - 36 < 0 GOTO 920 ELSE GOTO 1870
1650 PRINT #1, "PARAMETER VALUES VIA REGRESSION "
FOR I = 1 TO NP
TH(I) = TB(I)
NEXT I

```

```

ITYPE = 1: GNQ = NP: FOR ks = 1 TO NP
  GAS(ks) = TH(ks): NEXT ks
GOSUB 3160: PRINT #1,
PRINT #1, "LAMDA = "; GA; "  SUM OF SQUARES AFTER REGRESSION "; SUMB
PRINT "  SUM OF SQUARES AFTER REGRESSION "; SUMB
IF EPS2 > 0 GOTO 1750
IF EPS1 > 0 GOTO 1810
1750 FOR I = 1 TO NP
  IF ABS(P(I)) / (9.999999E-21 + ABS(TH(I))) - EPS2 < 0 THEN GOTO 1780
  IF EPS1 <= 0 GOTO 1840 ELSE GOTO 1810
1780 NEXT I
  PRINT #1, "ITERATION STOPS..REL CHANGE IN EACH PARAM < "; EPS2
  GOTO 1890
1810 IF ABS(SUMB - SSQ) - EPS1 * SSQ > 0 GOTO 1840
  PRINT #1, "ITERATION STOPS..REL CHANGE IN SUM OF SQRS < "; EPS1
  GOTO 1890
1840 SSQ = SUMB
  nit = nit + 1
  IF nit - MIT <= 0 GOTO 550 ELSE GOTO 1890
1870 PRINT #1, "THE SUM OF SQRS CANNOT BE REDUCED TO THE SUM OF "
  PRINT #1, "SQRS AT THE END OF THE LAST ITERATION ..ITERATING STOPS"
1890 GOSUB 8000
  PRINT #1,
  PRINT #1, "      RESPONSES      "
  PRINT #1, "  MEASURED  PREDICTED  RESIDUAL"
  FOR mags = 1 TO NOB
    PRINT #1, USING "#####.###^"; Y1(mags); F(mags); r(mags)
  NEXT mags
  PRINT #1,
  PRINT #1, " X TRANSFORM X MATRIX"
  ITYPE = 4: FOR ks = 1 TO NP: FOR KX = 1 TO NP: KJS = KX + NP * (ks - 1)
  GC(KX, ks) = d(KJS): NEXT KX: NEXT ks

```

```

GOSUB 3160
SSQ = SUMB
IDF = NOB - NP
PRINT #1, : PRINT #1, " CORRELATION MATRIX"
NB = 0: NNVAR = NP
FOR ks = 1 TO NP: FOR KX = 1 TO NP
KJS = KX + NP * (ks - 1)
XA(KX, ks) = d(KJS): XB(ks, 1) = P(ks): NEXT KX: NEXT ks
GOSUB 2770
FOR ks = 1 TO NP: FOR KX = 1 TO NP
KJS = KX + NP * (ks - 1)
d(KJS) = XA(KX, ks): P(ks) = XB(ks, 1): NEXT KX: NEXT ks
DET = XDET
FOR I = 1 TO NP
II = I + NP * (I - 1)
E(I) = SQR(d(II)): NEXT I
FOR I = 1 TO NP
JI = I + NP * (I - 1) - 1
ij = I + NP * (I - 2)
FOR J = I TO NP
JI = JI + 1
A(JI) = d(JI) / E(I) / E(J)
ij = ij + NP
A(ij) = A(JI): NEXT J
NEXT I
ITYPE = 3: FOR ks = 1 TO NP: FOR KX = 1 TO NP: KJS = KX + NP * (ks - 1)
GC(KX, ks) = A(KJS): NEXT KX: NEXT ks
GOSUB 3160
IF IDF = 0 GOTO 2740
SDEV = SSQ / IDF
PRINT #1, : PRINT #1, "VARIANCE OF RESIDUALS"; SDEV; " DEGREES OF FREEDOM";
IDF

```

```

SDEV = SQR(SDEV)
FOR I = 1 TO NP
P(I) = TH(I) + 2! * E(I) * SDEV
TB(I) = TH(I) - 2! * E(I) * SDEV
NEXT I
PRINT #1,
PRINT #1, "INDIVIDUAL CONFID LIMITS ON EACH PARAM (UNDER LIN HYPOTH)"
ITYPE = 2: FOR ks = 1 TO NP: GAS(ks) = TB(ks): GB(ks) = P(ks): NEXT ks
GOSUB 3160
LAOS = 1
GOTO 580
2410 FOR K = 1 TO NOB
TEMP = 0!
FOR I = 1 TO NP
FOR J = 1 TO NP
ISUB = K + NOB * (I - 1)
DEBUG1 = DELZ(ISUB)
REM DEBUG1=DELZ+NOB*(J-1)
ISUB = K + NOB * (J - 1)
DEBUG2 = DELZ(ISUB)
REM DEBUG2=DELZ+NOB*(J-1)
ij = I + NP * (J - 1)
DEBUG3 = d(ij) / (DIFZ(I) * TH(I) * DIFZ(J) * TH(J))
TEMP = TEMP + DEBUG1 * DEBUG2 * DEBUG3
NEXT J
NEXT I
TEMP = 2! * SQR(TEMP) * SDEV
r(K) = F(K) + TEMP
F(K) = F(K) - TEMP
NEXT K
PRINT #1, : PRINT #1, "APPROX CONFID LIMITS FOR EACH FUNCTION VALUE"
IE = 0

```

```

FOR I = 1 TO NOB STEP 7
PRINT #1,
IE = IE + 7
IF NOB - IE >= 0 GOTO 2670
IE = NOB
2670 FOR ks = I TO IE
PRINT #1, USING "###.###^"; r(ks);
NEXT ks: PRINT #1,
FOR KX = I TO IE
PRINT #1, USING "###.###^"; F(KX);
NEXT KX: PRINT #1,
NEXT I
2740 RETURN
PRINT #1, "PARAMETER ERROR"
GOTO 2740
2770 REM THIS SUBROUTINE DETERMINES THE INVERSE OF ANY SQUARE MATRIX
REM
REM XB IS THE INVERSE OF XA
PIVOTM = XA(1, 1)
XDET = 1
FOR ICOL = 1 TO NNVAR
PIVOT = XA(ICOL, ICOL)
IF PIVOT < PIVOTM THEN PIVOTM = PIVOT
XDET = PIVOT * XDET
REM
REM DIVIDE PIVOT ROW BY PIVOT ELEMENT
REM
XA(ICOL, ICOL) = 1
IF PIVOT < 9.999999E-21 THEN PIVOT = 9.999999E-21
PIVOT = XA(ICOL, ICOL) / PIVOT
FOR L = 1 TO NNVAR
XA(ICOL, L) = XA(ICOL, L) * PIVOT

```



```

NEXT L
IF NB <= 0 GOTO 3020
FOR L = 1 TO NB
  XB(ICOL, L) = XB(ICOL, L) * PIVOT
NEXT L
REM
REM REDUCE NON PIVOT ROWS
REM
3020 FOR L1 = 1 TO NNVAR
  IF (L1 - ICOL) = 0 GOTO 3130
  T = XA(L1, ICOL)
  XA(L1, ICOL) = 0
  FOR L = 1 TO NNVAR
    XA(L1, L) = XA(L1, L) - XA(ICOL, L) * T
  NEXT L
  IF NB = 0 GOTO 3130
  FOR L = 1 TO NB
    XB(L1, L) = XB(L1, L) - XB(ICOL, L) * T
  NEXT L
3130 NEXT L1
  NEXT ICOL
  RETURN
3160 GNQ = NP
  REM
  NR = FIX(NP / 10)
  LOW = 1
  LUP = 10
3210 IF NR < 0 THEN RETURN
  IF NR > 0 GOTO 3260
  LUP = GNQ
  IF LOW - LUP > 0 THEN RETURN
  PRINT #1, SPC(7);

```

```

3260 FOR J = LOW TO LUP
    PRINT #1, J; SPC(8);
    NEXT J: PRINT #1,
    IF ITYPE = 1 GOTO 3410
    IF ITYPE = 2 GOTO 3450
    IF ITYPE = 4 GOTO 3380
    FOR I = LOW TO LUP
        PRINT #1, I; SPC(2);
        FOR ks = LOW TO I
            PRINT #1, USING "##.###^"; GC(ks, I);
        NEXT ks: PRINT #1,
    NEXT I: GOTO 3490
3380 FOR I = LOW TO LUP
    PRINT #1, I; SPC(2);
    FOR ks = LOW TO I
        PRINT #1, USING "##.###^"; GC(I, ks);
    NEXT ks: PRINT #1,
    NEXT I: GOTO 3490
3410 FOR ks = LOW TO LUP
    PRINT #1, USING "##.###^"; GAS(ks);
    NEXT ks: PRINT #1,
    GOTO 3660
3450 FOR ks = LOW TO LUP
    PRINT #1, USING "##.###^"; GB(ks);
    NEXT ks: PRINT #1,
    GOTO 3410
3490 REM
    LOW2 = LUP + 1
    IF LOW2 - GNQ > 0 GOTO 3660
    IF ITYPE = 4 GOTO 3600
    FOR I = LOW2 TO GNQ
        PRINT #1, I; SPC(2);

```

```

FOR ks = LOW TO LUP
PRINT #1, USING "##.###^~^~"; GC(ks, I);
NEXT ks: PRINT #1,
NEXT I
GOTO 3660
3600 FOR I = LOW2 TO GNQ
PRINT #1, I; SPC(2);
FOR ks = LOW TO LUP
PRINT #1, USING "##.###^~^~"; GC(I, ks);
NEXT ks: PRINT #1,
NEXT I
3660 LOW = LOW + 10
LUP = LUP + 10
NR = NR - 1
GOTO 3210
RETURN
7000 REM
REM Initialization for RK optimization

COMPDAT = 2
K1 = XTH(1)
K2 = XTH(2)
K3 = XTH(3)
K4 = XTH(4)
K5 = XTH(5)
CH2CAL(1) = 0
CCH4CAL(1) = 0
TIME0 = 0
TS0 = 1
TCH3S0 = 0
THS0 = 0
TCH3S20 = 0

```

```

TCHXS20 = 0
CMETH0 = 0
CHYDR0 = 0
7500 IF TIME0 > TIMEMX THEN 10000

REM RK Parameters
REM K1
REM PRINT TIME0, TS0, TCH3S0, THS0
REM PRINT TCH3S20, TCH3SX0
RK1(1) = H * FNS(TS0, TCH3S0, THS0, TCH3S20)
RK1(2) = H * FNCH3S(TS0, TCH3S0, THS0, TCH3S20)
RK1(3) = H * FNHS(TS0, TCH3S0, THS0, TCH3S20)
RK1(4) = H * FNCH3S2(TS0, TCH3S0, THS0, TCH3S20)
RK1(5) = H * FNCHXS2(TS0, TCH3S0, THS0, TCH3S20)
REM K2
RK2(1) = H * FNS(TS0 + RK1(1) / 2, TCH3S0 + RK1(2) / 2, THS0 + RK1(3) / 2, TCH3S20 +
RK1(4) / 2)
RK2(2) = H * FNCH3S(TS0 + RK1(1) / 2, TCH3S0 + RK1(2) / 2, THS0 + RK1(3) / 2,
TCH3S20 + RK1(4) / 2)
RK2(3) = H * FNHS(TS0 + RK1(1) / 2, TCH3S0 + RK1(2) / 2, THS0 + RK1(3) / 2, TCH3S20
+ RK1(4) / 2)
RK2(4) = H * FNCH3S2(TS0 + RK1(1) / 2, TCH3S0 + RK1(2) / 2, THS0 + RK1(3) / 2,
TCH3S20 + RK1(4) / 2)
RK2(5) = H * FNCHXS2(TS0 + RK1(1) / 2, TCH3S0 + RK1(2) / 2, THS0 + RK1(3) / 2,
TCH3S20 + RK1(4) / 2)
REM K3
RK3(1) = H * FNS(TS0 + RK2(1) / 2, TCH3S0 + RK2(2) / 2, THS0 + RK2(3) / 2, TCH3S20 +
RK2(4) / 2)
RK3(2) = H * FNCH3S(TS0 + RK2(1) / 2, TCH3S0 + RK2(2) / 2, THS0 + RK2(3) / 2,
TCH3S20 + RK2(4) / 2)
RK3(3) = H * FNHS(TS0 + RK2(1) / 2, TCH3S0 + RK2(2) / 2, THS0 + RK2(3) / 2, TCH3S20
+ RK2(4) / 2)

```

```

RK3(4) = H * FNCH3S2(TS0 + RK2(1) / 2, TCH3S0 + RK2(2) / 2, THS0 + RK2(3) / 2,
TCH3S20 + RK2(4) / 2)
RK3(5) = H * FNCHXS2(TS0 + RK2(1) / 2, TCH3S0 + RK2(2) / 2, THS0 + RK2(3) / 2,
TCH3S20 + RK2(4) / 2)
REM K4
RK4(1) = H * FNS(TS0 + RK3(1), TCH3S0 + RK3(2), THS0 + RK3(3), TCH3S20 + RK3(4))
RK4(2) = H * FNCH3S(TS0 + RK3(1), TCH3S0 + RK3(2), THS0 + RK3(3), TCH3S20 +
RK3(4))
RK4(3) = H * FNHS(TS0 + RK3(1), TCH3S0 + RK3(2), THS0 + RK3(3), TCH3S20 +
RK3(4))
RK4(4) = H * FNCH3S2(TS0 + RK3(1), TCH3S0 + RK3(2), THS0 + RK3(3), TCH3S20 +
RK3(4))
RK4(5) = H * FNCHXS2(TS0 + RK3(1), TCH3S0 + RK3(2), THS0 + RK3(3), TCH3S20 +
RK3(4))
REM NEXT STEP

REM Coverage of species
TS1 = TS0 + RK1(1) / 6 + RK2(1) / 3 + RK3(1) / 3 + RK4(1) / 6
TCH3S1 = TCH3S0 + RK1(2) / 6 + RK2(2) / 3 + RK3(2) / 3 + RK4(2) / 6
THS1 = THS0 + RK1(3) / 6 + RK2(3) / 3 + RK3(3) / 3 + RK4(3) / 6
TCH3S21 = TCH3S20 + RK1(4) / 6 + RK2(4) / 3 + RK3(4) / 3 + RK4(4) / 6
TCHXS21 = TCHXS20 + RK1(5) / 6 + RK2(5) / 3 + RK3(5) / 3 + RK4(5) / 6

CMETH1 = H * MC0 * K1 * TS1 ^ 2 + CMETH0
CHYDR1 = H * MC0 * (K3 * THS1 ^ 2 + K4 * TCH3S1 + K5 * TCH3S21) + CHYDR0
TIME1 = TIME0 + H
REM MATCH RATES
IF ((TIME(COMP DAT) < TIME1) AND (TIME(COMP DAT) > TIME0)) THEN
CH2CAL(COMP DAT) = CHYDR0 + (CHYDR1 - CHYDR0) * (TIME(COMP DAT) - TIME0)
/ H
CCH4CAL(COMP DAT) = CMETH0 + (CMETH1 - CMETH0) * (TIME(COMP DAT) -
TIME0) / H

```

```

REM    PRINT "RATE="; COMPDAT, CONS * CH2EXP(COMPDAT); CH2CAL(COMPDAT);
CONS * CCH4EXP(COMPDAT); CCH4CAL(COMPDAT)

```

```

    COMPDAT = COMPDAT + 1

```

```

END IF

```

```

TIME0 = TIME1

```

```

TS0 = TS1

```

```

TCH3S0 = TCH3S1

```

```

THS0 = THS1

```

```

TCH3S20 = TCH3S21

```

```

TCHXS20 = TCHXS21

```

```

CMETH0 = CMETH1

```

```

CHYDR0 = CHYDR1

```

```

GOTO 7500

```

```

10000 REM

```

```

    SUM = 0

```

```

    FOR I1 = 1 TO NDAT

```

```

        F(I1) = (WH2 * (CH2CAL(I1) - CONS * CH2EXP(I1)) ^ 2 + WCH4 * (CCH4CAL(I1) - CONS
* CCH4EXP(I1)) ^ 2) ^ .5

```

```

        SUM = SUM + F(I1) * F(I1)

```

```

    NEXT I1

```

```

    PRINT K1, K2, K3, K4, K5, "SUM="; SUM

```

```

    RETURN

```

```

REM    Use optimum parameters to find the coverages and rates

```

```

8000 REM CALCULATE FINAL FORM

```

```

REM    Initialize

```

```

    S(1) = 1

```

```

    CH3S(1) = 0

```

```

    HS(1) = 0

```

```

    CHXS(1) = 0

```

```

    S2(1) = 1

```

CH3S2(1) = 0

CHXS2(1) = 0

K1 = XTH(1)

K2 = XTH(2)

K3 = XTH(3)

K4 = XTH(4)

K5 = XTH(5)

CH2CAL(1) = 0

CCH4CAL(1) = 0

COMPDAT = 2

CONS = 2410.7

MC0 = 40.75

TIME0 = 0

TS0 = 1

TCH3S0 = 0

THS0 = 0

TCH3S20 = 0

TCHXS20 = 0

CMETH0 = 0

CHYDR0 = 0

RMETH0 = 0

RHYDR0 = 0

RH2CAL(1) = 0

RCH4CAL(1) = 0

CH2CAL(1) = 0

CCH4CAL(1) = 0

CUMXCAL(1) = 4

CUMXEXP(1) = 4

TIMEMX = TIME(NDAT)

8500 IF TIME0 > TIMEMX THEN 11000

```

REM K1
PRINT TIME0, TS0, TCH3S0, THS0
REM PRINT TCH3S20, TCH3SX0
RK1(1) = H * FNS(TS0, TCH3S0, THS0, TCH3S20)
RK1(2) = H * FNCH3S(TS0, TCH3S0, THS0, TCH3S20)
RK1(3) = H * FNHS(TS0, TCH3S0, THS0, TCH3S20)
RK1(4) = H * FNCH3S2(TS0, TCH3S0, THS0, TCH3S20)
RK1(5) = H * FNCHXS2(TS0, TCH3S0, THS0, TCH3S20)
REM K2
RK2(1) = H * FNS(TS0 + RK1(1) / 2, TCH3S0 + RK1(2) / 2, THS0 + RK1(3) / 2, TCH3S20 +
RK1(4) / 2)
RK2(2) = H * FNCH3S(TS0 + RK1(1) / 2, TCH3S0 + RK1(2) / 2, THS0 + RK1(3) / 2,
TCH3S20 + RK1(4) / 2)
RK2(3) = H * FNHS(TS0 + RK1(1) / 2, TCH3S0 + RK1(2) / 2, THS0 + RK1(3) / 2, TCH3S20
+ RK1(4) / 2)
RK2(4) = H * FNCH3S2(TS0 + RK1(1) / 2, TCH3S0 + RK1(2) / 2, THS0 + RK1(3) / 2,
TCH3S20 + RK1(4) / 2)
RK2(5) = H * FNCHXS2(TS0 + RK1(1) / 2, TCH3S0 + RK1(2) / 2, THS0 + RK1(3) / 2,
TCH3S20 + RK1(4) / 2)
REM K3
RK3(1) = H * FNS(TS0 + RK2(1) / 2, TCH3S0 + RK2(2) / 2, THS0 + RK2(3) / 2, TCH3S20 +
RK2(4) / 2)
RK3(2) = H * FNCH3S(TS0 + RK2(1) / 2, TCH3S0 + RK2(2) / 2, THS0 + RK2(3) / 2,
TCH3S20 + RK2(4) / 2)
RK3(3) = H * FNHS(TS0 + RK2(1) / 2, TCH3S0 + RK2(2) / 2, THS0 + RK2(3) / 2, TCH3S20
+ RK2(4) / 2)
RK3(4) = H * FNCH3S2(TS0 + RK2(1) / 2, TCH3S0 + RK2(2) / 2, THS0 + RK2(3) / 2,
TCH3S20 + RK2(4) / 2)
RK3(5) = H * FNCHXS2(TS0 + RK2(1) / 2, TCH3S0 + RK2(2) / 2, THS0 + RK2(3) / 2,
TCH3S20 + RK2(4) / 2)
REM K4
RK4(1) = H * FNS(TS0 + RK3(1), TCH3S0 + RK3(2), THS0 + RK3(3), TCH3S20 + RK3(4))

```


RK4(2) = H * FNCH3S(TS0 + RK3(1), TCH3S0 + RK3(2), THS0 + RK3(3), TCH3S20 +
RK3(4))

RK4(3) = H * FNHS(TS0 + RK3(1), TCH3S0 + RK3(2), THS0 + RK3(3), TCH3S20 +
RK3(4))

RK4(4) = H * FNCH3S2(TS0 + RK3(1), TCH3S0 + RK3(2), THS0 + RK3(3), TCH3S20 +
RK3(4))

RK4(5) = H * FNCHXS2(TS0 + RK3(1), TCH3S0 + RK3(2), THS0 + RK3(3), TCH3S20 +
RK3(4))

REM NEXT STEP

TS1 = TS0 + RK1(1) / 6 + RK2(1) / 3 + RK3(1) / 3 + RK4(1) / 6

TCH3S1 = TCH3S0 + RK1(2) / 6 + RK2(2) / 3 + RK3(2) / 3 + RK4(2) / 6

THS1 = THS0 + RK1(3) / 6 + RK2(3) / 3 + RK3(3) / 3 + RK4(3) / 6

TCH3S21 = TCH3S20 + RK1(4) / 6 + RK2(4) / 3 + RK3(4) / 3 + RK4(4) / 6

TCHXS21 = TCHXS20 + RK1(5) / 6 + RK2(5) / 3 + RK3(5) / 3 + RK4(5) / 6

CMETH1 = H * MC0 * K1 * TS1 ^ 2 + CMETH0

CHYDR1 = H * MC0 * (K3 * THS1 ^ 2 + K4 * TCH3S1 + K5 * TCH3S21) + CHYDR0

RMETH1 = MC0 * K1 * TS1 ^ 2

RHYDR1 = MC0 * (K3 * THS1 ^ 2 + K4 * TCH3S1 + K5 * TCH3S21)

TIME1 = TIME0 + H

REM MATCH RATES

IF ((TIME(COMP DAT) < TIME1) AND (TIME(COMP DAT) > TIME0)) THEN

CH2CAL(COMP DAT) = CHYDR0 + (CHYDR1 - CHYDR0) * (TIME(COMP DAT) - TIME0)

/ H

CCH4CAL(COMP DAT) = CMETH0 + (CMETH1 - CMETH0) * (TIME(COMP DAT) -

TIME0) / H

RH2CAL(COMP DAT) = RHYDR0 + (RHYDR1 - RHYDR0) * (TIME(COMP DAT) - TIME0)

/ H

RCH4CAL(COMP DAT) = RMETH0 + (RMETH1 - RMETH0) * (TIME(COMP DAT) -

TIME0) / H

CUMXCAL(COMP DAT) = 4 - 2 * CH2CAL(COMP DAT) / CCH4CAL(COMP DAT)

```

CUMXEXP(COMP DAT) = 4 - 2 * CH2EXP(COMP DAT) / CCH4EXP(COMP DAT)
S(COMP DAT) = TS0 + (TS1 - TS0) * (TIME(COMP DAT) - TIME0) / H
HS(COMP DAT) = THS0 + (THS1 - THS0) * (TIME(COMP DAT) - TIME0) / H
CH3S(COMP DAT) = TCH3S0 + (TCH3S1 - TCH3S0) * (TIME(COMP DAT) - TIME0) / H
CH3S2(COMP DAT) = TCH3S20 + (TCH3S21 - TCH3S20) * (TIME(COMP DAT) - TIME0) /
H
CHXS2(COMP DAT) = TCHXS20 + (TCHXS21 - TCHXS20) * (TIME(COMP DAT) -
TIME0) / H
S2(COMP DAT) = 1 - (CH3S2(COMP DAT) + CHXS2(COMP DAT))
CHXS(COMP DAT) = 1 - (S(COMP DAT) + HS(COMP DAT) + CH3S(COMP DAT))
PRINT "RATE="; COMP DAT, CONS * CH2EXP(COMP DAT); CH2CAL(COMP DAT);
CONS * CCH4EXP(COMP DAT); CCH4CAL(COMP DAT)
COMP DAT = COMP DAT + 1
END IF
TIME0 = TIME1
TS0 = TS1
TCH3S0 = TCH3S1
THS0 = THS1
TCH3S20 = TCH3S21
TCHXS20 = TCHXS21
CMETH0 = CMETH1
CHYDR0 = CHYDR1
RMETH0 = RMETH1
RHYDR0 = RHYDR1
GOTO 8500

11000 REM
REM REcord the results in the file
REM WRITE DATA FOR TIME(20), RH2EXP(20), RCH4EXP(20)
SUMH = 0
SUMC = 0
EXC = 0

```

```

EXH = 0
FOR I1 = 1 TO NDAT
SUMH = SUMH + (CH2CAL(I1) - CONS * CH2EXP(I1)) ^ 2
SUMC = SUMC + (CCH4CAL(I1) - CONS * CCH4EXP(I1)) ^ 2
EXH = EXH + (CONS * CH2EXP(I1)) ^ 2
EXC = EXC + (CONS * CCH4EXP(I1)) ^ 2
NEXT I1
OUTPT$ = "C:\soltan\KINETICS\OUTPUT" + A$ + ".PRN"
OPEN OUTPT$ FOR OUTPUT AS #2
WRITE #2, "H=", H, "SUM H=", SUMH, "SUM C=", SUMC
PRINT "SUM H="; SUMH, "SUM C="; SUMC
WRITE #2, "DT# PT=", NDAT, "EXS H=", EXH, "EXS C=", EXC
PRINT "EXS H="; EXH, "EXS C="; EXC
WRITE #2, "K1=", K1, "K2=", K2, "K3=", K3, "K4=", K4, "K5=", K5
WRITE #2, "t (MIN)", "sigH2(EX)", "sigH2(CL)", "sigCH4(EX)", "sigCH4(CL)", "X(EX)",
"X(CL)", "rtH2(CL)", "rtCH4(CL)", "Tet(S1)", "Tet(CH3S1)", "Tet(HS1)", "Tet(CHxS1)",
"Tet(S2)", "Tet(CH3S2)", "Tet(CHxS2)"
FOR I = 1 TO NDAT
WRITE #2, TIME(I), CONS * CH2EXP(I), CH2CAL(I), CONS * CCH4EXP(I), CCH4CAL(I),
CUMXEXP(I), CUMXCAL(I), RH2CAL(I), RCH4CAL(I), S(I), CH3S(I), HS(I), CHXS(I), S2(I),
CH3S2(I), CHXS2(I)
NEXT I
CLOSE #2
RETURN

```